NEAR SURFACE EVALUATION OF STRUCTURAL, ELECTRONIC AND CHEMICAL PROPERTIES OF TEMPLATED PT MONOLAYERS

A Dissertation
Presented to
The Academic Faculty

by

Adam J. Vitale

In Partial Fulfillment
of the Requirements for the Degree
Doctor of Philosophy in Materials Science and Engineering

Georgia Institute of Technology
August 2016

NEAR SURFACE EVALUATION OF STRUCTURAL, ELECTRONIC AND CHEMICAL PROPERTIES OF TEMPLATED PT MONOLAYERS

Approved by:

Dr. Faisal Alamgir, Advisor
Materials Science and Engineering
Georgia Institute of Technology

Dr. Eric Vogel
Materials Science and Engineering
Georgia Institute of Technology

Dr. Meilin Liu
Materials Science and Engineering
Georgia Institute of Technology

Dr. Krista Walton
Chemical & Biomolecular Engineering
Georgia Institute of Technology

Dr. Preet Singh
Materials Science and Engineering
Georgia Institute of Technology

Date Approved: June 15, 2016

ACKNOWLEDGEMENTS

I wish to take this space to acknowledge my family for always being there for me throughout my life and academic career. My parents Stephen and Gail and my brothers Drew and Daniel have always made their loving support available in a number of ways. My brother Bryan has been especially supportive and took the journey through graduate school alongside me.

The many professors and colleagues I've met during my time at Georgia Tech have also been incredibly helpful, influential, and supportive. I owe my deepest gratitude to Dr. Faisal Alamgir, who gave me the opportunity to participate in his lab and has become a trusted advisor and friend. I want to also acknowledge the other members of my dissertation committee: Dr. Eric Vogel, Dr. Preet Singh, Dr. Meilin Liu, and Dr. Krista Walton for their important insights towards my research. I would also like to show gratitude to my colleague, Dr. Samson Lai for his advice among numerous research discussions.

I would also like to thank Dr. Peter Albrecht, Dr. Sanjaya Senanayake, and Dr. Erik Farquhar from National Synchrotron Light Source for their guidance and assistance during various synchrotron experiments.

Finally, I would like to acknowledge the ACS Petroleum Research Fund #50934-DNI10 for financial support and the National Science Foundation Nanostructured Materials for Energy Storage and Conversion (NESAC) IGERT program for traineeship support under Award Number 1069138.

TABLE OF CONTENTS

Page

LIST OF FIGURES

Page

SUMMARY

Platinum group metals are the choice catalysts for a wide variety of catalytic reactions, including oxygen reduction. The focus of this study is to explore the dimensional aspect of both electronic and structure-driven surface properties of Pt monolayers grown via templating on Au. Surface limited redox replacement is used to provide precise layer-by-layer growth of Pt to synthesize well-controlled 'core-shell' catalyst architectures.

The interaction between core and shell manifests itself through both a structural contribution of epitaxial strain and d-electron orbital mixing. The cumulative effect of the secondary support on the surface Pt and its interaction with adsorbate species is referred to as a ligand effect. The main goal of the research is to investigate how these ligand effects contribute to the structural and electronic properties of Pt monolayer catalysts.

One focus of this study is to explore the incorporation of single layer graphene into the core-shell catalyst architecture. Fully wetted 4-5 monolayer Pt films can be grown on graphene, maximizing the exposed catalyst surface with high Pt activity and stability. The research also looks to investigate the use of single-layer graphene as an intimate capping sheet to prevent surface dissolution of electrode metals into the electrolyte, without adversely affecting activity.

X-ray photoelectron spectroscopy and extended x-ray absorption fine structure techniques are used to examine surface composition and local atom-atom correlations (bond distance, strain, coordination) as well as core-shell charge transfer effects. Cyclic voltammetry and the oxygen reduction reaction are used as probes to examine the electrochemically active area of Pt monolayers and catalyst activity, respectively.

CHAPTER 1: INTRODUCTION

1.1 Topic and Motivation

Mounting concerns around the exhaustion of traditional energy resources and their effects on the environment and climate change have spurred development and research into renewable energy technologies. One of the most prominent areas of focus today is that of fuel cell technology, due to the potential of high energy efficiencies and low carbon emissions. In brief, fuel cells are electrochemical devices that convert chemical energy stored in hydrogen-based fuels to electrical energy with water and heat as the only byproducts.[1] However, fuel cell performance and lifetime are in many ways governed by the limitations of the electrocatalysts working at each electrode, and examination of a multitude of electrocatalytic properties is required in order to improve fuel cell technology among other catalyst-driven systems.

Polymer electrolyte membrane (PEM) fuel cells have the potential to reduce our energy use, pollutant emissions, and dependence on fossil fuels. PEMFCs also hold the advantages of low operating temperature and are being developed as electrical power sources for vehicles and portable applications.[2-5] Despite a great deal of effort to advance PEM fuel cell technology, factors such as electrocatalyst lifetime, durability, and cost still remain as the major barriers to fuel cell commercialization.[1]

The key PEMFC components under the most scrutiny are the catalysts employed. These types of catalysts are generally referred to as ‘heterogeneous’, which are solid-phase materials that act as reaction sites for adsorbing and desorbing reactants and products, and are responsible for a variety of reactions. The atomic interactions between

an electrolyte and a catalyst surface are fundamental to a large variety of practical applications. When such a material can decrease the temperature or energy required to drive a reaction, and the surface itself does not take place in the reaction, this effect is said to be catalytic in nature. Or in short, catalysts lower the energy required to generate a reaction of one material converting into another. Catalysis is of high importance to many technologies and industries, especially when it comes to energy generation. The development of new catalyst systems that can help to solve the challenging problems of energy security is of utmost importance when it comes to environmentally clean energy production.[6] By lowering required activation barriers, improving catalyst lifetime, and decreasing the cost, electrocatalytic systems such as PEMFCs have the potential to become viable source of power. Decreased energy requirements are of utmost importance as that can lead to decreased monetary costs associated with running catalytic processes.

Catalyst-driven reactions are used in a wide variety of applications, from chemical refining in the oil industry, to conversion processes necessary for the proper operation of advanced fuel cells and batteries. Understanding and facilitating oxygen reduction is considered one of the most challenging tasks in current research surrounding both fuel cell technology[1, 3, 7, 8] and lithium air batteries.[9-11] Electrocatalysts for use in water oxidation is also pertinent to promising energy conversion technologies such as solar water-splitting devices and water electrolyzers.[12, 13]

Fuel cells themselves are versatile in their utilization, finding service in transportation as well as both stationary and portable power applications. PEM fuel cells, specifically, are a key focus in the field. Many major automotive companies work solely on PEM fuel cells due to high power density, low operation temperatures, and excellent

dynamic characteristics as compared with other types of fuel cells.[1] Transportation is one of the most interesting and pervasive applications of PEM fuel cells and electrocatalyst research primarily because of potential impact on the environment and the control of emission of greenhouse gases.[14]

Platinum group metals are the material of choice in a wide variety of catalytic reactions, including the oxygen reduction reaction (ORR), hydrogen oxidation reaction (HOR), and the methanol oxidation reaction (MOR), all of which are partial reactions in electro- and photo-electrochemical devices. However, some primary drawbacks of platinum such as its high cost, low poisoning resistance, and loss from corrosion pose significant problems in the continuing development of catalysts, spurring research efforts to modify the catalyst architecture in order to increase activity and robustness while decreasing the cost. The possible impact of rising platinum prices has been raised as a potential barrier to the commercialization of fuel cell vehicles.[15] In order for these technologies to be more readily adapted, it is necessary to develop energy systems that use catalyst material more efficiently over long term application.

One of the most important factors in the catalysis research community pertains to the limited supply of valuable noble metals, which comprise a large portion of catalytically relevant systems. For many fuel cell reactions, precious metals are the material of choice for electrocatalysts. Namely, platinum (Pt) exhibits the highest electrocatalytic activities for electro-oxidation of alcohol fuels on the anode and the ORR on the cathode. However, Pt alone has several obvious disadvantages which greatly inhibit its application for use fuel cells and other catalyst systems. The metal is limited in nature, resulting in high-costs and hindering more widespread commercialization of fuel

cell technology. Pt is also prone to severe poisoning effects, most notably strong CO adsorption on the surface, decreasing both performance and lifetime of Pt-based catalysts.

Pt is primarily produced from ores mined in only two locations: South Africa and Russia.[16] Demand for Pt continues to rise, with these elements playing important roles in automobiles, chemicals synthesis, and petrochemical refining. Currently, Pt demand is most easily attributed to catalytic converters, which detoxify gases and pollutants in exhaust coming from combustion engines. In 2014, automotive demand for Pt rose by 7% to its highest level since 2008, owing to higher car manufacturing output and tighter emissions limits globally.[17] European and North American platinum recoveries in autocatalyst recycling also rose at a lower rate than predicted by Johnson Matthey PLC.

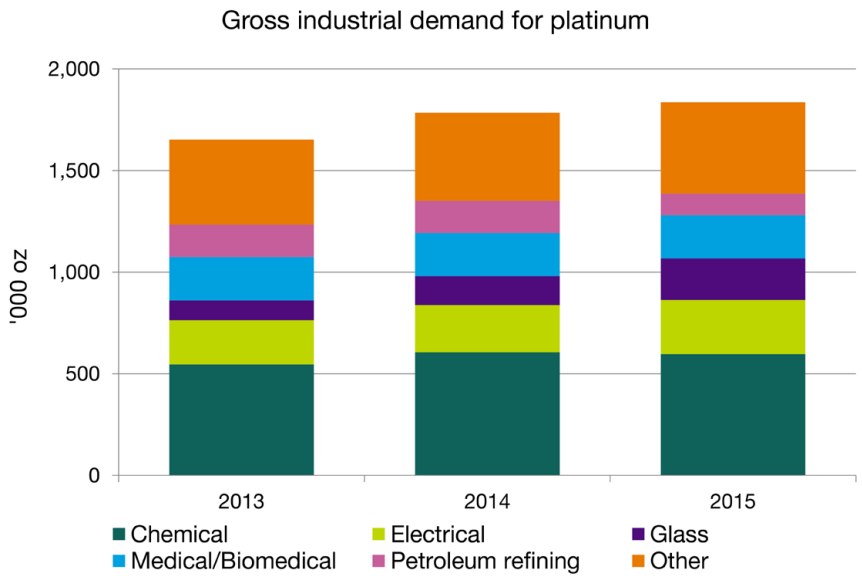

Figure 1: Forecasted gross industrial demand for Pt. (PGM Market Report May 2015)[17]

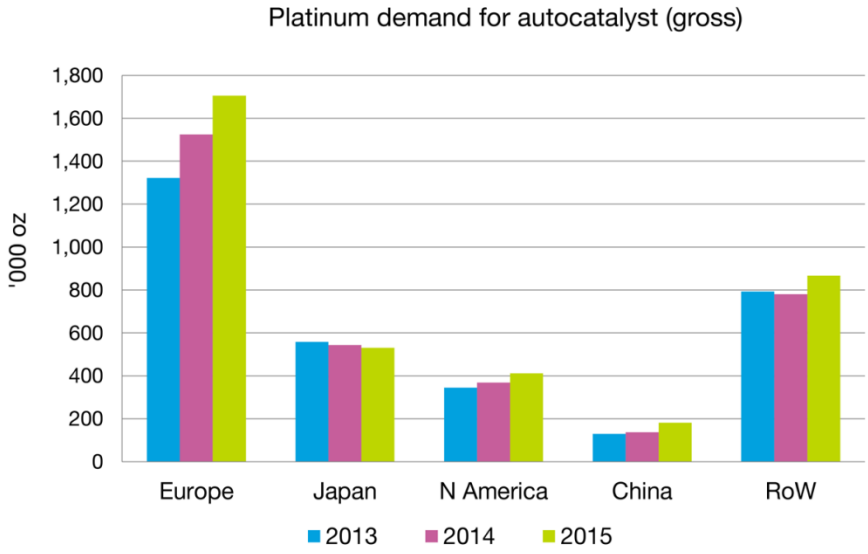

Figure 2: Forecasted autocatalyst Pt demand. (PGM Market Report May 2015)[17]

1.2 Catalytic Fundamental Research

One large avenue of current research in the field aims for improved understanding of the principles of fuel cell processes. There are many interrelated, complex, and subtle phenomena that occur during fuel cell operation, which include mass transfer,

electrochemical reactions, and ionic/electronic transport. The materials properties which influence reactions at the catalyst surfaces are of particular importance. Subtle changes in surface electronic structure can arise due to variation in catalyst composition or architecture, and in turn influence its interaction with a reactant. The development of new material architectures and improving our understanding of the subtleties of surface properties and their relation to catalysis are principally significant for current fuel cell development. Further, the capability to model the electrochemical reactions at the electrodes is crucial, particularly at the cathode where the sluggish ORR often limits the performance of a fuel cell as a whole.

Due to the scarcity of Pt, many problems still need to be solved regarding catalyst lifetime when noble metal materials are involved.[18] The lifetime of a catalyst system is one of its most critical properties, as evidenced by the emerging interest in understanding how catalysts deteriorate over time.[19-21] In order for these technologies to be more readily adapted, it is necessary to develop catalyst systems that are used more efficiently and over longer terms.[15] To obtain ideal electrocatalysts for fuel cells with high catalytic performance, high stability, and low price, much effort has been devoted to designing novel structured catalysts.[22] Specifically, current research aims for nanostructured materials to meets the requirements of large catalytic surface area, increased surface active sites, and low metal loading.[23] One major avenue to accomplish this is the incorporation of other, more abundant transition metals into Pt-based catalysts. Various Pt-based bimetallic and ternary catalysts, such as Pt-Ru,[24, 25] Pt-Fe,[26, 27] Pt-Ni,[28] Pt-Cu,[29] Pt-Co,[30] Pt-Mn,[31] Pt-Ir,[32], and Pt-Au,[33, 34]

etc., have been designed to improve their catalytic performance and reduce the costs.[22, 35]

The influence of catalyst supports is also of key consideration when it comes to studying and developing novel architectures. Carbon materials are the support of choice for PEMFC electrocatalysts due to their high electronic conductivity, high specific surface area (~50-1000 m^2/g_{carbon}), and ability to form highly porous structures.[5] In general, a catalyst's specific activity is often used when attempting to compare the activity of catalysts when taking into account different surface areas or loadings. Due to the various definitions of specific activity used, reports of specific activity must be explicit in their writing.[12] However, while higher surface areas offered by supports intrinsically allow for more reaction sites on a catalyst surface, sometimes complications arise when it comes to support durability as well as pore shape and size.

One longstanding area of research devoted to alleviating the numerous difficulties with catalytic materials is the development of bimetallic catalysts. It is now well known that these architectures often show electronic and chemical properties that are markedly changed from those of their base consitutent metals, and allow the opportunity to obtain new catalyst systems with improved activity and stability. Bimetallic catalysts are very widely researched utilized in many catalysis applications.[28, 36, 37] Modifications to these systems are especially significant when the admetal composition is on the monolayer scale. However, it is difficult to know with certainty how the properties of monolayer bimetallic architectures (MBA) will be affected. There are two major factors that contribute to the properties of MBAs: modifications of electronic structure through the so called ligand effect, and a strain effect that arises from bond length changes along

interfaces. In some cases there are also teritary effects, such as the so-called ‘bifunctional’ effect, in which two surface metals co-exist on a surface such that reactant molecules may interact with two different components in sequence.[38] Measuring these multiple effects arising from multiple metal presences requires meticulous study and characterization.

As the loadings of precious metals in surface-chemical systems continue to decrease for photo-and electro-catalysts for energy and environmental applications, the study of near-surface electronic and atomic structure in functional materials becomes critically important. Extremely small quantities of active elements, whether grown as clusters or ultrathin films, exhibit changes in catalytic activity that arise from both size effects and electron-transfer effects.

1.2.1 Catalyst Performance, Lifetime, and Durability

PEM fuel cell efficiencies and power outputs have been limited by the achievable reaction rates and overpotentials associated with both electrodes. The reaction with the most amount of attention is the oxygen reduction reaction (ORR) which takes place electrocatalytically at the cathode. About 20–35% of cell fuel efficiency in a PEM fuel cell is sacrificed to create an overpotential to drive oxygen reduction.[39] ORR is a multi-electron reaction that includes a number of elementary steps involving different reaction intermediates. It is established that the reaction rate of the ORR is sensitive to the structure of the catalyst surface, arising from the adsorption of spectator species during the reduction.[40] Oxygen reduction is well known to be extremely slow, resulting in large overpotential losses under typical fuel cell operating conditions.[8]

In addition to the major issues involving ORR, anode inefficiencies also contribute to fuel cell limitations, particularly with respect to alcohol oxidation.[41, 42] Much like catalysts for cathode-side ORR, much research has investigated developing more efficient and durable Pt-based catalysts for oxidation of various hydrogen containing fuels, aiming to increase achieved current densities at low overpotentials. While alcohol oxidation reactions are markedly slower and more complex than direct oxidation of hydrogen, using alcohols is practically attractive due to their energy density and easier storage and transport.[5] The most commonly examined anode reaction is that of the methanol oxidation reaction (MOR) in acidic media. MOR is a slow process involving six electron transfers in total for complete oxidation to CO_2.[43].

Several other factors can reduce the useful life of a PEM fuel cell, including Pt dissolution, carbon-support corrosion, and thinning of the polymer membrane.[44] While a catalyst surface does not actually participate in generated chemical reactions at the electrodes, it still exhibits a limited lifetime due to corrosion and other inherent processes. Corrosion of the electrocatalyst especially is one fundamental mechanism that strongly influences cell lifetime and is a major hurdle in commercialization of the technology. This mechanism is frequently addressed in the existing literature and is one of the better understood degradation mechanisms of PEM fuel cells.[45] The range of potential cycling, the total number of cycles, overall cell temperature, and the cell humidification level are the most important factors contributing to corrosion.[46] The lifetime required by a commercial fuel cell is over 5000 operating hours for light-weight vehicles and over 40,000 h for stationary power generation with less than a 10%

performance decay. Many fuel cells exhibit major performance decay after around a thousand hours of operation.[46]

A primary degradation mechanism of the catalyst layer is Pt agglomeration, causing loss of activation sites. Especially when discussing catalyst material on the nano-scale, nanoparticles tend to coalesce due to their high specific surface energy.[47, 48] For nanoparticles, the smaller the size, the higher the specific surface area, and the easier to agglomerate. When this occurs, the electrochemical surface area of Pt catalysts decreases, directly causing the performance of PEMFC degrades, shortening its lifetime. Ferreira *et al.* showed that Pt particles can easily dissolve and subsequently reform as larger particles, a process called Ostwald ripening.[49] Borup *et al.* showed through XRD analysis that Pt particles may not be sufficiently anchored to the carbon support and during cycling will coalesce onto bigger particles.[50] Direct dissolution of Pt from the carbon support has also been shown to occur under most fuel cell conditions. Several studies indicated that Pt moves from the electrode into the electrolyte, reducing the active catalyst area.[20, 51] Both Pt agglomeration and dissolution are illustrated in Figure 3.

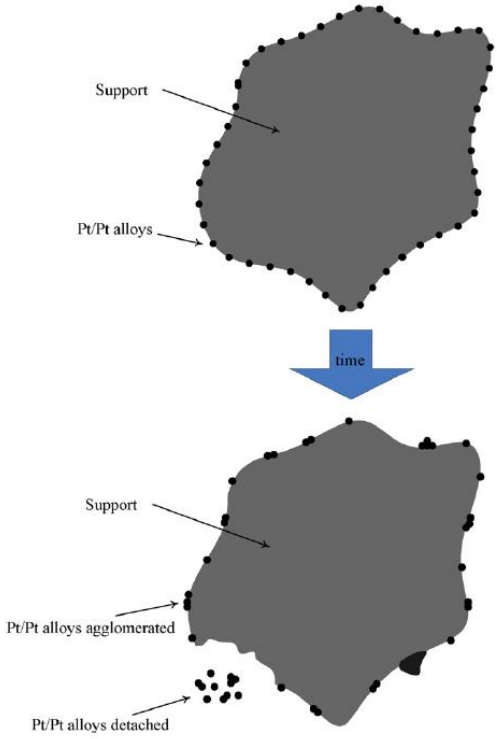

Figure 3: Schematic representing Pt agglomeration and Pt detachment from support material surface.[20]

As to the degradation of electrocatalyst supports, the widely understood mechanism is of carbon oxidation. Carbonaceous species formed during this oxidation understandably decreases the amount of support available for Pt loading, causing catalyst nanoparticles to detach, decreasing the electrochemical surface area.[20] The issue is linked, too, as Pt is known to catalyze the oxidation of carbon, observed in an electrochemical system by $C+H_2O \rightarrow CO_2 + 4H^+ + 4e^-$.[52] In a review paper on PEM durability, Shao *et al.* describe that it is possible that: the more active a catalyst is towards ORR, the more likely it the carbon support can degrade, specifically through a water–gas reaction.[20] Additionally, it is expected that degradation rate of a carbon support increases with temperature. It is also noted how other properties of carbon can also

influence its degradation rate. For example, a support with a higher degree of graphitization is shown to exhibits less degradation. [53]

In addition to cost and propensity to corrosion, Pt catalysts are susceptible to adsorption of molecular intermediates on the surface, blocking reaction sites in a method known as poisoning.[54, 55] Carbon monoxide poisoning, specifically, is considered to be one of the major technical barriers to the commercialization of PEM fuel cells, most notably arising from alcohol electro-oxidation process at the anode. CO tends to form a strong bond to a Pt surface and effectively blocks reactions sites, essentially decreasing the amount of Pt available for catalysis. Thus it is of great importance that CO adsorption be mitigated as much as possible by constructing catalyst surfaces to circumvent it. This poisoning causes dramatic current loss over the performance lifetime of a catalyst, and the ability to resist poisoning is one of the most important parameters to consider when choosing or designing a catalyst system. Many studies, both experimental and mathematical, have been conducted to investigate CO poisoning and its effects.[56-60] PEM fuel cell anodes are tasked with the oxidation of alcohol-based fuels, which can involve the presence of CO. CO is well known to cause poisoning effects to noble metal catalyst material, but unfortunately, fuel gas without CO content cannot be easily used.[61] This is because the use of pure hydrogen as a fuel source has numerous formidable limitations, namely storage and transport.[58] During the catalytic process, CO chemisorbs on the Pt sites to the exclusion of hydrogen. This is possible because CO is more strongly bonded to platinum than hydrogen, as indicated by a greater potential required for the oxidation of CO than hydrogen. Analysis of Gibbs free energy also clearly indicates that CO will preferentially adsorb to Pt due to a more negative energy of

adsorption. The result of this is that even a relatively small concentration of CO can result in the complete coverage of the anode platinum surface.[45, 58]

While problems at PEM cathodes are not always considered poisoning, intermediates of the ORR, such as OH-, can affect the catalysis of oxygen reduction. Spectroscopy studies showed that OH- chemisorption was closely related to oxygen reduction activity on cathode catalysts, indicating the important role of OH- poisoning on Pt sites.[62] Desorption of OH- species from the catalyst surface is a crucial process in allowing completion of the electronic reduction of O_2 to H_2O.[63]

1.2.2 Monolayer Catalyst Design

Current research efforts surrounding electrocatalysts are focused on new catalyst structures that improve on the reaction kinetics, catalyst activity, and cost effectiveness. There has been a considerable amount of research focused on improving catalysts through the use of monolayer/submonolayer coverage of the catalyst adlayers on support materials.[63-69] These so called ‘core-shell’ structures utilize monolayer levels of Pt as the surface shell while using other metal components acting as the core. Monolayer (ML) Pt catalyst architectures appear to provide several unique features that make them attractive from the viewpoint of high Pt utilization and enhanced activity.[63] Adzic recently outlined the tunable nature of the activity for these types of catalysts, which can be manipulated depending on the properties of the top atomic layer and of the core support.[69] Examples include variations to the core of the structure, such as composition, shape, or size to optimize the core-shell interaction. Adzic *et al.* summarizes the advantages of the tunable activity of a Pt monolayer, resulting directly from the

modification of the structural and electronic properties of core-shell structure, which opens extensive opportunities for designing core-shell electrocatalysts.[63]

Not only is the deposition of continuous monolayer-scale Pt films essential for efficient utilization of nanostructured catalysts with highly active Pt shells and cost-effectiveness, but much research also aims at careful tailoring of the electronic structure of the Pt coatings.[70] Various electrochemical deposition techniques allow one to precisely control the growth of deposited catalytic material through the manipulation of experimental parameters.[71] In particular, deposition speed and growth mode can be manipulated via the tuning of solution composition and electrodeposition voltage. The amount of electrodeposited metal can be varied through self-limiting techniques with submonolayer scale precision, or by varying deposition times. By combining precisely electrodeposited layers with galvanic replacement, where a more noble metal preferentially replaces a baser metal, ML replacement is exceptionally precise and can be used to achieve well-defined monolayer bimetallic structures.[66]

Pt monolayer catalysts enable attaining the most direct correlation between catalytic activity and structural properties because all Pt atoms involved in the reaction in the sample shell are sampled by the measuring technique. For conventional catalysts, material properties are determined mostly by bulk Pt atoms, many of which do not actually participate in catalysis because they are not exposed to the reactants.[63] This opens up new avenues of mechanical understanding, as the intimate processes involved can more easily be examined and deconvuluted through careful and systematic experimentation of well-controlled monolayer catalysts.

In addition to precise dimensional control, Pt ML catalysts are also suitable to alteration of the architecture through incorporation of additional 2D materials. One material that has been especially interesting for modifying the core-shell catalyst is a sandwiched 2d material, such as a single layer of graphene, between the Pt adlayers and a host support. With its unique structure and electronic configuration, graphene has become a choice material for incorporation into many high performance electronic devices[72], such as high speed optical modulators, integrated circuits and transistors. The inherent advantage of graphene for many applications is not only limited to its mechanical strength, chemical stability, and super aromatic electrical conductivity through its 2d planar structure, but also due to the versatile tuning of electronic structure at the graphene-metal interface.[73, 74] In the area of catalysis, sandwiched single graphene sheets can potentially transform the catalyst/support architecture by introducing interface stress. Early studies testing this concept, for example, have been carried out in electrocatalysts to enhance activity for oxygen reduction and methanol oxidation reactions.[75] Induced strain along the catalyst surface caused by the insertion of graphene holds the potential to induce surface electrons to more readily catalyze such reactions.[76]

As described earlier, platinum, as one of the most active catalyst metals, suffers from high cost and loss of electrochemically active area due to dissolution during operation. Incorporation of graphene as a catalyst support for Pt has already shown improvements for boosted catalyst activity and lifetime.[33, 77-79] Li *et al.* investigated the catalytic activity of Pt/graphene nanocomposites towards the methanol oxidation reaction via cyclic voltammetry and analysis of redox peaks, finding that Pt/Graphene

nanocomposites compared favorably in catalytic aptitude to nanocomposites composed of Pt/Vulcan carbon.[79] Shang *et al.* deposited platinum over both graphene nanoflakes and carbon nanotubes to compare catalyst durability towards the MOR, and demonstrated more stability for the nano-flakes support.[80]

The advantages of metal-graphene coupling can be utilized in the formation of new fuel cell catalyst architectures. Monolayer-scale platinum can exhibit weak chemical stability and unevolved metallic bonding.[81, 82] Graphene has shown potential to improve the properties within this field of monolayer architectures. By placing a monolayer sheet of graphene between the core substrate metal and overlayer, the graphene will bond to the core and act as a template for the overlayer material.

The main goal of this research is to systematically investigate Pt monolayer formation as well as the role of single-layer graphene in potentially modifying the core-shell platinum monolayer catalyst architectures. Incorporation of graphene at the interface between Pt and Au is expected to give a versatile tunability of electronic configuration and mechanical strain which will affect the binding energy of surface electrons. The proposed research provides a thorough examination of the growth mechanism of Pt monolayers, the strain induced at the interface between Pt and Au and the direct impact on the electrochemical catalytic activity -using spectroscopic and electrochemical analysis. Chapter 2 will thoroughly outline previous work conducted in related literature that informs this study. Chapter 3 discusses the synthesis and characterization techniques employed.

CHAPTER 2: LITERATURE REVIEW

2.1 Traditional Nanoparticle Catalysis

The original concept of catalysis actually dates back 1000s of years to the earliest days of civilization, when mankind learned the art of producing alcohol by fermentation. In medieval times, a nebulous field of alchemy was dominated by the search for a method that could convert commonly found metals into precious metals like gold and silver. However, the knowledge of chemical reactions before the 19th century was largely empirical, where any discoveries made were often isolated and collaboration between scientists of the period was sparse.[83] Most experiments at the time were sporadically documented without much effort made to explain the results. The first proper defining of catalysis as a wide-ranging natural phenomenon is attributed to Swedish chemist Jöns Jacob Berzelius in 1835, although research documentation of catalytic processes came about a few decades beforehand. Berzelius summarized his observations in 1835 as *"…simple or compound bodies, soluble and insoluble, have the property of exercising on other bodies an action very different from chemical affinity. By means of this action they produce, in these bodies, decompositions of their elements and different recombinations of these same elements to which they remain indifferent."* Berzelius then proposed the presence of a new force which he called the "catalytic force" and he called "catalysis" the decomposition of bodies by this force.[84] While early studies of catalysts often employed solid Pt foil as the catalyst material, catalyst research quickly progressed towards more dedicated use catalysts by the 20th century.[83] As catalytic processes became more generally understood by scientists, an increased demand for products generated through catalysis followed, such as ammonia, petroleum products,

pharmaceuticals, and polymers.[85] In the latter half of the 20th century to today, the amount of new insights, discoveries, materials, and processes has become one of the largest research fields, and one of the first to focus on nanoscale research and technology.

Nanoparticle (NP) focused research is extremely prevalent in today's scientific reporting. Due to extremely small length scales, NPs have an obvious application in catalysis due to their considerable specific surface area, which is extremely advantageous for surface reactions. When it comes to NP synthesis, the main goal is the ability to control composition along with size, morphology, and distribution. Control of the primary NP assembly structure is widely utilized to tune their catalytic aptitude, specifically by ensuring the distance between NPs. For optimal properties, NP surfaces have to be well organized in order to get regular spacing between them. While most applications benefit from high nanoparticle density, inter-particle distance has to be long enough to avoid NP aggregation. Catalyst NPs can be synthesized in a variety of ways, such as template-assisted deposition, layer-by-layer deposition, evaporation-induced deposition, through a molecular linker, or electrochemical methods. Depending on the type of structure and composition desired, different methods will lend themselves more readily to a successful fabrication process.

In general, each type of NP synthesis method uses a solution derived from a precursor form of the element of interest, and fabrication routes are based on the ultimate chemical reduction of these metal precursors, often with the appropriate reducing reagents in the presence of stabilizing ligands.[86] Basic chemical methods of deposition are the most common, involving the use of reducing agents or pH-changing additives to encourage the synthesis process. Thermal techniques manipulate the temperature of the

solution to influence the thermodynamic reaction behaviors. However, chemical and thermal methods do not provide an easy route to the control of structure or size distribution. Linker-assisted synthesis uses a molecule introduced between NPs which remain in the final material. However, linker molecules could potentially interfere with the intended application of the NPs. By manipulating the size and shape of the linker molecules in between NPs, one can control the distance between them. Templated assisted methods also use supporting molecules to the organization of NPs, but these processes must undergo additional steps to subsequently remove the 'template'. With template-assisted procedures, very precise control of NP size and distribution can be obtained. These techniques are constantly being revised and improved, and innovation in nanoparticle synthesis abounds.[87]

The research presented concentrates on electrochemical methods for nanoscale catalyst formation. Electrochemistry is advantageous largely because it is inherently surface-sensitive. In brief, these fabrication methods consist of an electrochemical cell where applied current at an electrode surface can be controlled by setting a voltage. These are often performed in 'three electrode' cells, which typically contain a voltage reference electrode, a counter electrode to collect current, and a specially designed working electrode (the sample substrate in question). The working electrode serves as the dominant reaction sites for electrochemical processes in the cell, on which electrodeposition of the desired nanostructure takes place. Using the surface of the working electrode as a template, various chosen nanostructures can be synthesized for the desired application.[88] Electrodeposition synthesis processes can vary based on the procedures utilized, and can involve the formation of either 'instantaneous' or

‘progressive’ nucleation. In the case of the former, nuclei form instantaneously and simultaneously on any available location on the electrode substrate, subsequently growing with electrodeposition time. For progressive nucleation, the number of nuclei that are formed is a function of time of electrodeposition.

Since this work focuses on nanoscale film interactions, the most easily employed technique for synthesis is an iterative electrochemical technique known as surface limited redox replacement (SLRR). Electrochemical set-up and techniques are further detailed in the next chapter.

2.2 Bimetallic and Monolayer Catalysts

2.2.1 Bimetallic Catalyst Overview

The primary approach to solving modern catalysts issues focuses around researching the surface structure and composition to develop novel catalyst architectures with higher ORR activity and less Pt. In many areas of catalysis, nanoscale bimetallic systems are exhibiting higher activities for a variety of reactions when compared to their monometallic counterparts. These architectures can be incorporated into innovative catalysts with improved activity and stability, exhibiting properties that are enhanced from those of their individual parent metals. Bimetallic electrocatalysts, as indicated by their name, incorporate two or more metal catalyst materials achieved either through alloying or layering. These are seen to be an attractive solution to many catalysts problems and have been well researched over the last few decades.

Bimetallic catalysts originally started to gain substantial interest in the 1960s for their use in hydrocarbon reforming as they exhibited faster reaction rates unlike

compared to traditional monometallic catalysts.[89] These initial discoveries of synergistic catalytically properties motivated what would become an enormous experimental field investigating other possible applications for bimetallic systems. Because it is difficult to know without direct observation how the electronic and chemical properties of parent metals will contribute to multi-metal catalysis, and because of the numerous metal systems and reactions available to investigate, the study of bimetallic surfaces in the field of catalysis is incredibly vast and varied.

There are two commonly considered factors that contribute to property modification of catalyst in bimetallic architectures. The first of these is referred to as a 'ligand effect', which is a surface electronic modification that arises when dissimilar metals are incorporated into a single catalyst structure. Secondly, a 'strain effect' between two metals occurs due to bond size differences, such that the geometry of the bimetallic structure induces compressive or tensile strain on surface atoms, affecting their bonding with reaction intermediates.[90] More details of these effects are given in the upcoming sections of this chapter. There are other components of catalyst architectures that influence the reactions that take place on their surface. One of these is a 'bifunctional' effect where two distinct surface metals work in tandem to progress a reaction.[91]

There are many examples of bimetallic catalysts showing enhanced catalytic aptitude in the literature. With Pt-based bimetallic catalysts, the second metal can facilitate a reaction by alleviating CO poisoning that often occurs during the oxidation of alcohols. [92] As an example of a bifunctional effect, Chen *et al.* describe a Pt-Ir system where Ir aids in the dissociation of water to form adsorbed OH species, which then helps to oxidize stuck CO species adsorbed on neighboring Pt atoms.[32] A similar example

comes from Souza-Garcia *et al.* who showed a similar synergy with Pt and Ru for the electro-oxidation of ethanol. In brief, the process involves the breaking of the C-C bond and the subsequent formation of CO_2. In this case, a Pt sites catalyzes the breaking of the C-C bond, and neighboring Ru then transfers absorbed OH to the CO molecule adsorbed in the neighboring Pt site, resulting in a net catalysis.[93] A third example comes in Au-Ag systems, where Au adsorbs CO molecules and the neighboring Ag adsorbs oxygen species to ultimately oxidize CO.[94]

Au-Pd has also been shown to be a catalyst system that benefits from its bimetallic nature. Wang *et al.* correlated that system's alcohol evolution capability with the degree of Au-Pd segregation, such that closer to a monolayer coating of Pd on Au show higher catalytic activity.[95] The same Au-Pd system also exhibits better H_2O_2 evolution rates, reported by Edwards *et al.*.[96] For a different kind of example, the water gas shift reaction (WGS) is also of much attention due to the generation of H_2 as a product. Pt-based systems have shown enhanced activity for the WGS reaction and show enhanced activity when alloyed with Re, Co, and Au.[90] Addition of Ag to Ni(111) has been shown to enhance the activity towards ethylene epoxidation increase the stability of ethylene oxide.[97] While examples of bimetallic systems can be found for many pairs of metallic elements, this work will focus mainly on Pt-based bimetallic architectures.

Pt alloyed or layered with 3d transition metals series have been extensively studied as cathode catalysts for the oxygen reduction reaction (ORR). In general, Pt-alloy nanoparticles in such architectures have been shown increase ORR activity by about a factor of 2 to 2.5 when compared to traditional Pt/C catalysts.[3] Extensive studies have been conducted in Pt and Pt-alloy electrocatalyst development.[58, 98-109] For example,

one of the most significant ORR catalyst reported in the literature is a Pt-Ni system, reported by Stamenkovic *et al*.[28] Pt-Ru catalyst structures have also been shown to exhibit enhanced ORR activities. Inoue *et al.* demonstrated dependence in O_2 reduction capability based on structurally-dependent variations of Pt-modified Ru catalyst surfaces.[110] Strasser *et al.* showed that Pt-Cu nanoparticles can also exhibit high catalytic reactivity for the oxygen-reduction reaction, and the group detailed a reactivity-strain relationship to provides a guideline for tuning electrocatalytic activity for Pt-alloy systems.[111] Further, Greeley *et al.* alloyed Pt with early transition metals such as Sc or Y, determined to be among the most stable Pt systems.[7] Pt-Au has also been suggested as a candidate for a methanol-resistant fuel cell cathode material, when it comes to mitigating the effects of methanol crossover.[112]

2.2.2 Pt Monolayer Catalysts

M.K. Debe of the Energy Components Program at 3M (formally Fuel Cell Components Program) reviewed in *Nature* the primary Pt-based catalysts for cathode side oxygen reduction.[3] He categorized the various approaches to new architectures by overall geometries, catalyst support, and composition. One of the most capable categories detailed was that of core-shell bimetallic systems. As introduced in Chapter 1, core-shell nanoparticle electrocatalysts, founded by groups at Brookhaven National Laboratory, form a highly promising set of catalysts.[63-69] These architectures, oftentimes referred to as ‘monolayer catalysts’ optimize surface electronic and structural effects, and have been well summarized by R. Adzic.[63, 69] Many monolayer catalysts with bimetallic cores and multilayered Pt-skin surfaces have been fabricated, showing the potential of

utilizing multi-metallic nanostructures in tuning their catalytic and durability properties. [113, 114]

One of the biggest advantages of Pt ML catalysts is the relative ease of modification of the structural and electronic properties through careful selection of substrate material. This level of architecture control opens wide-ranging possibilities for designing electrocatalysts with specified catalytic properties. There are many potential avenues from which Pt monolayer architectures can be modified and tuned depending on the surface reaction desired. Other than changing the composition of the core or shell materials, a monolayer of some other metal can be placed as an interlayer between the core and Pt shell. Additionally, modifying the number of low-coordination sites and imperfections can affect how reactive a surface is to bonding with catalytic intermediates.[69] Atoms at low-coordination sites such as edges and kinks have been shown to have a stronger binding with OH than those at 2D terrace sites, which could inhibit the reactions like oxygen reduction.[115] Stronger binding with adsorbates can also lead to Pt nanoparticles more prone to dissolution. In brief, improving a Pt monolayer's reactivity to ORR can be achieved by placing it on the core which forces a slight contraction of Pt-Pt bonds. Compressive strain is known to weaken the bonding strength of oxygen adsorbates, which ultimately speeds up the kinetics of ORR. Lattice contraction can also prevent catalyst dissolution.

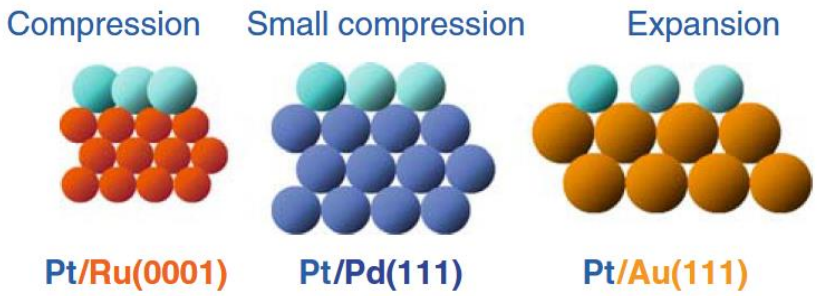

Figure 4: Models of Pt monolayers on three different substrates inducing compressive strain (Ru(0001) and Pd(111)) and expansive strain (Au111)) [63]

Enhanced activity of the ORR reaction of Pt monolayers on alloyed substrates has been reported.[116] Adzic *et al.* have reported a systematic study regarding platinum monolayer catalysts for the electro-oxidation of alcohol molecules on single-crystal and nanoparticle supports, supporting a proposed correlation between substrate-induced lateral strain in a Pt overlayer and its activity towards catalytic reactions.[117] Even further, some studies have examined placing a monolayer of a third metal as an interlayer, such as one by Mavrikakas.[116] The same group recently reported on carbon supported core-shell composition-tunable Pt/PdNi nanostructures with high structural uniformity and high electrochemical durability.[118] In addition to ORR, Pt MLs have also exhibited high potential for the oxidation of methanol and ethanol. In contrast to strain effects on ORR, MOR exhibits significant enhancement in the catalytic activity associated with the tensile strain and decreased activity associated with the compressive strain. Li *et al.* established a correlation between substrate-induced lateral strain and MOR activity.[117]

2.3 Theoretical Background

Bimetallic catalysts are a significant avenue of research when it comes to developing new catalyst structures, due to their ability to improve a multitude of catalytic properties. The goal of much of this research is both to understand the fundamental concepts of heterogeneous catalysis and how to design the best catalysts with better performance and lifetime. For the last century of research in the field, the Sabatier principle has offered the theoretical framework in understanding what would constitute the optimum catalyst.[119-121] The general concept behind the principle focuses on the bonding strength between a catalyst surface and reaction molecules. If this bond is too strong, reaction products cannot be easily desorbed from the surface. If this bond is too weak, the catalyst isn't able to initially activate the reactants. This idea results what is commonly referred to as a 'volcano plot', where the reaction rate's dependence on bond strength appears with an optimal point between the two competing influences. Determining how to best reach optimal reaction rates is a key focus in the area of research when designing new catalyst systems.

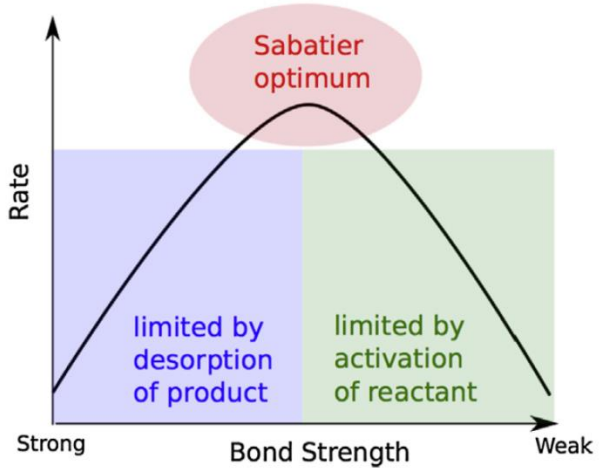

Figure 5: Schematic representation of the Sabatier principle.[119]

However, as Medford *et al.* describe, the Sabatier principle only provides a general qualitative understanding of the concept, and it has the major shortcoming that it is not quantitative, especially when it comes to developing new heterogeneous catalysts.[119] The characterization of reaction rates and bond strengths is not explicitly stated, and the Sabatier principle isn't enough to solely be used as a basis for catalyst design.

The two most important surface-chemical properties that influence the behavior of reactions in catalyst systems are the chemical state and local atomic structure of the surface. Even subtle changes in the chemical identity, electronic structure, and atomic arrangement of the outer few layers of atoms in a catalyst material can have profound influences on the type and rate of reactions that proceed in a given system. One of the initial challenges in describing the change of surface properties is determining an appropriate representation of the state of the surface and its tendency to bond to reaction

intermediates. To that effect, Mavrikakis *et al.* discovered that there is a correlation between adsorption energies, activation energy barriers, and how they relate to surface strain. More accurately, their research described how a material's reactivity can be attributed to a shift in the center of the surface metal *d* bands.[77]

Hammer and Norskov summarized the beneficial effects of bimetallic catalysts by describing *d* band centers in catalytically interesting metals and how they are affected.[122] Their discussion on adsorbate-surface reactions is rooted in density functional theory, where models of adsorption properties attempt to discern the important quantities that affect the reactivity of a catalyst surface. Norskov further describes how modification by alloying or through monolayer bimetallic architectures can lead to shifts of the *d* band centers, which in turn affect the activity for reactions such as the ORR. According to further theoretical considerations, the energy of the *d* band center relative to the Fermi level is a suitable descriptor of the resulting catalytic behavior of a monolayer surface.[123] It is important to note that the *d* band correlates with hybridization energy, in that interaction strength between adsorbates and a catalyst is related to the filling of the anti-bonding states.[119, 124, 125] When the energy level of the *d* band shifts upwards towards the Fermi level, antibonding state energy also increases. This results in more empty antibonding states, which leads to stronger interactions between a catalyst surface and reaction intermediate. It follows that lowering the energy of the *d* band (relative to the Fermi level) decreases the energy of antibonding states, increases their electron population, and weakens surface-adsorbate interactions. [125] This theory is shown as a schematic in Figure 6.

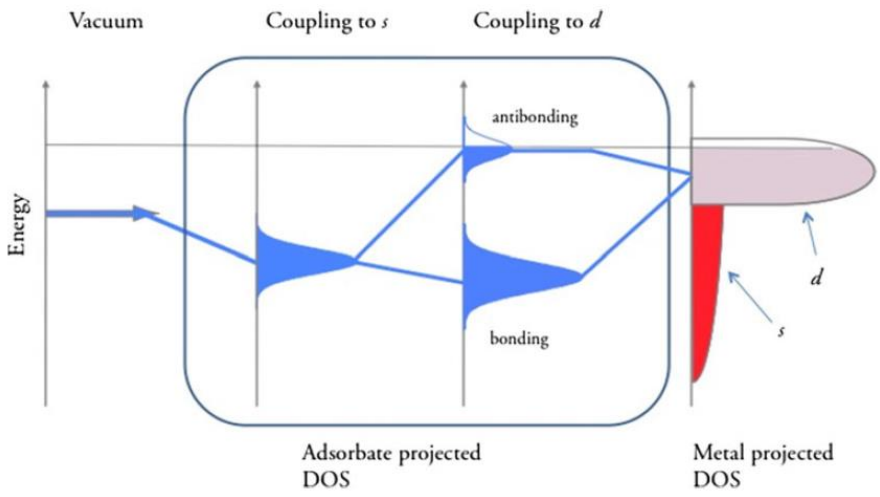

Figure 6: Schematic representation of the *d* band model showing the interaction of an adsorbate adatom level with the *s*- and *d*- states of a transition metal surface.[125]

In looking at the relationship between adsorbate and surface more closely, bonding strength can be estimated through the Newns-Anderson (NA) model approach for various transition metals.[126, 127] According to the model, the electronic valence state of a catalyst surface forms an almost continuous band, and the shape of these bands can widely varied based on the transition metal elements employed and their coordination. When an adsorbate approaches the surface its one-electron states begin to interact with all valence surface states. If the surface band is especially broad, the resulting interaction will exhibit a broadened adsorbate resonance with energy lower than the original gas phase adsorbate level. If the surface associated band is narrow, the adsorbate state will split into bonding and anti-bonding bands, with energies above and below the original gas phase adsorbate level, respectively.[124]

When it comes to monolayer architectures, the interaction between core and shell manifests itself through both a structural contribution of epitaxial strain and *d*-electrons

orbital mixing. The formation of a bond between a surface metal and core metal often produces significant changes in the electronic properties of the metal overlayer, and pronounced differences can be observed in the reactivity of a Pt monolayer scale surface compared to a pure Pt(111) surface. The cumulative effect of the secondary metal on the surface Pt and its interaction with adsorbate species is commonly referred to as a ligand effect.[123] This influence can arise from two separate sources, either as a function of strain-mismatch or from transfer of electron density, both affecting the *d* band centers of the catalytic material.[91] This type of effect has been shown for several Pt-metal systems and has long been the subject of much DFT and STM study.[128] Measuring these ligand effects requires meticulous growth and characterization of the core-shell interface.

For many catalytic reactions of core-shell monolayer systems, the activity of catalysts also exhibits 'volcano-type' dependence based on the supporting metal, which affects how strongly the surface bonds to reaction intermediates. The catalyst that shows the best activity toward ORR specifically strikes a balance between two competing influences. While the mechanistic issues are still being debated in literature, it is generally understood that O_2 electro-reduction must involve both the breaking of an O-O bond and the formation of an O-H bond. It is known that optimal ORR catalyst should strike a balance between O-O bond breaking and O-H bond-making activity.[129] Architecture tuning is required to tweak the activity of these catalyst surfaces to be optimal to promote the given reaction.

2.4 Ligand, Strain, and Size Effects

The commonly cited ligand effects and strain effects are often difficult to uncouple from each other, as both often arise simultaneously in bimetallic catalyst systems. The cumulative contributions of electronic ligand effects and strain effects together can result in upshifts or downshifts the *d* band depending on each effect's individual influence. Moreover, the subtleties of strain alone can require careful meticulous consideration to properly ascribe changes in properties to changes in bond distances. A great example comes from recent studies by Gokcen *et al.* who investigated Pt monolayers on Au nanoparticles.[130] They describe that in an ideal Pt monolayer in a Pt-Au core-shell system, surface Pt atoms must conform to the same in-plane interatomic distance as core Au atoms. The resultant misfit at the surface leads to a tensile strain in the Pt monolayer, leading to an upshift according to the *d* band model and resulting in increased reactivity and stronger adsorption to the surface.[123]

It is important to note that this deduction does not take into account any potential electronic effects caused by the underlying Au, which is expected to exhibit electron transfer towards the Pt shell.[82] However, even disregarding electronic effects, catalyst morphology of Pt MLs in practice may not form wetted monolayers, and instead may resembles 2D clusters instead. The morphology of Pt monolayers has shown some dependence on the subtleties of the slightly varied desposition methods. Gokcen *et al.* show that if Pt exhibits a 2D nanocluster configuration, the cumulative strain is a convolution of the expansive strain due to the epitaxial misfit and a unique compressive strain due to the finite size effects.[130]

The same group explains further how the cumulative strain in nanoclusters has a radial dependence such that compressive effects are stronger at cluster edges. If deposited clusters are small enough, this compressive strain component is significant, and the Pt surface will exhibit a much different overall reactivity when compared to wetted Pt monolayers. Fundamental understanding of this 'size effect' can be also used to tune catalytic properties by controlling morphology. In practice, Grabow *et al*. recently developed a 'core-edge' architecture which consisted of Ru cores surrounded by Pt deposited on Au, or 'RuPtML-CE/Au(111)'. Electrochemical analysis showed that this architecture exhibited higher CO electro-oxidation activity than more typical ML catalysts by an order of magnitude. The group achieved this by understanding the combinations of large lattice mismatch, weak electronic ligand effects, and strong finite size effects and exploiting them to best effect.[131]

To complement, Rettew *et al.* demonstrated a combined methodology of element-specific atomic and electronic structure measurements following monolayer-scale deposition of Pt MLs on Au, and incorporated DFT calculations in their studies. The group concluded that the average valency of ultrathin Pt films in dependent on its overall thickness as a shell on top of crystalline Au. It was shown how the film undergoes a phase transition around a distance of 2-3 monolayers, where Pt initially exhibits a largely cationic valency state with low durability with regard to methanol oxidation. Past this thickness threshold, Pt begins to exhibit a more typical metallic configuration, and the films no longer rapidly dissolve with cycling. Importantly, they also show that films around this threshold are still thin enough to exhibit enhanced CO stripping due to electron transfer from the underlying Au.[82] The enhanced CO stripping is attributed to

the ability of Pt to nucleate OH- species onto its surface through a CO adlayer. While OH- adsorption bonds can be seen as problematic when it comes to catalysis of the ORR at the cathode, they have been shown to lead to lower potentials required for electro-oxidation of CO at the anode.[132] Thus it has been shown that how the valence state of a Pt surface comes into play and how subtle electronic affinities outside of strain can effect catalytic processes.

Strain has long been recognized as a key determinant of ORR activity in Pt alloyed nanoparticles that generally possess altered bond distances compared to pure Pt.[62, 63, 133] Unlike strain effects, the role of electronic ligand effects in ORR activity of Pt nanoparticles has been more obscure, best summarized by Jia et al.[134, 135] Their calculations showed that Pt surfaces on another metal (M) exhibit enhanced activity due to the complex nature of ligand effects, such that the *d* band moves upwards as alloyed M atom radius decreases.[135]

Jia *et al.* review how poor fundamental understanding of the subtleties of ligand effects can lead to seemingly conflicting conclusions in literature.[134] For example, Chen *et al.* attributed high ORR activity of Pt_3Co nanoparticles to cooperative strain and ligand effects induced by the abundant Co.[136] Likewise, Cui *et al.* reported similarly that Pt-Ni exhibited the highest ORR activity in their stoichiometry study, attributing the improvement to ligand effects brought by subsurface Ni.[137] However, other studies by Xin *et al.* and Wang *et al.* show that the enhanced activity of Pt_3Co nanoparticles should be ascribed to strain effects instead of ligand effects, due to the dimensional thickness of Pt shells around Co as Co cannot survive in exposure to acidic environments.[138, 139]

It has been established that properties of nanoscale heterogeneous Pt catalysis embody a sum of contributions in the form of strain, size, and ligand effects. The review of Jia *et al.* surmises that the ambiguity around the role of ligand effects could partially arise from the limitations of characterization techniques along with the exceptionally wide variation in catalyst architectures and synthesis methods. Techniques such as X-ray absorption spectroscopy (XAS) offers the capability to provide inclusive understanding of catalysis mechanisms through quantitative determination of many simultaneous material properties such as bond distance and composition, and can even be performed under operating conditions. The versatility of XAS in sensitivity to chemical species and oxidation state, along with its high spatial resolution, is a powerful tool when examining surface properties. Such measurements can be then directly attributed to the related strain, ligand, and particle size effects. This information is crucial to tie improved synthesis to functionality and even to computational efforts in understanding novel catalyst architectures.[140]. Jia *et al.* performed meticulous in situ XAS analysis on two different Pt-Co nanoparticle catalysts with different morphologies, systematically showing that their ligand effects, bond distances, and coordination were similar to each other, and thus the catalysts exhibited similar ORR activity despite morphological differences.[134] In further recent study via *in situ* XAS, the same group concluded that ORR activity enhancement of the Pt-Co is dominated by strain induced by Co substitution in the Pt lattice, and stoichiometric experimentation shows how varying precursor composition can tune said strain.[141]

2.5 Catalyst Supports and Graphene in Catalysis

2.5.1 Carbon Catalyst Supports

Pt electrocatalysts for PEM fuel cells are usually supported on high surface area materials, traditionally carbon, in order to increase their electrochemically active surface area while lowering the amount of Pt necessary. It has already been well established that electrochemical surface area is of primary importance in a catalyst system, since the rate at which reactants can interact with the catalyst material is limited by the amount of that material's surface available. The size and morphology of platinum particles depend on the nature of the support. One of the primary drawbacks to carbon-based supports is the tendency to oxidize, resulting in the separation of Pt particles from the carbon support. Pt particles would become electronically isolated, leading to a less effective Pt utilization as well as degraded fuel cell performance.[20] The electrochemical properties of catalysts, including both their reactivity and stability, are strongly affected by the physical properties of the carbon support. In general, the primary requirements of a catalyst support most suited for use in fuel cells include: high surface area, appropriate porosity, high electrical conductivity, and high stability under fuel cell operational conditions.[142]

Throughout the 1990s, carbon blacks - essentially pure elemental carbon in the form of colloidal particles - were almost exclusively used as catalysts support in low-temperature fuel cells. Carbon black, while exhibiting moderately high surface areas (~250 m^2g^{-1}), has randomly distributed pores of varying sizes which can result in inefficient diffusion effects. Carbon black materials also suffer from enhanced oxidation rates at high potentials as well as the presence of organo-sulfur impurities.[143] In recent

years, various catalyst support materials have been proposed to address the challenges. In order to improve the electrochemical activity and stability of catalysts, much more attention has been placed on specifically designed carbon supports. Novel carbon supports, such as carbon nanotubes (CNTs), nanoporous carbon, or graphene, offer improved electrical and mechanical properties through their versatility in terms of their structural conformation or pore texture.[142] In addition to carbon materials, non-carbon materials, such as oxides, titania nanotubes, and conductive polymers, have also been proposed as catalyst supports.[144, 145] Brief descriptions of CNT and nanoporous carbon supports are presented in the following paragraphs. However, graphene is the main support material examined in the research presented, detailed in the next subsection.

In brief, CNTs consist of cylinders made of graphite layers with diameters of a few nm and lengths of the order of 1 mm. CNTs exist in two general categories: single- (SWCNTs) and multi-walled nanotubes (MWCNTs).[146] However, pristine CNTs are inert and need to be functionalized before they can act as a support for catalyst materials. Functionalization is most often achieved through chemical treatment in HNO_3 or H_2SO_4/HNO_3 acids, which in essence creates defects on the external walls of CNTs for catalyst nanoparticles to attach to. Other functionalization methods include CNT treatment through surfactants or polymer materials.[147] CNT-supported Pt nanoparticles exhibit high catalyst utilization and especially improved durability compared to other carbon supports. One proposed reason is that hydroxyl intermediates cannot easily penetrate the rigid structure of CNTs, while other supports like carbon black have excessive presence of dangling bonds which oxygen atoms can easily attach to, leading to higher corrosion rates. [148] MWCNTs especially exhibit superior stability even severe

potential cycling conditions.[149] While these structures show notably higher durability than other catalysts on carbon-based supports, catalytic activities have yet to show significant improvements.[147, 150] Zhao *et al.* recently investigated the effect of multi-wall CNTs with different specific surface areas on the stability of supported Pt catalysts.[151] While CNT supports show higher electrical conductivity when compared to alternatives, the advantage is only minimal as electrode impedance is a nearly negligible contributor to overall performance losses. However, carbon nanotube supports do have potential to exhibit enhanced transport or water management. Further, there are concerns about processing factors of CNTs that make them unappealing when it comes to manufacturing in high volumes.[3]

Nanoporous carbon supports are characterized by high surface area and porosity leading to higher activity and stability than carbon black. Nanoporous surfaces provide interesting opportunities for catalysis, since they offer an extremely high electrochemical surface area per unit mass or nominal electrode size. Nanoporous structures facilitate diffusion of the reactants, making them very attractive materials as catalyst supports. Supports with a high specific surface area and optimal pore structure could significantly improve energy conversion efficiency and activity.[4] In order for a catalytic reaction to take place, reagent molecules must run across the porous systems and the reaction products have to leave the catalyst. One interesting side effect of nanoporous supports is that porous structures can act as diffusion sinks, slowing the diffusion of ionic species through their pores. Also deactivation phenomena are greatly affected by pore size, such as carbonaceous blocking on reaction sites.[152] Despite the added complications,

nanoporous surfaces are still an important consideration as they provide more applicable, economically feasible substrates.

In general, when it comes to carbon-based supports, the extent of carbon graphitization has been shown to play important role on carbon support stability. Carbon that exhibits more graphitic properties are typically more thermally and electrochemically stable, due to a smaller amount of defect sites on carbon structure where carbon oxidation reactions tend to initiate.[153, 154] Further, as increasing the degree of graphitization leads to the increasing support strength on the support, Pt can be more strongly anchored resulting in more durably metal–support interaction and resistance of Pt to sintering.[155, 156] Additionally, the crystalline structure of the supported catalyst metal is also affected by the metal-support interaction. Metal particles supported on CNTs, for example, have a highly crystalline structure due to strong metal-support interaction, whereas Pt particles supported on carbon black have a more dense globular morphology due to weak metal-support interaction. Hence, the more amorphous the carbon support, the higher the platinum size and the more dense the globular morphology.[157] Additionally, catalysts have been shown exhibit increased activity at boundary sites orders of magnitude greater than non-boundary sites. This leads to engineering targets dedicated to increasing the surface area of boundaries as much as possible.[158]

2.5.2 Graphene-based Catalyst Supports

Graphene is a two-dimensional planar sheet of bonded carbon atoms which is one atom in thickness. The carbon bonds are sp^2 hybridized, where the in-plane C-C bond (called σ) is one of the strongest common bonds in materials. The out-of-plane bond (called π) contributes to a delocalized network of electrons. These π bonds are chiefly

responsible for the electron conduction of graphene and provide the interaction among the surface of graphene sheets. With its unique structural configuration, graphene has shown exceptional physical properties, such as mechanical strength and chemical stability, which have attracted vast research interest in many scientific and engineering communities.[159] In addition to its planar state, graphene can also be formed into spherical buckyballs, one-dimensional carbon nanotubes (CNT), or stacked into three-dimensional graphite.[160-162]

In comparison with CNTs, graphene not only possesses similar stable physical properties but also larger surface area. Additionally, production cost of graphene in large quantities is much lower than that of CNTs.[163] The use of graphene as a supporting material in catalyst architectures is also interesting for improving the surface properties of noble metal materials. As mentioned in the introduction chapter, incorporation of graphene as a catalyst support for Pt has already shown improvements for boosted catalyst activity and lifetime.[33, 77-79] Li *et al.* examined the catalytic activity of Pt/graphene nanocomposites towards the methanol oxidation reaction (MOR) via cyclic voltammetry and analysis of redox peaks, finding that Pt/graphene nanocomposites compared favorably in catalytic aptitude to nanocomposites composed of Pt/Vulcan carbon.[79] Shang *et al.* compared MOR durability between deposited platinum on graphene nanoflakes and carbon nanotubes, demonstrating that the graphene nanoflakes support exhibited a higher level of more stability over time.[80] The use of single-layer graphene as an intermediate layer in monolayer catalysts has also been shown to improve catalytic activity towards ORR due to compressive strain induced on the outermost Pt layers.[33, 76] Furthermore, the two dimensional nature of graphene allows both its edge

and basal planes to interact with the catalyst atoms, leading to high conductivity and electron transfer.[143]

Experimental and computation research on the growth (and the resulting properties) of various metals over graphene, was reviewed by Liu *et al*. The review summarized many metal systems, but most showed a similar tendency to cluster over graphene.[164] Dai *et al*. used first-principles energy calculations to investigate the formation and structures of Pt clusters on graphene. Their calculation found that, for a single Pt atom absorption, the most stable absorption site is the bridge site, and that it will preferentially form tetrahedral clusters.[165] Similarly, Chan *et al*. found through calculation that metals comparable to Pt, such as Pd and Au, induce a noticeable distortion of the graphene sheet upon adsorption.[166] He *et al*. synthesized Pt, Pd, Au and Ag nanoparticles onto graphene oxide nano sheets by a solution-based method, but was not able to achieve full coverage due to agglomerates.[167] Sun *et al*. found that depositing Pt nanoparticles via atomic layer deposition (ALD) methods tended to form clusters rather than wetted layers spread over the graphene.[168] Achieving full metal wetting of graphene-based support at monolayer level thickness remains a challenge.

For this work, graphene is used extensively as a modifier for Pt catalyst architectures. Graphene is expected to provide a variety of alterations to the properties of Pt monolayers, either as an inducer of strain when used as a surface template, or as a protective barrier in mitigating catalyst dissolution.

CHAPTER 3: METHODS

3.1 Electrochemical Methods

3.1.1 Electrochemistry Experimental Set-up

Before discussing the electrochemical synthesis and characterization methods employed in this work, it is worthwhile to detail the experimental set up used to performed such processes and experiments. The most common setup for evaluating electrochemical processes includes a potentiostat device and an electrochemical cell.

3.1.1.1 Potentiostats and Three Electrode Cells

Potentiostats are instruments which allow for precise control and measurement of current and potential in an electrochemical system. A typical potentiostat connects to two pairs of electrical leads (four total leads) which can be connected to electrodes in a conductive system. One pair of leads controls the potential difference (voltage) between electrodes and the other controls the electrical current running through the electrochemical system. Most experiments performed on potentiostats are in the category of voltammetry, where the potential is controlled and varied arbitrarily. The resultant current is measured in a plot known as a voltammogram, and the shape of the voltammogram depends on nature of potential variation, electrolyte employed, and any reactions that are generated.

Such electrochemical experiments require at least two electrodes, like is common in batteries. A two electrode cell will allow a measurement of current and voltage difference between those two electrodes. While this setup might be suitable for a small subset of electrochemical analysis, there are numerous limitations. Most analytical

electrochemical experiments are interested in the potential at only one electrode in order to more closely study it and the chemical processes that occur on its surface. In a two electrode cell, the potential measured by the potentiostat is actually the potential difference between the two electrodes. It is very unlikely for either electrode to maintain a set potential while passing current to counter redox events occurring in the cell. In other words, the absolute potential of each electrode will be simultaneously changing, making it difficult or impossible to isolate either.

In order to separate the potential at the electrode of interest, the roles of supplying electrons and providing a reference potential are divided between two distinct electrodes. Three electrode cells allow an experimenter to study the potential at a single electrode surface. The three electrodes are known as the working electrode (WE), a reference electrode (RE), and a counter electrode (CE). The WE is the electrode in an electrochemical system on which the reaction of interest is occurring, or in simpler terms, the experimental sample in most cases. The RE is a half cell with a steady and well-known reduction potential, and it is used as the main point of reference in the electrochemical cell for the voltage control and measurement. Its only task is to act as reference when applying the potential at the WE. Additionally, the current flow through the RE should be kept close to zero which is accomplished by using the CE to close the current circuit. The counter electrode (sometimes called auxiliary electrode), is usually made of an inert material like Pt, Au, or glassy carbon, as it must not participate in any reactions within the voltage range of interest. The CE's main role is to collect all the current needed to balance the current observed at the WE.

By introducing a third electrode into the system, an experimenter can monitor the current between the WE and the CE, and the voltage between the RE and the WE. This is incredibly useful because the potential at the CE will constantly shift to generate the current demanded by the WE. By this three-electrode method, any measured current can be attributed to reactions at the WE, as the RE has no current flowing through it. Finally, provided that the RE maintains a constant and known potential of its own, the potential applied between the WE and RE can be set to an 'absolute' potential on an arbitrary scale. Referring back to the four leads common to most potentiostat systems, the WE will be attached to one lead of each of pair, which connects it to both the current supply loop and the voltage probe loop. The RE is connected to the other end of the voltage probe, while the CE will be attached to the current loop. Thus, cell current runs between two electrodes and the voltage is set between two electrodes, with the two loops sharing one electrode in common (the WE).

Most potentiostats can be operated in two ways: either by controlling the potential at the WE or by controlling current flow. In controlled-current mode, one pair of potentiostat leads holds a current while the other pair is used to measure the potential exhibited at the WE. When operated in a more commonly used controlled potential mode, the equipment uses the measurement from the voltage probe pair as a sort of feedback loop. Essentially, at any given point in a voltammetry experiment, the potentiostat compares the measured cell voltage with the desired voltage and appropriately drives an amount of current into the cell to force the voltages to be the same. This allows the device to either maintain a constant potential setpoint, or to precisely conduct dynamic potential sequences such as sweeps, steps, cycles, or other waveforms.[169]

3.1.1.2 Reference Electrodes and Redox Potentials

In three electrode electrochemistry, the reference electrode is key component of the system. The primary requirement of the RE is that its potential be stable throughout any electrochemical experiment. In brief, this means that the ionic concentration of species involved at RE must be held constant. The most common method to achieving this is to use a RE involving a half-cell reaction redox system with saturated concentrations of the participants of the redox reaction at the electrode. A redox reaction simply means reduction or oxidation (hence, redox for short), that is, any reaction that requires an electron transfer to proceed. In other words, one side of a redox reaction will have the species in its oxidized form, and the other will have the same species in its reduced form. Any electrochemical reaction must necessarily have an equilibrium reaction potential. The value of the potentials for redox reactions are known as redox potentials or standard potentials (when given standard pressure and temperature). In brief, redox potentials are a measure of the propensity for a chemical species to either oxidize or reduce. Each redox reaction of each species exhibits an intrinsic redox potential, and more positive redox potentials indicate a high affinity for electrons, meaning the species tends to be reduced. Noble metal species, such as Pt, exhibit high redox potentials and thus are difficult to oxidize. Various redox potentials for a range of metal systems are provided in Figure 7.

Rather than using an absolute scale for standard redox potentials for any given half reaction, instead they must be compared to each other for relevance. To give a real-world metaphor, in the realm of geography, redox potentials can be compared to values of ‘sea level’ where there is no intrinsic origin point to measure from. Instead, some

arbitrary zero point is collectively decided on to which all other values can be compared. The RE which sets the basis for the thermodynamic scale of oxidation-reduction potentials is known as the standard hydrogen electrode (SHE). The SHE's standard redox potential, that is, the potential for the reaction $2H^+ + 2e^- \rightleftharpoons H_2$ is arbitrarily declared to be 0.0 volts (at standard temperature and pressure). However, SHEs are seldom used in actual electrochemical three electrode systems because they are more problematic to prepare. Firstly, the redox reaction occurs at a platinum surface which has to be specially treated by preliminary electrolysis. Secondly, there is need for storage and supply of hydrogen gas, which makes using SHEs somewhat unwieldy and hazardous.

Reaction	Equilibrium Potential (V)
$Au^{+} + e^{-} \leftrightarrow Au$	1.692
$Pt^{2+} + 2e^{-} \leftrightarrow Pt$	1.18
$Pd^{2+} + 2e^{-} \leftrightarrow Pd$	0.951
$Ag^{+} + e^{-} \leftrightarrow Ag$	0.7996
$Rh^{3+} + 3e^{-} \leftrightarrow Rh$	0.758
$Ru^{2+} + 2e^{-} \leftrightarrow Ru$	0.455
$Cu^{2+} + 2e^{-} \leftrightarrow Cu$	0.3419
$Ru^{3+} + 3e^{-} \leftrightarrow Ru$	0.2487
$2H^{+} + 2e^{-} \leftrightarrow H_2$	0.00
$Pb^{2+} + 2e^{-} \leftrightarrow Pb$	-0.13
$Ni^{2+} + 2e^{-} \leftrightarrow Ni$	-0.257
$Co^{2+} + 2e^{-} \leftrightarrow Co$	-0.28
$Cr^{3+} + 3e^{-} \leftrightarrow Cr$	-0.7
$Zn^{2+} + 2e^{-} \leftrightarrow Zn$	-0.7618
$Cr^{2+} + 2e^{-} \leftrightarrow Cr$	-0.913
$Ti^{2+} + 2e^{-} \leftrightarrow Ti$	-1.6
$Al^{3+} + 3e^{-} \leftrightarrow Al$	-1.662
$Ce^{3+} + 3e^{-} \leftrightarrow Ce$	-2.336
$Li^{+} + e^{-} \leftrightarrow Li$	-3.04

Figure 7: Selected standard reduction potentials.[170]

One reference electrode that is in fact commonly used in practical electrochemistry is the silver-silver chloride (Ag/AgCl) electrode, which is the RE used throughout this work. This electrode usually takes the form of a piece of silver wire coated with AgCl. The coating is most commonly done by placing the silver in an electrolytic cell containing HCl and running and oxidizing current through it. Ag^{+} ions combine with Cl^{-} ions in solution ions as fast as they are formed at the silver surface. The wire can then be stored in a KCl or NaCl solution of known concentrations (usually

saturated). It is important to note that a good RE must be robust and not contaminate the electrolyte. In Ag/AgCl reference electrodes, the silver chloride film is insoluble, making it both very durable and stable in most cases. As aforementioned, reference electrode stability is crucially important to electrochemical measurements so that the potential measured at the WE can be recorded with certainty, especially for long-term or high precision experiments. Using a AgCl coated Ag wire alone would not be a suitable RE over time because, despite no current flowing through it, being in direct contact with the electrolyte can alter the composition of the RE, affecting the reference point and throwing off any potential measurements in the long run. It is important to ensure that the half-cell maintains its potential value while keeping those same conditions throughout experimentation.

In order to employ Ag/AgCl in a way so that it does not contact the electrolyte directly but still completing the circuit to the WE, some sort of barrier must be installed. This barrier must allow ionic transport but prevent mass flow of the electrolyte to the RE surface. This is most often done using porous frits, usually made of materials such as porous silica (Vycor), or other porous plastic or porous ceramic materials, depending on the specifics of the electrolyte in use. This way, the Ag/AgCl electrode can be placed in a NaCl or KCL solution of known concentration (usually saturated) in order to keep its redox potential stable while remaining in electrical contact with the WE. It's worth noting that ions associated with Ag/AgCl equilibrium, such as Cl^-, can still contaminate the electrolyte if the RE is not properly maintained.

The last major potential problem area regarding the reference electrode might arise due to electrolyte solution resistivity. Firstly, this can be mitigated by ensuring a

sufficient amount of non-reactive ionic species in the solution to allow for charge transport through the electrolyte. Additionally, a so-called Luggin capillary can also be employed to offer a more direct conductive path. The capillary is essentially a tube in the cell that shortens the average path between the RE and the WE, resulting in a sensing point close to the WE.

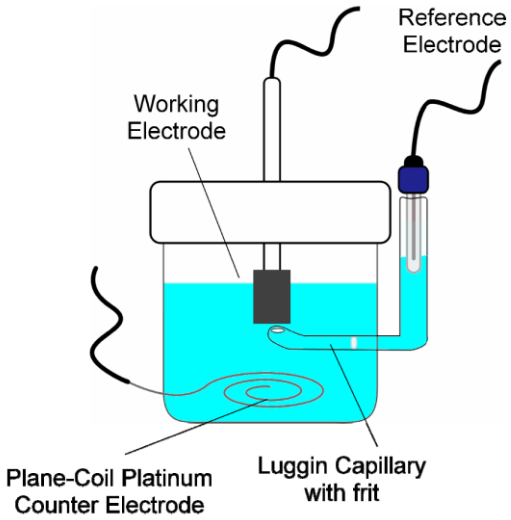

Figure 8: Illustration of electrochemical cell geometry employed. Adapted from [171]

3.1.1.3 Nernst Potential and Overpotentials

As explained in the previous section, any reaction involving an electron transfer must exhibit an equilibrium reaction potential, called the standard redox potential. In practice, the thermodynamically predicted equilibrium potential is actually the standard redox potential modified by temperature and concentrations of reactant and product. This is given by the Nernst equation:

$$E_{eq} = E_0 - \frac{RT}{nF} \ln \frac{a_{Red}}{a_{Ox}}$$

Where E_{eq} is the Nernst equilibrium potential, E_0 is the standard redox potential, R is the universal gas constant, T is the temperature (K), n is the number of electrons exchanged per reaction, F is Faraday's constant, a_{Red} and a_{Ox} are activities of reduced and oxidized forms of the species in question, respectively. The Nernst potential for any given ionic species is the thermodynamically determined potential at which the species are in equilibrium and there is no net ion movement. This can also be referred to as the equilibrium potential, such that chemical and electrical gradients are equal and opposite in direction.

Further, redox reactions actually require some additional energy past the Nernst potential before the reactions are experimentally observed. In order for a potential to be reducing for a given species, it must be at sufficiently lower value than the desired species' Nernst potential. Likewise, an oxidation potential must be sufficiently above the Nernst potential before oxidation can take place. In electrochemistry, this additional amount of energy required is call the overpotential, which arises due to kinetic hindrances inherent to any given redox reaction. This can be represented by:

$$\eta = |E_{observed} - E_{eq}|$$

Where η is the overpotential, $E_{observed}$ is the experimentally observed potential, and E_{eq} is the equilibrium Nernst potential.

3.1.2 Electrodeposition Methods

3.1.2.1 Electrolytic Deposition

Deposition of a material film by passing a current through an electrochemical cell using an external source is called electrolytic deposition, or more colloquially, electroplating. Most commonly, metal cations are dissolved in the electrolyte solution and a reducing potential is applied to the cell, forcing the ions to reduce into a zero-valent metal on the electrode surface, provided that the external potential surpasses the overpotential required. Electroplating can also occur by applying an oxidizing potential, which can deposit conductive metal oxides instead of metallic surfaces, called anodic electrodeposition. All electrolytic deposition done in this work is that of cathodic reduction of cations to metal.

Electrodeposition methods have been used for more than a century, largely due to their ease of implementation and high level of experimental versatility. There are many reasons why these techniques are still widely used in current research. Firstly, film thickness and morphology can be well manipulated because these properties are dependent on numerous experimental factors that can be controlled, such as electrolyte composition and potentials used. The uses of various electrode shapes and structures also be implemented easily to alter the resultant structure of the electrodeposited film. Most importantly though, electrodeposition experiments can typically be easily performed without a need for sophisticated equipment, vacuum environment, or high reaction temperatures.

As with many types of synthesis, deposited film growth can be described through nucleation and growth kinetics. With electrochemical methods, this is largely governed

by the level of current flowing through the electrochemical cell. Since the reactions observed are based on the transfer of electrons, ensuing electrochemical currents are directly proportional to reaction rates. Higher reaction rates mean more cations reducing, which means a faster rate of film growth. Higher reaction rates can be achieved either with higher ion concentration or by more applying more reducing potentials - providing more energy to drive the reaction. It follows that by controlling the voltage applied and ion concentration, a high level of precision is offered when it comes to the properties of electrodeposited films.

In addition to thickness, growth morphology is also affected by electrodeposition rates. For example, high reaction currents can cause the area closest to the electrode surface to become depleted of the dissolved cationic species being electroplated. This region in the electrolyte is sometimes referred to as an electrochemical depletion region or depletion zone. Continuing electrodeposition cannot occur until more cations in solution move close enough to the electrode in order to be reduced onto the surface. This means the reaction has become diffusion-limited, such that the reaction is now dependent on the movement of cations in the electrolyte, either due to induced electric fields or by normal Fickian diffusion. When electrodeposition becomes diffusion limited, the encroaching cations will preferentially begin to reduce at the outermost protrusions of the already grown film, eventually leading to the formation of dendrite-like structures. Considering one of the typical goals of electroplating is the synthesis of homogenous films, this can clearly be problematic.

The most evident solution to mitigating dendrite growth would be to slow the growth rate, and hence the creation of the depletion zone, by decreasing the potential

applied. However, this solution introduces several problems, which boils down to the fact that a depletion zone will occur eventually no matter the deposition rate. Instead, a simple modification in the electrodeposition process is that of pulse electroplating. This is process where the applied potential can be alternated between two different voltages in a series of pulses. One voltage can represent a deposition period, where the plating reaction will proceed. The other voltage is a relaxation period, where the potential is not reducing enough to drive the reaction, allowing active cations to diffuse close to the electrode and eliminate the depletion zone before depositing again. While pulsed-deposited films are often void of dendritic morphologies, they may exhibit smaller grain size or more porous structures. Pulse electrodeposition introduces even more variables to manipulate, and by changing the pulse amplitude and time, the deposited film's properties will be altered.

There are other solutions to avoiding electrolytic dendrite growth. One is to slowing the reaction's charge-transfer kinetics enough so that cation diffusion can keep up. This relies on the use of complexing agents in the electrolyte. Another alternative is to force cation movement through convection in addition to diffusion. This involves agitation of the bath solution using a stirring mechanism or rotating electrode to bring cations to the surface at a much higher rate.

3.1.2.2 Electroless Deposition

Contrary to electrolytic deposition, electroless deposition is a process which places a deposit metal on a surface without the use of an induced electric current. Electroless methods largely avoid depletion zone issues, allowing a more consistent cation concentration to deposit evenly on an electrode surface - even on edges, inside

pores, or other surface irregularities. Electroless plating can even be used to deposit a conductive surface on a nonconductive material.

Electroless techniques rely on some alternative driving force to induce a charge transfer needed to reduce cationic species to metallic species. In some cases, this is done through a reducing agent, such as formaldehyde or with hydrogen gas. These additives are often easily oxidized, meaning spare electrons can be generated and transferred to the cations, resulting in their reduction onto the electrode surface. Another option is to place a precursor metal on the electrode. This precursor layer effectively functions as a reducing agent, but has an additional the advantage of being confined to the surface in a recognized quantity. This layer is considered a ‘sacrifice’ because its role is to be replaced by a more easily reduced metal, in a process called galvanic replacement. Methods that rely on galvanic replacement reactions are limited to certain electrolyte-substrate systems in that they rely on the standard redox potentials of the species involved. Because it is an electroless method, no external voltage is applied and the driving force for the reduction can be equated as the difference between the redox potentials of precursor metal and the replacer. In order for the replacement reaction to proceed, the redox potential difference must be a negative value, so the selection of this sacrificial metal will depend on the desired metal to be plated. This difference in potentials must also be large enough to thermodynamically overcome any kinetic barriers to the process.

3.1.2.2 Underpotential Deposition

Underpotential deposition (UPD) is similar to electrolytic deposition in that it requires an externally applied potential to entice metal cations to reduce onto an electrode surface. Unlike electrolytic deposition however, UPD is a deposition reaction that takes place at a *more positive potential* with respect to the Nernst thermodynamic prediction for that species. While the name 'underpotential deposition' may initially seem counter-intuitive considering UPD occurs at more positive potentials than thermodynamically expected, it is given that name because it marks a contrast with the typical overpotentials required for cation reduction. Because reduction is an cathodic process, an applied potential *lower* than the Nernst potential is usually required in order to surpass the kinetics barrier and create a driving force. However, in the case of UPD, a reducing reaction occurs even when the applied potential sits above the Nernst potential. Thus, the level of overpotential required is less than or 'underneath' what is usually required for the deposition reaction.

The UPD phenomenon arises in cases where one material *A* is electrochemically deposited on a second material *B*. In short, UPD occurs due to a difference in which the electrodeposition energy required to nucleate *A* on a *B* is less than what is required to deposit *A* on itself. This leads to an situation where the energy applied to the system can be specified directly between these the UPD and bulk activation thresholds for material *A*, and all exposed *B*-sites at the solid-electrolyte interface will be covered with nucleated material *A*. The resulting *A* surface is then called a monolayer, due to the outer layer being one atom thick. This monolayer is self-limiting and can grow no further than a single atom, unless the energy supplied to the system increases past the bulk deposition

threshold activation energy, which would allow *A* to continue reducing on itself. This works well practically, as most potentiostat systems are well-suited to exploiting UPD in this way, allowing precise application of voltages to grow the UPD monolayers but not any following multilayers. It follows that UPD cannot be performed on top of itself. Thus, UPD is in the incredibly useful position of being a self-limiting electrochemical technique, where only a monolayer of a deposited layer or less is formed.[172, 173] The utility of UPD allows for a controlled degree of coverage of an adsorbate metal on the substrate surface. The theory behind the existence of UPD phenomena is still not fully understood, especially when it comes to nanoscale surfaces. For the last two decades, research into applications and theory of metal UPD has been spearheaded by Leiva *et al.*[172-175] There are many components that contribute to the properties of UPD, including surface composition, nanoparticle size, and anion co-adsorption. Several bimetallic systems do not exhibit UPD behavior at all, while others may evidence multiple UPD features.

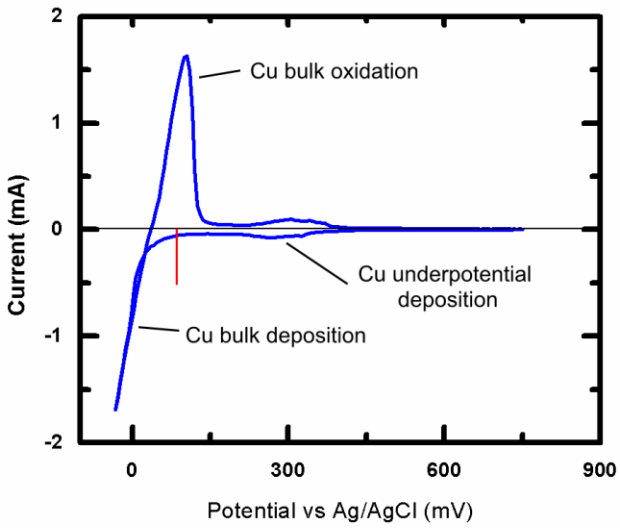

Figure 9: A cyclic voltammogram showcasing Cu UPD relative to Cu bulk deposition. The red line is an estimate of the Nernst potential for the $Cu^{2+} + 2e^- \rightleftharpoons Cu(s)$ system.

Due to this, the primary obstacle to the application of UPD is that the phenomenon is limited to certain bimetallic systems in which the depositing metal exhibits a UPD feature on the underlying metal. In many cases this means the deposition of a less noble metal on top of a nobler one. For the synthesis of catalysis nanostructures, this is the inverse of what is usually desired. Electroless galvanic replacement comes in handy here, such that UPD-deposited monolayer can be placed in a solution with a nobler cation, leading to a reduction of the cation and simultaneous oxidation of the UPD layer. Essentially, the UPD-grown can act as a 'sacrificial' monolayer for the cathodic reduction of one monolayer of a more noble metal to be grown. After galvanic replacement, it is possible to perform a successive use of UPD on the surface, followed by a second galvanic replacement, and so on. In this manner, the repeated substitution of a sacrificial UPD monolayer by a desired noble metal allows a film to be grown with atomic-scale precision. This iterative layer-by-layer growth technique has been called surface limited redox replacement (SLRR) among other acronyms, including electrochemical atomic layer deposition (E-ALD). This synthesis method is used extensively in this work, and is further detailed later in section 3.3.

3.1.3 Linear Sweep and Cyclic Voltammetry

3.1.3.1 Overview and Characterization

Some of the most fundamental electrochemical analysis techniques include potentiodynamic methods performed in a three electrode cell where an applied voltage is

varied in a linear fashion, referred to as a ‘sweep’. By sweeping the applied potential exhibited on the working electrode surface, a resulting current flow can be measured and analyzed, where any changes dues to oxidation or reduction (redox) reactions can be attributed to the working electrode sample. The most simple potentiodynamic experiment of this type is linear sweep voltammetry (LSV), where the potential is swept linearly in time from a set starting potential to a set ending potential at a constant rate (V/s). Cyclic voltammetry (CV), then, is essentially a repeated linear sweep and its reverse sweep in a cyclic manner, and can be repeated as many times as desired.[176, 177] Fundamentally, when a potentiostat moves a potential setpoint in liquid electrolyte, it must also continually flow some current to achieve the desired potential at the specified rate. CV is measured as a plot of resulting current vs set potential, noting that potential windows devoid of electrochemical reactions will exhibit slopes of zero. When a potential sweep reaches a voltage value where a chemical redox reaction occurs, charge accumulates on the working electrode surface and the potentiostat must change the current flow to accommodate the now-activated reaction but maintain the potential sweep rate. The resulting current due to the reaction is then measured as a function of potential in a plot called a voltammogram, where the current is proportional to the amount of reaction occurring. CV, as implied by its name, will progress with both a rising potential sweep and a falling potential sweep in a cyclic manner, showcasing both oxidation and reduction reactions exhibited in the electrochemical cell. By convention, positive currents correspond to oxidation reactions and negative currents correspond to reduction reactions.

There are a handful of different kinds of reactions that can be measured utilizing CV. For example, if O_2 gas is dissolved in electrolyte, CV can be used to measure its reduction. For acidic electrolytes, depending on the working electrode surface, the adsorption/desorption of H^+ ions can be measured at certain potential ranges. If a potential applied to the system is too high or too low, a current will result from the breakdown of the electrolyte itself. And of course as described in the previous section, CV is often used to measure the redox behavior of redox-active species like metals or metal oxides. Due to its cyclic nature, CV experiments can examine both the oxidation and reduction reactions for a redox system as a pair, as long as a given reaction is reversible. For fully reversible reactions, an oxidation reaction will occur along the positive potential sweep, a reduction reaction will occur at near the same potential on the negative going sweep, and the ratio of peak currents for the two reactions ideally should be 1. Sometimes, however, a redox reaction pair exhibits altered behavior in CV where the oxidation and reduction reactions occur at significantly different potentials on their respective sweeps, or that forward:reverse current ratio is not unity. This type of system is known as quasi-reversible, and can indicate that there is some kinetic barrier for one or both of the reactions.

The usual sweep rates used in CV range from about a minimum of 2 mV/s to 100 mV/s. Changes in potential sweep rates will alter the voltammogram shapes achieved, and can be used in various ways to analyze the reactions and/or electrode surface. Slower rates allow for more time for a reaction to progress, resulting in better resolved peak structures. Faster sweeps allow a potential range to be scanned through while minimizing the total amount of reaction driven. By performing a series of experiments altering sweep

rate, rate-constants for the examined reaction can be determined. Additionally, by carefully selecting the sweep rate and potential range limits, the resulting oxidation or reduction peaks of the catalyst surface will vary in shape and potential position. For example, regarding the reduction of Pt surface oxides, the presence of PtOH, PtO_2 or PtOOH oxide species depend on the oxidizing potential reached at the CVs upper limit. Each of these species reduces at a different potential, which can be used to further analyze Pt-based electrodes.

However, while this type of experiment is commonly performed using CV methods, this work does not aim to examine the kinetics or mechanisms of the progressing reactions. Thus, the sweep rate used for the experiments reported here is always held at a constant 20 mV/s.

One of the most important uses of cyclic voltammetry is the ability to quantitatively characterize surface reactions. When a given reaction is known to be surface-restricted, such as adsorption reactions, the electrode surface area can be derived from the current seen in CV by calculating the total amount of charge through signal integration. In the case of Pt, estimation of surface area can be via hydrogen adsorption/desorption reactions (sometimes called “hydrogen waves”) which occur in the -0.2 - 0.0 V regions (vs. Ag/AgCl). Secondly, an estimation of Pt amount can be conducted by studying the Pt oxide reduction feature at 0.45 V. Further, if a working electrode surface area is already known, the current in CV can be used to calculate a surface coverage percentage. When it comes to the field of catalysis, these techniques are very useful when examining electrocatalytic surface area, adsorption features, and can even be done iteratively to investigate catalytic durability.

3.1.3.2 Accelerated Aging Tests

Potential cycling methods are also commonly used to analyze the durability of an electrode surface. These cycling methods, referred to as electrochemical durability tests, potential cycling tests, or accelerated aging tests (AAT), are typically performed by sweeping the potential applied at an electrode surface between two extremes repetitively - up to several thousands of cycles. There are many factors that come into play when it comes to designing the type of durability test that is going to be conducted. First and foremost, the cycling potential 'window' between the ends of the potential sweep needs to be noted along with the sweep rate of the cycling itself. The cycling window must also force some reaction to repeatedly activate in order to validate the electrode's durability. Generally speaking, larger potential window are more aggressive and damaging on the stability of a sample surface.

These sorts of tests can either involve repetitive activation of a reaction at the electrode surface such as O_2 reduction or H_2 adsorption/desorption, or the probe reaction can be the direct oxidation/reduction of the material itself. In the case of Pt-based catalysts, the suggested durability-test protocols established by the U.S. Department of Energy places the endpoint voltages around 0.7 V and 0.9 V (vs SHE), which is bracketing the onset of Pt oxide formation.[46] It is important to consider that for electrochemical durability tests, changes in surface area the result can arise not only from loss of electrode material, but also from surface reconstruction during reversible oxidation/reduction cycling.

Additional experimental protocols can also be employed during long term durability testing, by which the catalyst is examined for performance under conditions

emulating real fuel cell processes. For example, such tests can include a specific measurement for a catalytic reaction, such its current to focus on tracking performance loss over time.

3.1.3.3 Oxygen Reduction Reaction Probing

In addition to surface characterization and durability measurements, sweep voltammetry methods can be used to judge the actual performance of catalytic materials by measuring the relative activity towards the catalysis of the ORR. The voltammograms generated from types of experiments are sometimes referred to as 'polarization' curves. Recently, rotated disc electrode (RDE) methods are most often used to perform such experiments, but they rely on the ability to deposit or attach the desired catalyst onto the RDE (usually glassy carbon). Using RDE method allows for analysis of ORR kinetic data by varying the electrode rotation speed, and can ultimately determine reaction orders or activation energies, without mathematical modeling. [178]

However, relative comparisons of ORR reaction currents can also be made using non-rotating electrodes in typical electrochemical set ups. This is done by saturating an electrolyte such as H_2SO_4 with O_2 gas, followed by performing a linear sweep negatively from above the ORR potential to below it in order to examine the current which results when O_2 reduces to H_2O There are numerous ways the comparisons between LSV voltammograms probing the ORR can be made: 1.) by analyzing the difference in onset potentials of the ORR, 2.) by examining the potential where the ORR reaction current reaches its highest value, 3.) the highest slope of the voltammogram, or 4.) a comparison of the current at any decided potential on the ORR voltammogram. These four components are certainly not isolated features, so ideal analysis would examine the

voltammogram as a whole, considering each component concurrently. Finally, since reactions are proportional to catalyst surface area, any ORR currents measured must be normalized to the surface area of the sample electrode.[179, 180]

3.2 X-ray Spectroscopic Methods

X-ray spectroscopic methods are some of the best suited characterization tools in providing element-specific structural measurements for the numerous materials used in catalysis and other energy applications. The flexibility of various core-hole spectroscopies lend themselves well to gaining better understanding of relating energy states and atomic structure to surface properties. Deducing the fundamental mechanisms stemming from local electronic structure to ultimate electrochemical properties is a key potential area of knowledge that can be gathered from such spectroscopic experiments. Additionally, synchrotron-based spectroscopies provide even further advantages in these techniques, due to their energy tunability in acquiring high resolution element-specific information for local structures and characteristic atomic phenomenon.

Core-hole spectroscopies involve excitation of electrons that are not on the outer shell of an atom, known as core electrons, by a photon source. With these methods, element-specific signals are generated when the core electron absorbs the energy of incident X-rays, gets excited beyond the Fermi level, leaving behind an electron hole. Some techniques, like X-ray photoelectron spectroscopy, can be done using common monochromatic X-ray emission lines, such as Al or Cu Kα. With synchrotron-based sources, the incident photons can be tuned to a wide range of possible energies, and by

selecting the appropriate wavelength, electron transitions that are most relevant to the desired chemistry can be achieved.

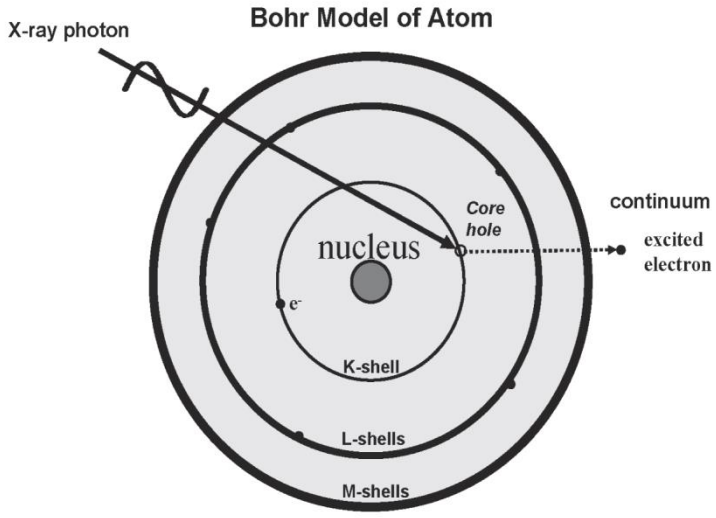

Figure 10: Schematic of a core electron absorbing the energy of an incident photon.[181]

3.2.1 X-ray Photoelectron Spectroscopy

3.2.1.1 XPS Technique Overview

X-ray photoelectron spectroscopy (XPS) is one of the main core-hole methods used for a multitude of research areas due to its elemental specificity, ease of implementation, as well as its high degree of surface sensitivity.[182] When incident X-rays come into contact with a sample, its electrons are transformed into an excited state within the bulk of the material. The majority of the excited electrons within the bulk interact with nearby atoms, and many are quickly relaxed back into core electronic states as electrons exhibit very short inelastic mean free paths (IMFP) in solid matter. However, core electrons from atoms near the top few nanometers of the sample surface can eject

themselves into the surrounding vacuum, allowing XPS to be a surface-sensitive technique, and the freed electrons subsequently head towards the XPS detector. These escaped electrons are referred to as photoelectrons - electrons freed from their original atomic states by interaction with incident photons.

While the incident stream of photons is monochromatic, electrons from several elements and many different atomic states will be excited simultaneously, resulting in photoelectrons with varying emission energies. XPS is element-sensitive, and these differing kinetic energies are what allow the XPS detector to distinguish between the different elements in the sample as well as different valencies of those elements. XPS detectors are curved with an electric field, such that electrons will impact the detector at different points depending on their kinetic energies. The system can measure the electrons' kinetic energies based on where they land and convert them to binding energies according to:

$$B.E. = h\nu - K.E. - WF$$

Where B.E is the binding energy, hν represents the incident photon energy, K.E. is the kinetic energy of the photoemitted electron, and WF denotes the energy needed to remove an electron from the sample to a point in the vacuum immediately outside the solid surface. The calculated binding energies represent the intrinsic energy securing a given core electron to an atomic nucleus. As each element has a unique nucleus, and each nucleus is surrounded by electrons in several energy levels, it is possible to study the photoemission spectrum of a specific electron at a particular energy level for a specific

element, such as the O 1s or the Pt 4f emission. The end result of XPS experimentation is a spectrum of overall photoelectron 'count' versus a binding energy scale. Values for the electron binding energies of pure elements are well known and recorded.

Importantly, characteristic binding energies will exhibit a variance in their values, often referred to as a 'shift', when said element is in a non-nominal valance state or participating in covalent bonding. For example, oxygen-bound electrons can exhibit many varying binding energies depending on the type of oxygen bond or the bonding coordination. Oxygen 1s electron binding energies are well recorded for molecular oxygen, atomic oxygen, and O^{2-} species in an oxide. However, it is important to recognize that formal charge is not the sole contributing factor to binding energy shifts. For example, electron binding energies in a Pt^{4+} ion will alter depending on the coordinating anions. Pt 4f electrons in H_2PtCl_6 and PtO_2, despite having a stoichiometric charge of 4+ in both compounds, will exhibit dissimilar binding energies relative to each other despite the same valence state.[183] These alterations stem from the differing electron interactions which depend on both individual bond strength, the number of total bonds, and bonding coordination. This type of change can also result from the ligand effect, which highlights the influence of a neighboring atom's electric field.

There is another way that binding energies can vary, distinguishable from oxidation state changes or bonding coordination. Known as a surface-core level shift, this phenomenon arises from immediate local geometric coordination and is generally well understood.[184] This alteration is what gives detail to binding energy deviations of near-surface atoms in a material when compared to bulk properties. Lower atomic coordination among surface atoms tend to exhibit lower binding energies for the

outermost layers of atoms, and in the case of ultrathin nanofilms, the entire shell may exhibit this type of shift. This shift is very subtle in nature, usually less than 1 eV in magnitude, but is very important to recognize when it comes to XPS research in the field of catalysis. As an example, surface core-level shifts have been shown to associate with a metal's *d* band and adsorption of reaction intermediates like CO.[128] For most bimetallic systems, the core-level shift is more complicated. In addition to normal surface effects, the system can be influenced by the interaction of a surface shell with its substrate material. Neighboring dissimilar atoms can cause a subtle transfer of electron density, which also affects the surface atoms' measured binding energies in addition to the normal surface-core and any ligand bonding effects.

Not only do XPS spectra qualitatively give information about the elements and valence states present on the surface of a sample, the data is also quantitative in nature, providing information about the percentage of elements present based on the number of photoelectrons counted from the sample elements. However, more often than not, quantitative analysis of XPS is relative instead of absolute, involving comparisons between several samples in a set. Relative quantitative measurement is also done through assessment of distinct photoemission peaks within the same spectra, relating peak size of one detected element to another to establish a comparative analysis. The best way to compare XPS intensities is through percentage atomic concentrations. That is, the ratio of the intensity of a particular photoemission to the total intensity of electrons in the measurement. Absolute quantitative analysis of XPS spectra is difficult due to varying characteristics of equipment, such as x-ray gun power output or vacuum conditions, and often requires the use of standard samples. Absolute peak intensities can change from

experiment to experiment, but all else being equal, should remain constant in relative terms. Furthermore, when it comes to layered samples with known architectures, quantitative analysis of peak-area ratios for multiple elements can provide information on the construction of the sample. For example, a Pt surface shell photoemissions can be compared to those of an underlying Au substrate, and thus indicate some idea of the shell thickness depending on the elemental photoemission ratio.

XPS experiments gain much more flexibility when performed at large scale synchrotron radiation facilities instead of traditional laboratory facilities. With a synchrotron light source, 'bunches' of relativistic electrons travel through a vacuum ring, passing through bending magnets and so-called 'insertion devices' to produce high intensity and flux photon beams. Insertion devices, such as wigglers and undulators, alter the relativistic electrons' paths through a series of dipole magnets, providing a wide array of energy ranges that can be utilized. Depending on the synchrotron facility and equipment, photon energies can be set down to UV wavelengths, which can then be filtered to desired incident energy through a monochromator. This is one of the greatest strengths of using a synchrotron source for XPS, the ability to tune incident photons' energies. By using low energy but high flux incident photons, resultant XPS spectra generated is even more sensitive to the sample surface due to smaller IMFPs of ionized electrons. Further, by performing experiments with a variety of incident photon energies, the atomic and electron state of a sample can be analyzed at more than one 'information depth'. By increasing the incident X-ray energy, energized electron IMFPs increase - meaning the sampling depth is increased, allowing a greater vertical slice of the sample to be studied. This is especially advantageous when analyzing samples with atomic-scale

surface shells, where careful selection of incident energies can be used to examine the shell and the core-shell boundary region.

3.2.1.2 XPS Data Analysis

After acquisition of sample data from XPS, analysis is performed often through peak-fitting. XPS spectra are largely quantified in terms of peak intensities and peak 'position' along a binding energy scale. The primary concept behind quantifying XPS data is that the count of electrons recorded is directly proportional to the number of atoms in any given state on the sample surface. As detailed in the previous section, photoemission intensities indicate the elements present at the surface, and the peak positions indicate the elemental and chemical composition of those elements. Peak fitting allows the experimenter to deconvolute and estimate the photoemissions of elements that exist in multiple valencies or oxidation states. Several dedicated XPS fitting programs are available, allowing a fit of calculated photoemission spectra to experimental data. However, if treated as a 'black-box' tool, XPS peak fitting will almost always yield incorrect results. Without careful construction involving parameter constraints, the resulting fit, regardless of how accurately it mathematically represents the data, may be of no meaning from a physical perspective. The problem is that a good fit is always achieved when optimized without restrictions.

In order to have actual physical meaning, peak-fitting procedures must be done with proper constraints. These constraints usually originate from knowledge of the sample being examined, and knowing what photoemissions and shifts to those emissions to expect. Understanding potential sample chemistries is of clear importance, as it can suggest which chemical states may be present and how many sub-peaks can constitute an

overall photoemission as well as relative intensities. Other parameter constraints to consider include peak widths, usually measured as the full-width at half-maximum, or FWHM. This is a useful indicator of chemical state changes and physical influences, such that broadening of a peak can indicate a change bonding nature contributing to a peak shape. In cases where XPS analysis of multiple chemical states is being performed, theoretical values of peak width, known area ratios, and relative position to each other. Additionally, many photoemissions exhibit a doublet resulting from spin-orbit coupling.[185] This coupling arises from the difference in angular momentum component between two electrons at the same energy level. The split energy levels will each have a different binding energy associated with it as well as a known area ratio, which can be used in proper fitting analysis.

Not all peaks in an XPS spectrum are due to simple photoelectric transitions. Secondary peaks may appear from other phenomena, most likely due to Auger transitions. Auger photoemissions are generated through a process by which electrons with characteristic energies are ejected from an atom in response to a downward transition by another electron. Auger peaks are usually ignored in XPS analysis, but in the case where Auger emission occurs at the same energy as the photoelectrons being studied for XPS, it can be problematic. The usual step-arounds for Auger emissions is to use another characteristic photoemission of the desired element being examined, or to use another energy source to change the kinetic energy of photoemissions - noting that Auger electrons always have the same energy regardless of source. Another difficulty that can arise during XPS analysis is due to charging of the sample surface.[186] XPS relies on electrons leaving the sample and unless emitted electrons are quickly replaced, the

sample will exhibit a subsequent charging effect. This results in the measured binding energies shifting due photoemission interaction with the surface electric field arising from the amassed charge. If the samples are conducting and electrically connected to the instrument, charge balance is easily restored. But for other more insulating materials, emitted electrons must then be replaced via an external source. One common way to achieve this is through the use of charge neutralization methods such as an electron flood gun. The purpose of flood guns is to provide a steady state electrical environment. Sometimes such methods are not easily available, and then charging effects must be accounted for in peak analysis.

3.2.2 X-ray Absorption Spectroscopy

The local atomic structure around a given atom can be investigated using X-ray absorption. This occurs when an atom acquires energy from an incident X-ray in order to excite electrons into higher unoccupied electron orbitals. A subsequent relaxation process occurs with the release of energy as an electron transitions from a higher-energy electron orbital to fill the leftover core-hole. The transition of an electron is accompanied by a release of energy, often in the form of fluorescence radiation. The energy above which a given electron transition is excited is known as an absorption edge.[181]

X-ray absorption spectroscopy (XAS) is a synchrotron-based technique that uses a tunable X-ray source to allow element-specific examination of chosen electron transitions.[187] In XAS, a monochromator sweeps incident photons from below a electron's absorption edge to above it, discerning the amount of electron transitions available in that material. This information can then be analyzed to deduce a number of details about a material, such as atomic structure or electron behavior. Therefore, XAS

can be used to probe various transitions across a range of excitation energies for the elements in a material. This gives the technique a component of element-specificity much like XPS.

XAS experiments are conducted in one of three modes: transmission mode, fluorescence mode, or via electron yield. When using a partial electron yield detector, one can selectively reject photoelectrons below a specified kinetic energy threshold. This allows the experimenter to eliminate a large portion of unwanted signal and preferentially measure a subset of the photoemission spectrum when desired.[188] In fluorescence mode, a detector is placed near a sample to measure the signal arising from fluorescing photons resulting from electron excitation. In transmission mode, the absorption spectrum is calculated by measuring the magnitude of a photon signal traveling through a sample and normalizing to incident signal originally present. Clearly, this mode of experiment imposes a limit on the overall thickness of a sample, considering a photon source must be able to be measured on the opposite end of the incident photon beam. This set up is best described by the Beer-Lambert Law:

$$I = I_o e^{\frac{-\alpha}{\mu}}$$

Where (I_o) is original intensity, (I) is transmitted intensity, (μ) denotes the absorption length, and (α) denotes the path length. From this, it can be seen that a single 'absorption length' is defined as the material distance required for the intensity of an incident beam to drop to 1/e of its original intensity, or about 37%.

XAS is a versatile technique in that all forms of XAS benefit from a wide selection of possible detectors to be employed. When done in vacuum, absorption measurements can be done by tracking the electron yield emitted or by tracking the photon signal emitted through excitation-fluorescence mechanisms. Other types of detectors include semiconductor-based solid state devices such as PIPS detectors, multi-element fluorescence detectors, or transmission detectors in the form of ionization chambers.

The absorption signal measured against the source X-ray energy constitutes two main data regions: the X-ray absorption near edge structure (XANES) and extended X-ray absorption fine structure (EXAFS) spectrum. XANES analysis was not used for this work.

3.2.3 Extended X-ray Absorption Fine Structure

Extended X-ray absorption fine structure (EXAFS) is one of the methods that can be used to analyze X-ray absorption spectrum. By gathering the transmitted signal hundreds of eV above an absorption edge, atomic structure information can be gleaned. The key components of EXAFS are the oscillations which the spectra exhibit in the region past the absorption edge – sometimes called the absorption ‘tail’. These oscillations are induced by interfering photoelectron waves arising from the material’s crystal structure. Analysis of this oscillating tail is performed by using Fourier transformation methods, which must be preceded by a series of normalization steps.

Before discussing experimental analysis of an EXAFS spectrum, it is necessary to discuss the physics that govern it. EXAFS is a specialized XAS technique, meaning an

electron absorbs energy from an incident photon and is subsequently shot into the continuum. This photoelectron can be described as a spherical wave propagating outward from an absorber atom. This photoelectron wave is then scattered from the neighboring atoms surrounding the absorber atom, such that the scattered wave and original outgoing wave now collide and interfere with each other. The type of interference that results depends on the energy (i.e. wavelength) of the photoelectron as well as the distance between atoms. If the outgoing and scattered waves are in phase with each other, then the interference is constructive. If the two colliding waves are out of phase, then the interference is destructive. Thus, the phase difference between the interacting electron waves will vary between constructive (in phase) and destructive inference (out of phase) as the energy of the electron is increased.

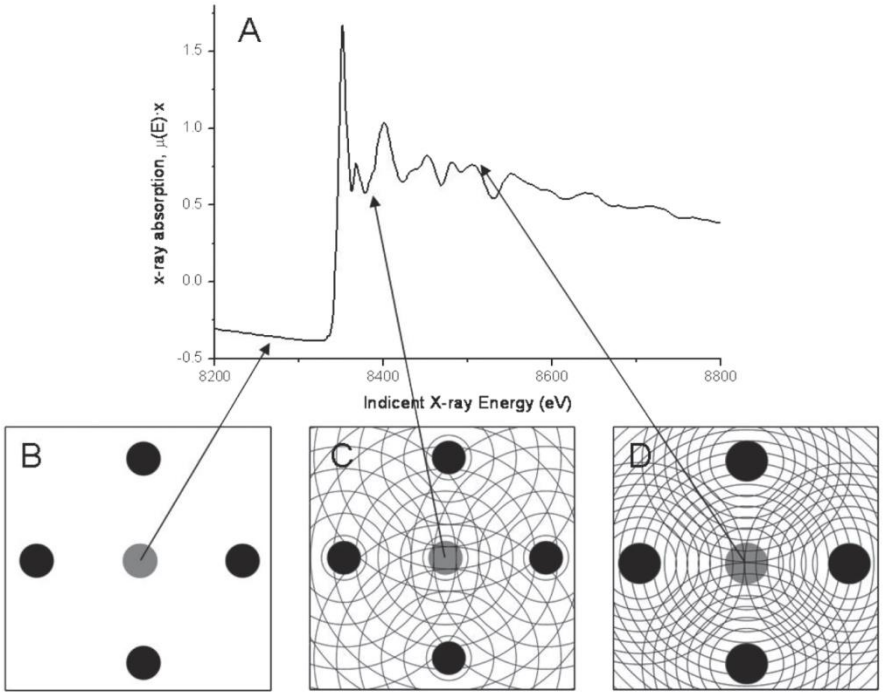

Figure 11: Example illustration of EXAFS spectra. A.) Nickel K-edge X-ray absorption spectrum example. (B-D.) Nickel absorber atom (gray) and four neighboring oxygen

scattering atoms (black). The crests of photoelectron waves produced by X-ray absorption are shown as concentric circles. B.) At X-ray energies below the absorption edge no photoelectron is produced. C.) A relative oscillatory minimum in the EXAFS spectra due to out of phase electron waves. D.) C.) A relative oscillatory maximum in the EXAFS spectra due to in phase electron waves.[181]

The type of interference is important because the relative phase affects the probability for X-ray absorption by the absorber atom. If the waves are out of phase, a relative minimum in absorption occurs which causes a drop in the oscillatory part EXAFS spectrum. If the waves are in phase, a relative maximum is exhibited instead. When an EXAFS experiment is being performed, the energy of the photoelectron increases (wavelength decreases), but of course the atomic bond distance in the absorbing material remains unchanged. This will alter the interference that results, and the colliding waves will progressively fall in and out of phase as the energy of the photoelectron is increased. This is what causes the oscillations seen in the EXAFS spectrum.

In summary, the sum of the outgoing photoelectron waves and the scattered waves at absorber atoms oscillate with a periodicity that is dependent on electron energies and the bond distances present in the sample material. Because an experimenter knows the experimental electron energy contribution to the oscillations already, it is possible to unearth information about the bond distance contribution to the oscillations through careful spectra analysis. It's worth noting the EXAFS oscillations only occur for elements with neighboring atoms, so in the absence of coordinated atoms, EXAFS oscillations are absent.

The EXAFS spectrum can be understood in terms of the EXAFS equation, which can be written in terms of a sum of the contribution from all scattering paths of the photoelectron. The EXAFS equation can be given as follows:

$$\chi(k) = \sum_{shells} \frac{n_x \cdot s_0^2 \cdot f_x(k) \cdot e^{-2k^2a^2}}{k \cdot r^2} \sin(2kr + a(k))$$

With the total absorption (χ) as a function of shell population (n_x), amplitude reduction factor (S_o), backscattering amplitude function (f_X), Debye-Waller term, interatomic distance (r), and phase shift (α).[187, 189]

EXAFS processing starts by normalizing the magnitude of the absorption edge-step to one, which accounts for sample to sample variation in the amount of material present and removes it from experimental consideration. Then, the pre- and post-edge regions of the absorption spectra are fitted with a background line and subtracted from the raw data. After normalization background signals from the experimental data, the structure-induced oscillations can be isolated and converted to k-space and subsequently Fourier transformed to a real space probability function. This final real-space plot gives information on the atomic bond lengths present in the sample. At this point, the real-space EXAFS data can be fitted using calculated distribution functions based on model crystal structures, allowing qualitative and quantitative conclusions to be drawn. By rigorous calculation of several hypothetical models and fitting to the data, the finer details of the crystal structures in the sample can be established. Through this type of analysis, information such as crystallinity and nearest-neighbor distance can be derived. This entire process is generally performed using a data processing suite such as ATHENA.[190]

After this step, a goodness-of-fit χ^2 test can be conducted to quantify the accuracy of the data treatment process employed.

3.3 Sample Synthesis

3.3.1 Surface-Limited Redox Replacement

Surface limited redox replacement involves the repeated process of electrodeposition of one sacrificial atomic monolayer, oftentimes via underpotential deposition (UPD) [172, 191-193] and its replacement by a second element via redox galvanic replacement.

The combination of UPD exploitation with galvanic replacement of the UPD-grown layer allows for the synthesis of pure metal films with high degree of atomic-scale precision. This technique, called surface limited redox replacement (SLRR) or sometimes electrochemical atomic layer deposition (E-ALD), first grows a monolayer of *A* on a substrate *B* via UPD methods, but then goes further to remove the *A*-monolayer through a replacement process. This in turn causes a deposit of a third material, *C*, to deposit on the surface. The process in full can then be repeated iteratively, resulting in a film of pure *C* material grown on top of the *B* substrate with a well-controlled level of thickness. Brankovic *et al.* were some of the first to deposit of single MLs of Pt and Pd through the use of SLRR.[194] Initial attempts at SLRR often used Pb and Cu as the so-called 'sacrificial' '*A*' material, due to the ease of which single UPD monolayers can be formed from simple electrodeposition baths of these metals.[193]

The driving force of the galvanic replacement reaction between two metals in the same system can be considered as the difference between their redox potentials. In the

case of SLRR, the redox potential of the sacrificial metal expresses the potential at which that layer will dissolve. The redox potential of the desired metal to be deposited, which for catalysis purposes is often Pt^{4+} or another noble metal ion, defines the potential at which that metal will galvanically reduce onto the substrate surface. Accordingly, when two such metals are placed in the same electro chemical system, the galvanic replacement reaction will take place with respect to their redox potentials. A metal with the more positive potential will preferentially be reduced and replace a metal with the lower redox potential, which will then oxidize and dissolve into solution.

Enactment of SLRR involves two ionic metal solutions, the first of which is used to underpotentially deposit the sacrificial metal layer, and the second to house the replacing layer of the desired noble metal. There is a range of experimental setups that can be used to carry out SLRR fabrication. For example, the substrate electrode could be manually moved from the UPD depositing solution to the second in an iterative manner. Conversely, a flow cell arrangement could be used where the working electrode remains stationary and the different ionic solutions are sequentially flowed past the electrode surface.[195] Flow-cell arrangements utilize a series of pumps to flow the requisite solutions in an automated manner, in addition to a rinsing bath to prevent cross-contamination between the UPD and galvanic reactions. This type of setup is especially convenient for large-scale growth of films via SLRR, as dozens of iterations of layer deposition and replacement can more easily be automated. However, manual operation of SLRR allows for a higher level of control regarding solution composition, given the potential of less dilution by avoiding the use of a rinsing solution in between steps.

Clearly, the major disadvantage would be that electrode switching is done by hand, limiting the number of layers which can be grown.

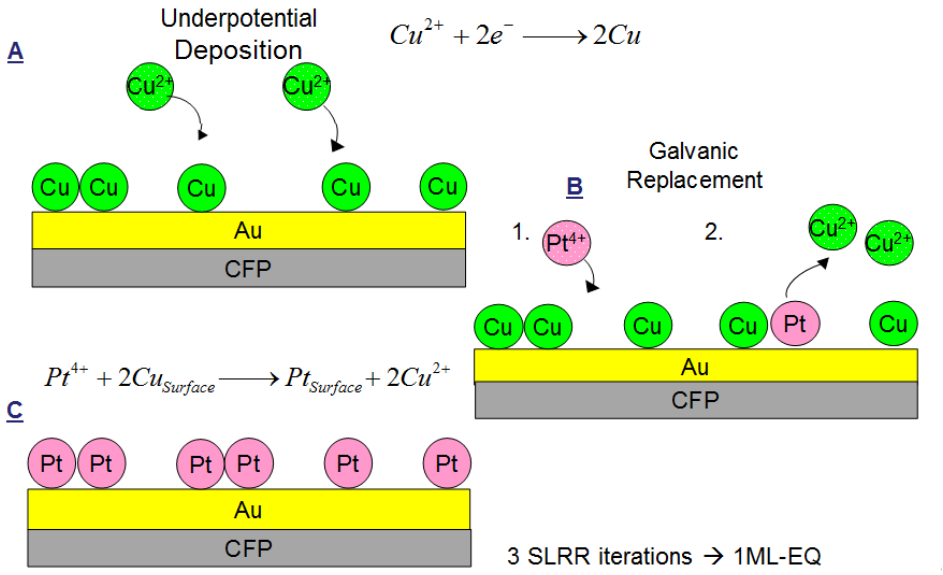

Figure 12: Schematic of surface limited redox replacement.

A notable element for SLRR techniques was discovered by Weaver *et al.*,[196] where film epitaxy and wetting could be improved by performing a 1:1 place exchange using a Pt^{2+} replacement solution, as opposed to a 1:2 place exchange sing Pt^{4+}, noting that Cu would oxidize in the galvanic reaction as Cu^{2+}. Furthermore, it has been shown that the coverage and morphology of the sacrificial layer plays an important role on the final chemical state and reactivity of the ultrathin film ultimately grown.

Challenges still remain on the road toward the development of SLRR Pt deposition strategies that would better meet today's requirements for Pt surfaces need for fuel cell catalysts. Most significant among those challenges are the relatively low efficiency of the SLRR reaction when Cu is used as sacrificial metal and the absence of information about the elemental composition of SLRR deposited Pt layers.[70, 193, 197]

There has been evidence that the metal grown by SLRR is not fully reduced, an effect suggested by previous work which indicated non-traditional stoichiometry in specific cases of SLRR growth.[197] It has been shown that the influence of support particle size is of critical important when it comes to the valence state of SLRR-grown overlayers.[68]

3.3.2 Graphene Synthesis and Transfer

Single layer graphene sheets have gained attention for the coverage of large substrate areas for large scale applications, such as for electrocatalysts. Synthesis of graphene layers has been conducted in a variety of manners. The first of these incorporates annealing of single-crystal SiC, which results in desorption of Si from the surface yielding a multilayered graphene structure that behaves like graphene.[198] Secondly, graphene oxide films have been fabricated through a liquid suspension followed by chemical reduction.[199] A third method is a chemical vapor deposition (CVD) / surface segregation method where carbon is dissolved in transition metals and then undergoes a precipitation process at high temperatures followed by cooling down with various rates.[200] For use in this work, graphene obtained uses high vacuum CVD methods on transition metals.[198, 201] However, several of these approaches require the use of a specific substrate material.

The growth of graphene monolayers on transition metals such as Co, Pt, Ir, Ru, Ni and Cu is well known. In general, the growth process involves exposure of the transition metal surface to a hydrocarbon gas, such as CH_4, at temperatures around 1000 °C under low pressure conditions. In a CVD process, graphene growth occurs due to the precipitation of graphite from gaseous carbon species within the surface of a metal film, forming a solid solution. After exposure to CH_4, the system is cooled to room

temperature. Since the solubility of carbon is temperature-dependent, it then precipitates as a graphene layer on the Cu surface upon cooling of the foil.[201] For this work, Cu foil was used as the metal of choice.

Following CVD growth of a large-area graphene monolayer on Cu, reliable transfer onto any desired arbitrary substrates is a crucial step for most practical applications. This is conducted by performing a wet-etching process of the underlying metal film. In order to protect the graphene, it is first coated on one side with a polydimethylsiloxane (PDMS) or poly-methyl methacrylate (PMMA) layer. PMMA has been more commonly used for purposes similar to this, such as a carrier material for transferring carbon nanotubes.[202] The etching is then carried out in steps by first floating the foil, PMMA coat side up, on an aqueous HCl or HNO_3 followed by floating on solutions such as ammonium persulfate for several hours.[203] This ultimately results in a free-standing PMMA/graphene sheet that can be transferred to any desired target substrate. The final step involves removal the PMMA protective coat by acetone. The newly attached graphene monolayer preserves it structure and can attach strongly to most materials, such as semiconductors, glass, metals and plastics, via van der Waals interactions. [204]

3.3.3 Experimental Sample Set

This study encompasses the previously described spectroscopic and electrochemical methods to analyze Pt monolayers grown on Au coated supports via the SLRR method. Au is used as a supporting core metal for two primary reasons. First, it allows for uncomplicated synthesis of SLRR because it allows Cu to exhibit a clean UPD

feature when used as a sacrificial layer. Secondly, Au has been shown to have synergistic effects when paired with Pt when it comes to its activity and stability.

Two different Au based supports are used throughout the research presented in the following chapters. One support will involve carbon fiber paper (CFP) as a catalyst backing, chosen due to its affordability, high surface area, easy synthesis incorporation, and efficiency as a current collector for fuel cells. Before any deposition, the CFP electrodes are cleaned by CV in a 0.1 M H_2SO_4 solution until a steady state was reached. The Au is then deposited using a 1 mM $AuCl_3$ solution via potentiostatic deposition (PSD) at 0 V for 30 minutes. The solution used for Cu UPD is 10 mM $CuSO_4$ + 50mM H_2SO_4 and Pt galvanic replacement of the Cu utilized 1 mM H_2PtCl_6.

The other support material is flat crystalline Au(111) deposited on glass substrates, which acts a more academic set of monolayers in analyzing architecture effects on the Pt surface. Glass substrates are first cleaned in Piranha solution (H_2SO_4: H_2O_2 – 4:1) for 15 minutes, followed by physical vapor deposition of a 15 nm Cr layer and a 50 nm Au layer, successively, using a Denton Explorer E-beam Evaporator. A slow deposition rate of 0.5 Å/sec is used in order to achieve to most uniform Au coating possible. AFM measurements of deposited Au on glass substrates show a surface roughness value of less than 1 nm (RMS). XRD analysis shows that the deposited Au surface is largely of a (111) orientation, and can be seen in Figure 13. The Cr acts as an adhesion layer for the Au, which acts as the core metal.

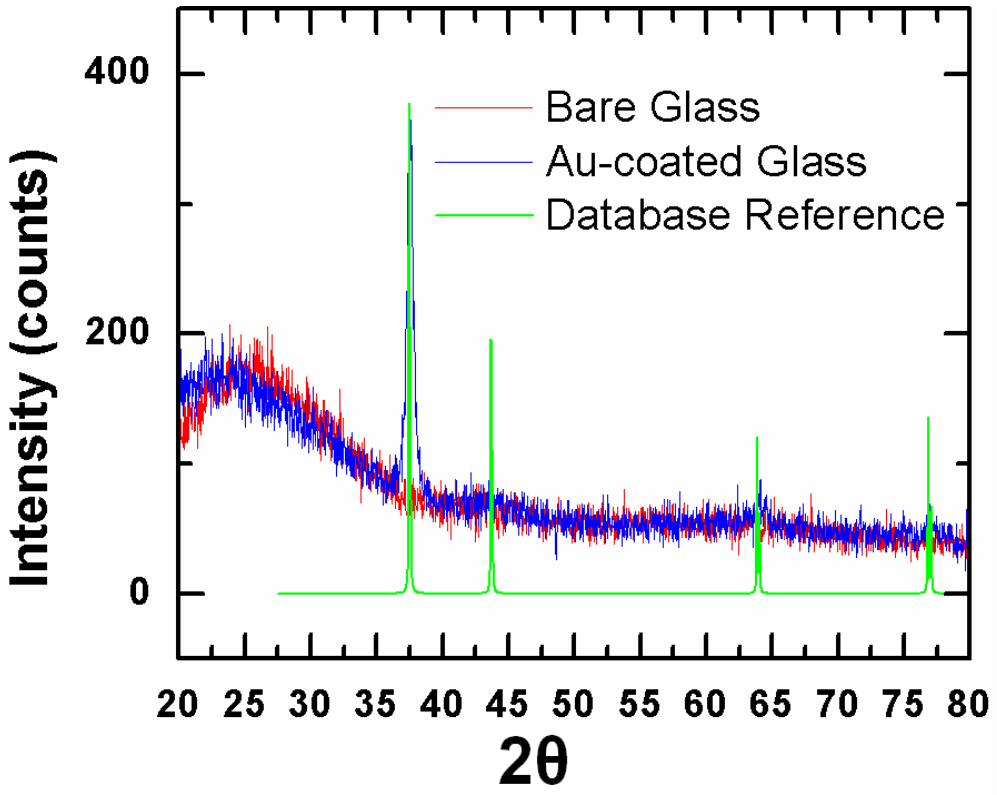

Figure 13: XRD spectra for bare glass substrate and Au/glass substrate, using a Cu Kα source.

For the Pt MLs grown on Au(111) thin films, this study also examines the effects of single layer graphene incorporated into the core-shell architecture. Graphene sheets have been added to the samples in two distinct manners. Firstly, the study examines graphene when placed in between the Au substrate and SLRR grown monolayers, such that the SLRR process grows Pt on top of a graphene-templated Au film. Secondly, graphene is placed at the top most layer of the Pt-Au structure, such that graphene acts as a cap covering the SLRR grown Pt. These two types of architectures will be denoted at Pt/GR/Au and GR/Pt/Au, respectively. A representation of all the sample types examined throughout this study is shown in Figure 14.

Individual monolayers of graphene were obtained from American Chemicals Supplier, previously synthesized by chemical vapor deposition over 25 μm Cu foil. A 100 nm thick PMMA layer is spin coated over graphene/Cu foil and left over night to dry. The underlying Cu foil is then etched away by floating on HNO_3 for 5 minutes, with the coated PMMA layer facing up and followed by floating overnight in an ammonium persulfate solution. This is succeeded by cleaning in 18.2 MΩ deionized water bath and isopropyl alcohol. After etching, the PMMA/graphene film is then transferred over to either the Au substrate in the case of Pt/GR/Au samples, or to the already grown Pt-Au architecture in the case of GR/Pt/Au samples. The PMMA/graphene/substrate is then annealed at 220 °C for 15 min with a ramp up from room temperature at 20 °C/min. After annealing, the substrate is placed in acetone to etch away the PMMA for 8 hours.

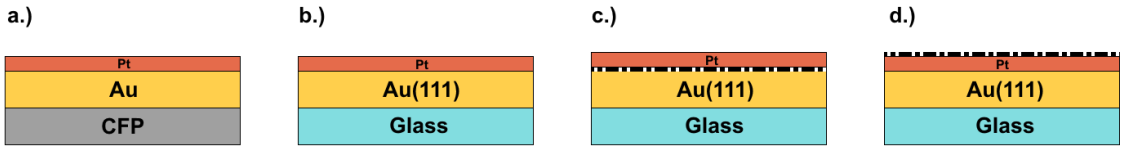

Figure 14: The main sample architectures examined in this study. a.) Pt monolayers on Au-coated carbon fiber paper. b.) Pt monolayers on Au-coated glass. c.) Pt monolayers on graphene-templated Au-coated glass. d.) Pt monolayers capped by single-layer graphene on Au-coated glass. Dark dashed line represents a graphene layer.

As a result of the SLRR process, Pt is nominally deposited on the surface in a 1:2 Pt/Cu ratio, which arises from the ratio of the valence states of the corresponding Pt^{4+} and Cu^{2+} ions in solution. Each SLRR iteration results in Pt replacing a 2/3 ML of Cu, therefore this nominally yields a 1/3 ML-equivalent (ML) of Pt.[68] This can be seen in

Figure 12. So, a sample with only 1 SLRR iteration can be denoted by 0.3 ML, while 3 SLRR iterations can be seen as equivalent to 1 ML, and 6 SLRR iterations can be denoted as 2 ML, etc.

The experiments performed on the samples are detailed in the following chapters, but a general outline of the characterization methods used can be seen in Figure 15. At least a subset of each type of sample architecture have been examined via XPS and CV as well as synchrotron EXAFS and some form of potential cycling to analyze surface durability.

Sample Type	Laboratory XPS	Synchrotron XPS	EXAFS	CV	LSV (ORR probe)	Potential Cycling (durability test)
Pt/Au/CFP	✓	✓	✓	✓	✓	(N_2, 0-1.5V, 300 cycles), (O_2, 0.4-0.75V, 1000 cycles)
Pt/Au(111)/Glass	✓		✓	✓	✓	(O_2, 0.4-0.75V, 1000 cycles)
Pt/GR/Au(111)/Glass	✓		✓	✓	✓	(O_2, 0.4-0.75V, 1000 cycles)
GR/Pt/Au(111)/Glass	✓		✓	✓	✓	(O_2, 0.4-0.75V, 1000 cycles)

Figure 15: A table summary of the experimental methods performed on the sample set detailed in Figure 14. Durability tests are summarized by the potential window, number of cycles, and whether the electrolyte was N_2 or O_2 saturated.

CHAPTER 4: STRUCTURAL SURFACE EVOLUTION OF PT MONOLAYERS ON AU

One of the goals of the research presented is to examine the structural and electronic properties of Pt monolayers grown using the SLRR method. Specifically, the aim is to examine the chemical state of the surface of the Pt monolayer catalysts formed via SLRR on varying supports and to determine the best methods and architectures of obtaining the most suitable surface for use in catalysis. Literature shows that many properties of a monolayer scale surface are dependent on the proximity of atoms to the supporting core material. Thus, one of the main variables this study look to examine is that of monolayer thickness, usually in the range of sub-monolayers to 5 monolayers, which can be controlled by the number of SLRR iterations performed in sample synthesis.

This research compares the chemical state of fabricated Pt architectures by XPS. Further, by using a tunable synchrotron source of light for these experiments, a very detailed examination of the Pt surface can be done, which can inform of the level of metallic and cationic state Pt that exists in the overlayer. LSV sweeps are used in oxygenated H_2SO_4 to examine the aptitude of the Pt surface for catalyzing the ORR. Catalyst durability is also a significant aspect for consideration, with instability oftentimes caused by metal dissolution or corrosion.[180] It is has been shown that Au can have a stabilizing effect on Pt even under high oxidizing conditions and thus can suppress Pt dissolution during reactions such as MOR, resulting in improved durability of the Pt catalysts.[37, 205] This study looks at the durability of Pt monolayer catalysts in two ways, firstly by subjecting samples to an aggressive potential cycling window and by

examining the activity of the surfaces towards the ORR during cycling in an oxygen environment with narrower cycling ranges. These three aspects of monolayer catalysts - chemical state, activity, and durability - are the primary basis for the study. Sample synthesis and characterization methodology is outlined in Chapter 3.

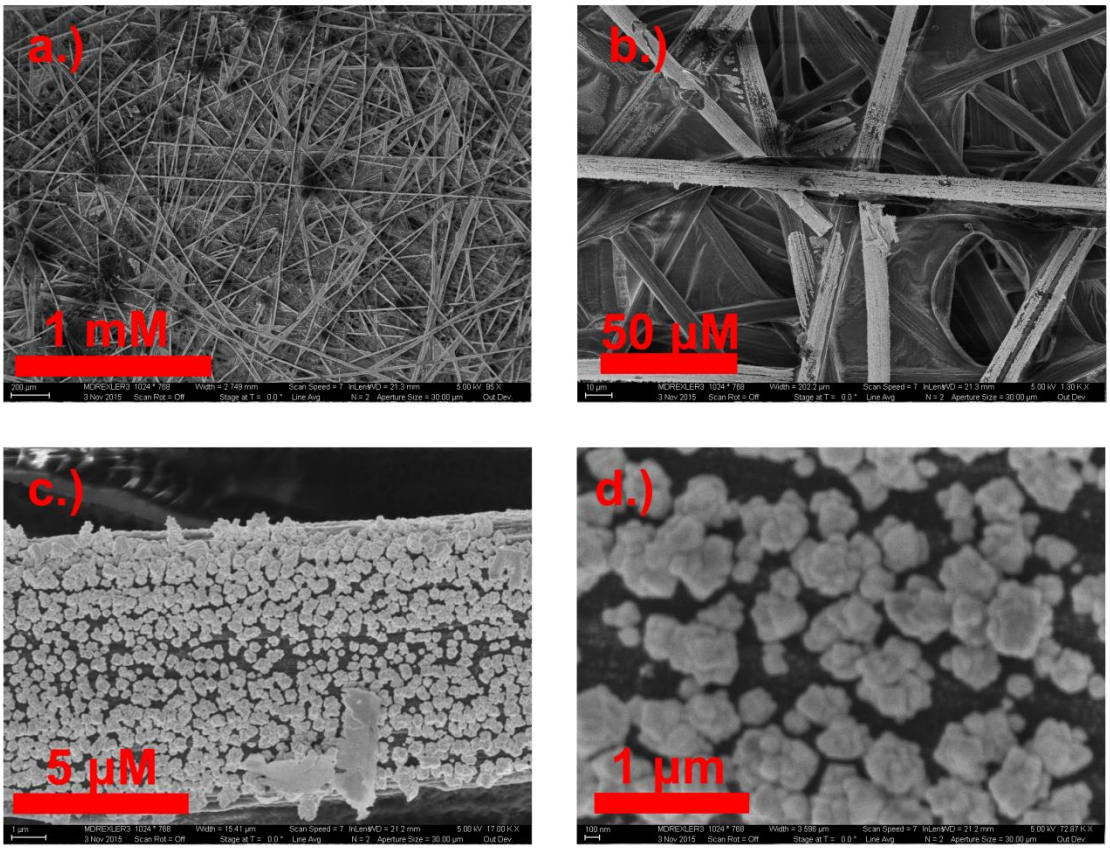

Figure 16: SEM images of potentiostatically deposited Au deposited on CFP.

Before sample characterization, SEM images of Au deposited on CFP were taken and can be seen in Figure 16. Notably, there is no useful purpose in taking SEM images for Pt/Au/CFP samples, due to the extremely small scale of the SLRR-grown Pt depositions. The Au deposit takes on the morphology of numerous large urchin-like

clusters with an average diameter of a few microns. The formation of Au clusters is sensible, due to diffusion-limited growth caused by electrochemical potentiostatic deposition. The rate-limiting step for the reduction of Au^{3+} to Au is the arrival of solution-phase Au^{3+} at the CFP surface, creating a depletion zone after initial Au nuclei formation. Once this region is formed, the arrival of further Au^{3+} ions to the Au-CFP surface will preferentially reduce at the outermost protrusions of the deposited Au into the depletion zone, leading to a cluster formation. SLRR grown Pt can then be expected to coat the surface of the Au clusters, as shown in Figure 17.

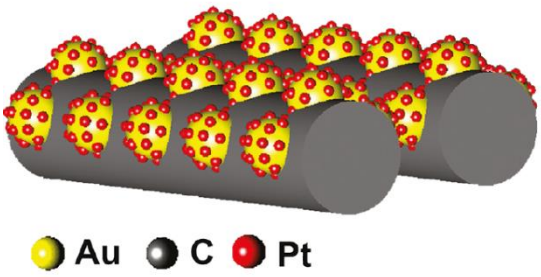

Figure 17: Representation of Pt growth on CFP containing Au clusters. Adapted from earlier report.[68]

Another goal of the research presented is to determine methods to readily achieve a reduced metallic state of the Pt overlayer, which can be done with both electrochemical methods as well as annealing. The Pt/Au/CFP sample set includes samples ranging from having undergone 1 SLRR iteration to 18 SLRR iterations (0.3 ML to 6.0 ML) in one of two states, as-is and after an electrochemical reduction step. Samples modified by electrochemical reduction were done so by cycling in a 0.1 M H_2SO_4 solution conducted from 0 V to .9 V. In this way, the chemical state of both as-is samples and reduced

samples can be compared, and variations in chemical state can be examined. This study also examines the effects of moderate temperatures on the state of the Pt catalyst samples and how the core-shell architecture is modified.

Several Pt/Au/glass samples are also characterized in the chapter. These architectures are flat academic samples largely utilized as a means of comparison to the Pt/Au/CFP samples.

4.1 Electrochemical Characterization & Durability Testing of Pt Monolayers

4.1.1 Pt/Au/CFP Sample Set

The samples used for this study can be referred to by the number of the equivalent number of monolayers rather than iterations of the SLRR technique. For example, 1, 3, and 6 SLRR iterations can be denoted as '0.3 ML', '1.0 ML', and '2.0 ML', respectively. Firstly, the surfaces of the samples were examined by CV in acidic media where the relative currents associated with Au or Pt surface oxide reduction can be seen. Figure 18 shows representative CV curves for varying thicknesses of Pt. The voltammograms presented here were recorded in N_2-saturated 0.1 M H_2SO_4 at 20 mV/s. Cycling the samples in such a manner also acts as a preliminary electrochemical reduction step when the sweep is terminated at 0 V.

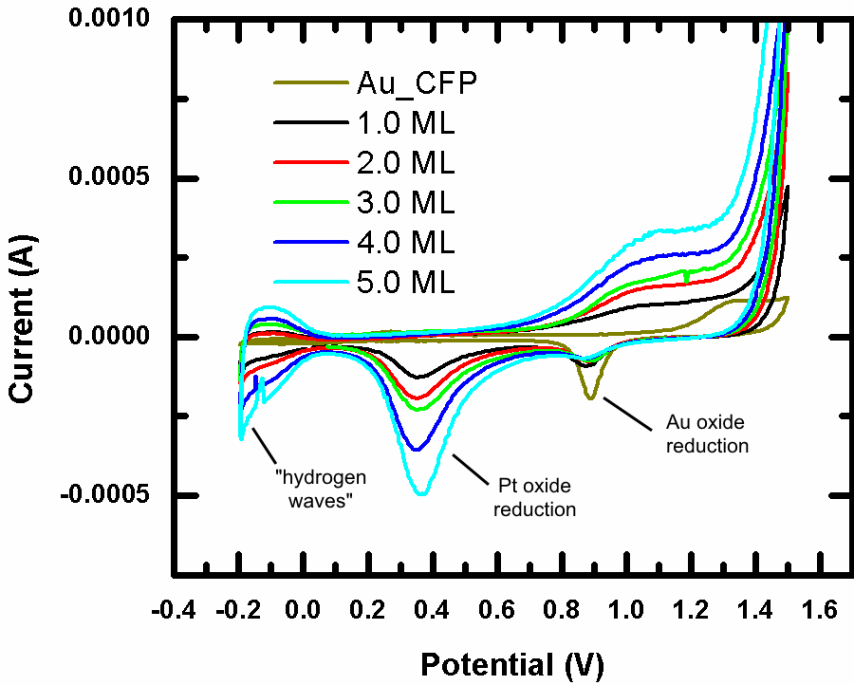

Figure 18: Cyclic voltammograms of Pt/Au/CFP electrodes in 0.1 M H_2SO_4 solution with a potential scan speed of 20 mV/s. Referenced against Ag/AgCl.

Figure 18 shows a set of cyclic voltammograms for SLRR grown Pt on Au on CFP. CV is a surface-sensitive technique, as currents seen are generated from reactions at the metal-electrolyte interface. For Pt specifically, a Pt surface area can be tracked either by studying the Pt oxide reduction feature at around 0.45 V or by the hydrogen adsorption/desorption curves that appear around the 0 V region of the voltammograms against an Ag/AgCl reference electrode. Similarly, the presence of a small Au reduction feature at 0.9 V indicates when Pt deposits are not fully masking the underlying Au.

It can be seen that most of the Au reduction feature is eliminated with a single monolayer coverage of Pt, but it never fully diminishes even after several SLRR iterations. With increasing amounts of Pt, the Pt surface area increases at the expense of the Au surface area, indicating that Pt deposition at Au sites is dominant. The Pt

reduction feature continues to increase in size up 5 ML (15 SLRR iterations) thickness. The use of these two reduction features can be used to track Pt's growth on Au via SLRR and has been employed successfully in the past, including previous research by this group. [68, 179, 206, 207] Additionally, the hydrogen wave feature also continues to increase in size as the amount of Pt deposit increases. Hydrogen adsorption is directly proportional to the amount of Pt exposed to the electrolyte, and indicates that the Pt surface area still continues to increase even after when a few monolayers are placed. This could be due to continuing clustering of deposited Pt in addition to surface roughening.

Further, the peak potential of the Pt reduction feature tends to shifts to more positive potentials with more monolayers placed. A positive potential shift can be indicative of the Pt surface exhibiting a more metallic structure rather than 'cationic' where Pt deposited on the surface is not fully reduced.[68] This shift has also been shown to indicate a benefit to the chemisorption of species such as OH- to help promote oxygen reduction kinetics.[179, 208] These results are also in accordance to recent research by Stickney et al. which show a similar progression for the Pt reduction charge shape as number of SLRR iterations increase.[195] The platinum reduction shape can be integrated to obtain the total Pt charge of the atoms, which is a representation of the amount of platinum atoms exposed to the surface. This information is used in normalization of electrochemical experiment data.

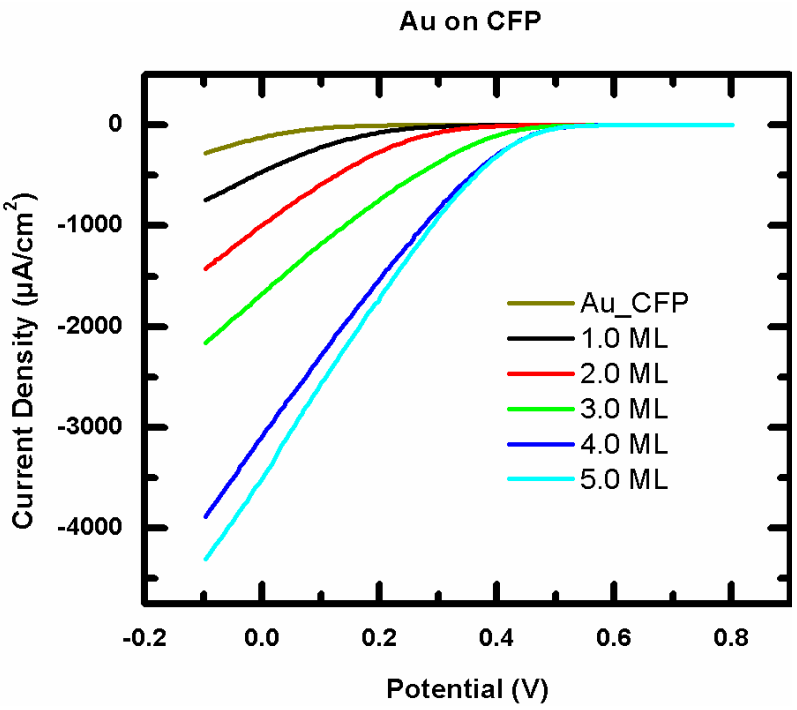

Figure 19: LSV sweeps for Pt/Au/CFP samples in O_2-saturated 0.1 M H_2SO_4. Referenced against Ag/AgCl.

In addition to Pt/Au/CFP characterization by cyclic voltammograms, the sample set was analyzed by LSV to probe ORR activity. Figure 19 shows the linear sweeps conducted in an oxygenated electrolyte, where the potential is swept negatively and the resulting current arises due to the reduction of O_2 to H_2O. It can be seen that with Au does not easily catalyze the ORR, and by increasing Pt overlayer thickness: 1.) the onset potential for ORR shifts positively, 2.) the current/potential slope increases, 3.) the maximum current achieved increases. For Pt/Au/CFP samples, an easy way to denote a sample's catalytic activity towards the ORR is simply to mark the current at the left-hand end of the sweep at 0.1 V.

Durability of Pt/Au/CFP catalysts was examined via electrochemical methods, using two different types of potential cycling approaches. First, an aggressive durability

test was conducted by repeating cyclic voltammetry (CV) cycles between 0.00 V and 1.50 V in N_2-saturated 0.1 M H_2SO_4 at a scan rate of 50 mV/s. While this potential range is much larger than what a catalyst would expect in a working fuel cell, this aggressive potential range was utilized simply to study the stability of the Pt overlayers and to compare varying overlayer thicknesses. The cycling repeated 300 times for each sample. After every 25 cycles, the electrochemically active surface area (ESA) of the Pt surface was estimated via integration of the Pt reduction charge in the cyclic voltammograms (see Figure 18).

In addition to this aggressive potential cycling, a stability test using a smaller potential window of 0.40 V to 0.75 V was also conducted in O_2-saturated 0.1 M H_2SO_4. After every 100 of these cycles, the electrochemical activity for oxygen reduction of the catalysts was investigated by linear sweep voltammetry (see Figure 19). This experiment uses a potential range for the sweep selected to illustrate performance in a fuel cell and gives insight on the activity of the catalyst. This also can describe how dynamic reconstruction of the surface during potential-cycling in fuel cell operation can affect the activity and stability of the surface.[180, 209]

The size of the potential cycling window will have immediate effect on the observed stability of Pt catalysts. In accelerated durability cycling tests, extremely rapid cathode particle coalescence and dissolution can be observed when cells are cycled to voltages above 1 V. For more representative testing for fuel cell purposes, the U.S. Department of Energy have recently established a set of suggested durability-test protocols. For electrocatalysts, the protocol places the endpoint voltages at .7V and .9V

against a standard hydrogen electrode (SHE), either for cycling or potential holds.[46] This protocol more closely matches the lese aggressive durability experiment performed.

The results for the durability experiments are shown in the following figures, both with larger aggressive potential windows (Figure 20) and more characteristic narrower potential ranges (Figure 21). All data reported is referenced against an Ag/AgCl electrode (SHE - .22 V).

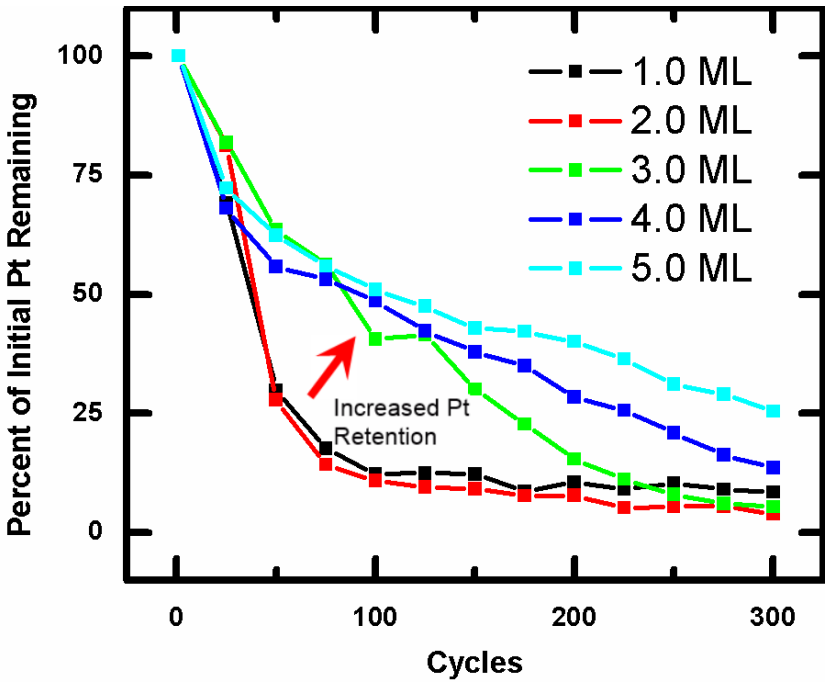

Figure 20: Percent remaining of the initial platinum overlayer on CFP every 25 cycles. Cycles were conducted from 0.00 V to 1.50 V in 0.1 M N_2-saturated H_2SO_4

Figure 20 shows us the percentage remaining of the integrated area of the Pt reduction charge every 25 cycles of an aggressive cycling experiment from 0 V to 1.5 V. The long-term stability of an ultrathin Pt film is a very important property for this type of fuel cell electrocatalyst. This shows that the charge obtained from the CV scans gradually decreases along with the successive CV scans. The shape and slope of the curve indicates

the relative durability of the Pt monolayers. Samples with an overlayer thickness of 2 monolayers or less show a more dramatic decay in ESA within the first 50 cycles, indicating that these samples show very poor durability and will dissolve readily. From this data, it can be seen that after about 100 cycles for the lower thickness samples, there is almost no remaining Pt reduction current which indicates that the Pt deposit has been mostly dissolved.

However, the shape of the curve significantly changes once the platinum surface is at least 3 ML in thickness, showing a slower decrease in the integrated charge as the cycling continues. This is especially noticeable in the 4 and 5 ML samples. This is in agreement with prior research done by this group that below which the film exhibits durability, due specifically to chemical state and thickness of the surface.[68] This previous report showed that Pt overlayers less than 2 MLs thick tend to exhibit more cationic Pt content, which can be inferred from the Pt reduction feature in Figure 18. This study investigates Pt chemical state further in Section 4.2.

Both the fact that the 3 monolayer overlayer shows significant increase in durability and a lesser decline in the Pt reduction charge in early cycles support the notion that cationic Pt species lead to less durable surfaces than more metallic-type Pt overlayers. The initial drop in the platinum reduction charge at 25 cycles may indicate a cleansing of the cationic content as it is quickly attacked during the initial cycles, before the curve starts to flatten out. The very thin oxide layer formed on the surface of Pt might not have a passivative nature and could accelerate the dissolution.[210] It can be said that after 3 monolayers (9 SLRR iterations) a thickness threshold has seemingly been

achieved, which allows the surface to achieve more metallic structure and gives it more stability.

In addition to this aggressive potential cycling, an activity/stability test using a smaller potential window of 0.40 V to 0.75 V was also conducted in O_2-saturated 0.1 M H_2SO_4. The electrochemical activity for oxygen reduction can be examined by linear sweep voltammetry experiments in H_2SO_4 solution at room temperature.[180] A LSV curve was taken from 0.8 V to -0.1 V and the final current achieved in the reaction was marked. Then the samples were cycled 100 times between 0.4 V to 0.75 V before performing another LSV curve. A total of 1000 cycles were performed, conducting a linear sweep after every 100 cycles. This experiment can give us some insight how dynamic reconstruction of the surface during potential-cycling in fuel cell operation can affect the activity of the surface.[180, 209]

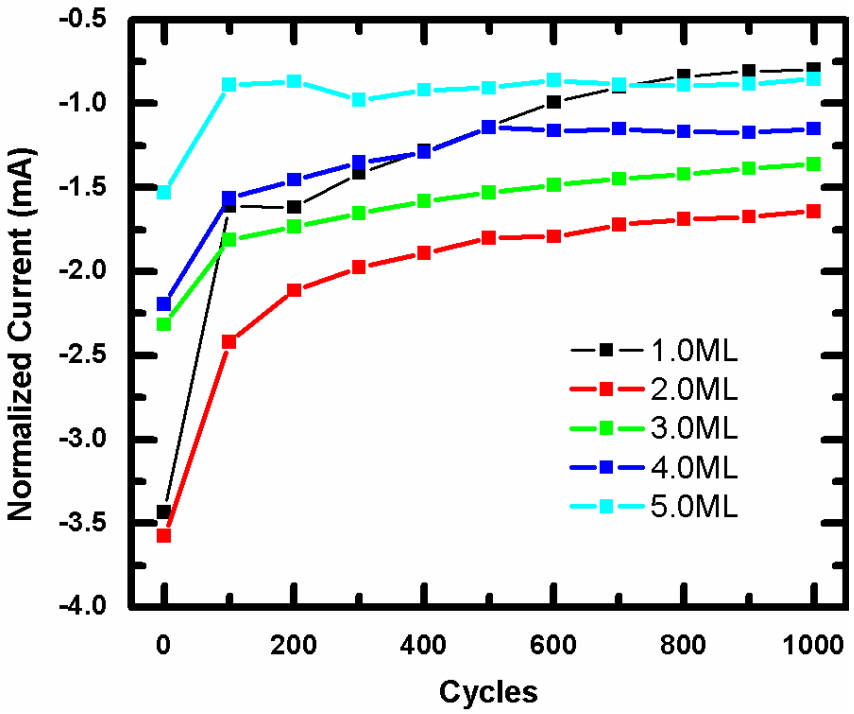

Figure 21: Normalized activities of after oxygen reduction reaction at -0.1V following negative potential sweep in 0.1 M O_2-saturated H_2SO_4 after every 100 cycles. Activities are normalized by the Pt reduction charge by CV in N_2-saturated 0.1 M H_2SO_4 (see Figure 18). Multicycles were conducted from 0.4 V to .75 V in O_2-saturated 0.1 M H_2SO_4.

Figure 21 shows the final currents achieved at the end of the potential sweep for each sample. Importantly, the currents have been normalized by the charge obtained by integration of the Pt reduction feature in the initial cyclic voltammogram of the sample (Figure 18). This Pt reduction charge essentially represents the exposed surface area of the Pt overlayer. By normalizing the ORR reaction current by this charge, a value that indicates *the activity of the surface-most platinum atoms* is obtained, not the activity of

the Pt/Au/CFP electrode as a whole. The cycling in oxygen-rich media show markedly enhanced currents for the ORR once a 2 monolayer Pt overlayer thickness is achieved.

When normalized by the Pt reduction charge in CV, it is seen that a surface coverage of 2.0 ML in thickness exhibits the highest activity towards the ORR relative to the amount of Pt present. One can see that the current obtained for a sample of 2.0 ML in thickness shows the highest (most negative) normalized current values, followed by 3.0 ML. Samples with higher surface coverages, such as the 4.0 and 5.0 ML thick surfaces, show a marked decrease in this normalized activity. It seems an overlayer thickness of 3.0 ML is most attractive, due to an increased durability as well as high activity towards the ORR relative to the amount of platinum exposed on the surface (see Figure 22).

Otherwise, each curve in Figure 21 shows a similar shape with regard to the activity after cycling. A significant current decrease the current is noted within the first 100 cycles, followed by a more gradual decline as cycling continues on the surface of the catalyst, much like Figure 20. Once again, the initial decrease may indicate a cleansing of a thin oxide layer formed on the surface of the Pt overlayer, potentially lowering the surface area for reaction and lowering the current before a more regular surface overlayer is achieved after initial cycling.

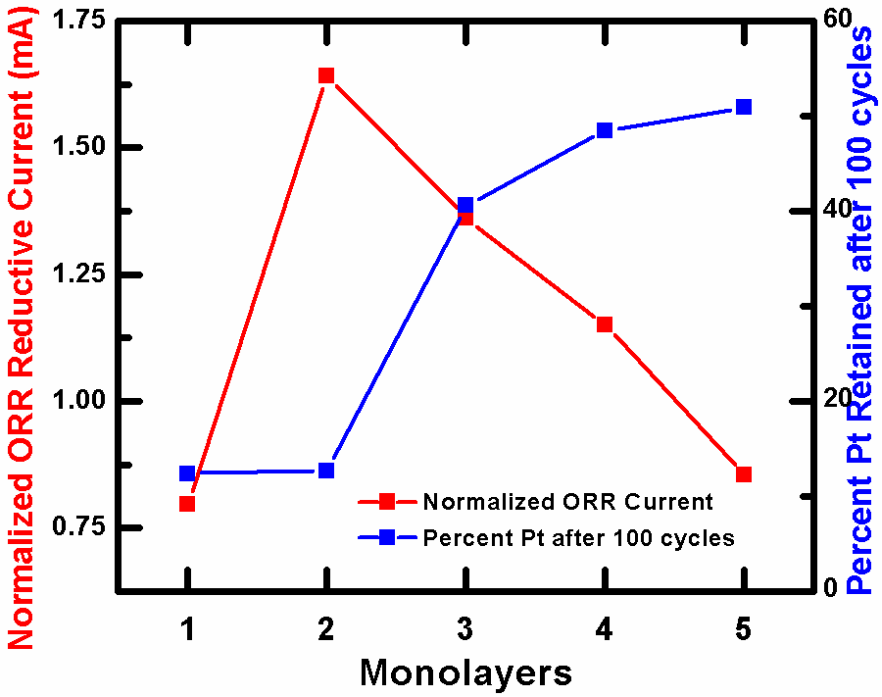

Figure 22: Normalized activities after 1000 (.4 V-.75 V) cycles of oxygen reduction reaction at -0.1V following negative potential sweep in 0.1 M H_2SO_4 plotted against Percent platinum retained after 100 (0.0 V-1.5 V) cycles. Activities are normalized by the Pt reduction charge by CV in nitrogen saturated 0.1 M H_2SO_4 (see Figure 18).

Figure 22 compares sample activity to durability by overlaying the normalized ORR current after 1000 cycles from .40 V to .75 V in O_2-saturated 0.1 M H_2SO_4 for each sample and the percent of Pt remaining on the surface after 100 aggressive cycles from 0 V to 1.5 V in N_2-saturated 0.1 M H_2SO_4. Although the increase in ORR activity is best for a sample with a Pt overlayer of 2 monolayers in thickness, when compared to the durability testing, the 3 monolayer samples seems to have the best overall activity and durability properties. This is in agreement with prior work by this group which showed that Pt films of 3 monolayers in thickness are spared the rapid metal dissolution from

repeated methanol oxidation cycles, but are thin enough to exhibit enhanced CO stripping due to electron transfer from the underlying Au.[82]

4.1.2 Pt/Au/glass Sample Set

SLRR grown Pt monolayers on glass are more thoroughly analyzed in the next chapter, however, this section includes the fundamental electrochemical characterization for the Pt/Au/glass sample set. Characterization voltammograms, LSV sweeps probing the ORR, and durability tests are conducted for comparative measure to the Pt/Au/CFP samples in the previous section.

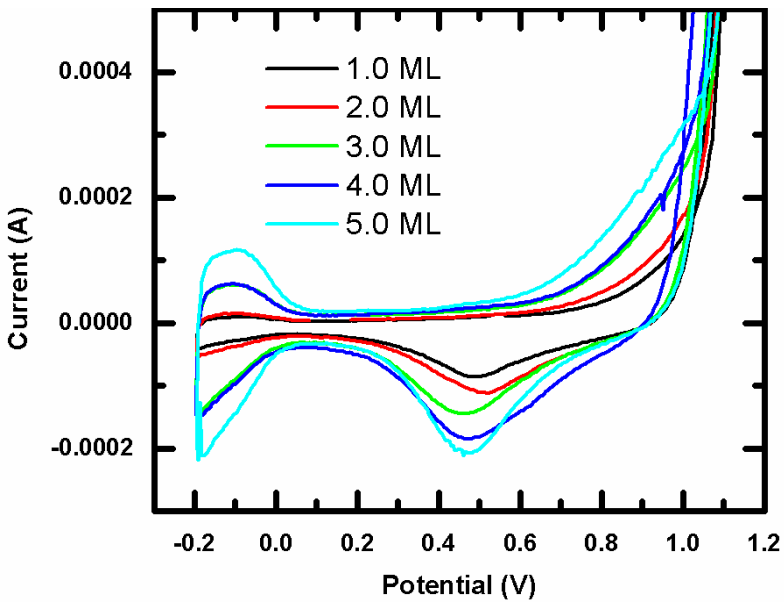

Figure 23: Cyclic voltammograms of Pt/Au/glass electrodes in 0.1 M H_2SO_4 solution with a potential scan speed of 20 mV/s. Referenced against Ag/AgCl.

Figure 23 shows cyclic voltammograms for Pt/Au/glass electrodes. Unlike the counterpart CFP based electrodes (Figure 18), the potential window only goes up to a maximum of 1.1 V. This is due to the Au adhesion to the underlying glass substrate. Higher oxidizing potentials of Au can easily lead to delamination of the Au from the support, effectively destroying the sample. It is worth noting that the absolute currents achieved are lesser than what was seen on carbon fiber paper, due to the lower specific surface area of flat Au substrates compared to CFP. Additionally, it is notable that the Au oxide reduction feature is not seen for any of the sample cases. There are two reasons for its absence, firstly, that oxidizing potentials up to 1.1 V may not be positive enough to oxidize a significant amount of Au. Secondly, Pt monolayers may effectively cover the entire surface of Au, even after only a single monolayer has been deposited.

It is possible to cycle up to 1.2 V, in order to see a higher amount of Au oxide formation and reduction as seen in Figure 24. However, if the Au is not well adhered to the glass surface, these potentials can be destructive to the sample. The presence or absence of the Au reduction feature at ~0.9 V is analyzed further in Chapter 5.

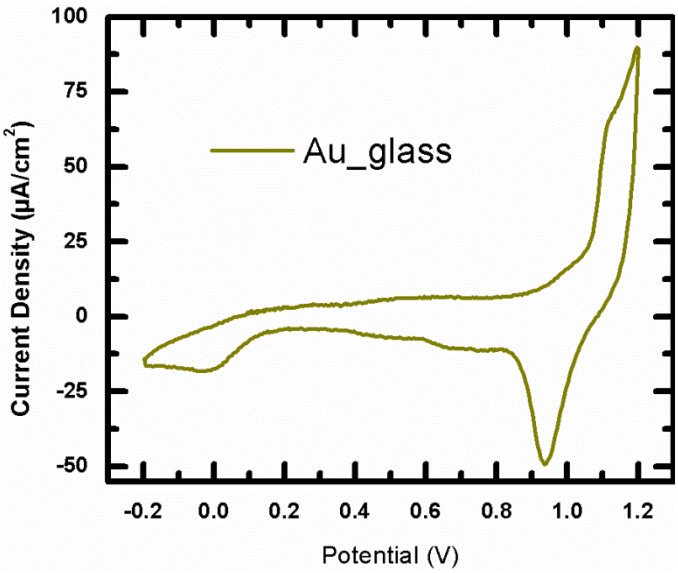

Figure 24: Cyclic voltammogram of Au on glass electrodes in 0.1 M H_2SO_4 solution with a potential scan speed of 20 mV/s. Referenced against Ag/AgCl.

The ORR activity of Pt/Au/Glass samples was also probed, and the results can be seen in Figure 25. Firstly, the ORR current densities (current per geometric surface area) achieved are much lower than the CFP counterparts (Figure 19), roughly by an order of magnitude, once again due to much lower surface area for the glass-supported samples. Secondly, the LSV shape is significantly different. Rather than a monotonically increasing current as potential is swept, a maximum is reached, after which the ORR current tails off. This is due largely to mass-transport limitations, which could normally be minimized with the use of a rotating electrode set up. However, due to the sample synthesis used in this report, rotating methods were not available.

This makes noting a sample's activity towards ORR a bit trickier than it was for CFP samples, where one can easily select the current at the end of the sweep. In the case of Pt/Au/Glass samples, the level of surface activity can be analyzed a number of ways:

1.) By examining the onset potential for ORR, 2.) By examining the maximum current value or reaction slope, 3.) By picking an arbitrary potential and marking the current value at that point for each LSV curve, 4.) some combination of 1-3. In analyzing ORR activities in the next chapter, this study examines both the slope of the curve - noting where the slope is at its maximum - and the current value at a chose voltage.

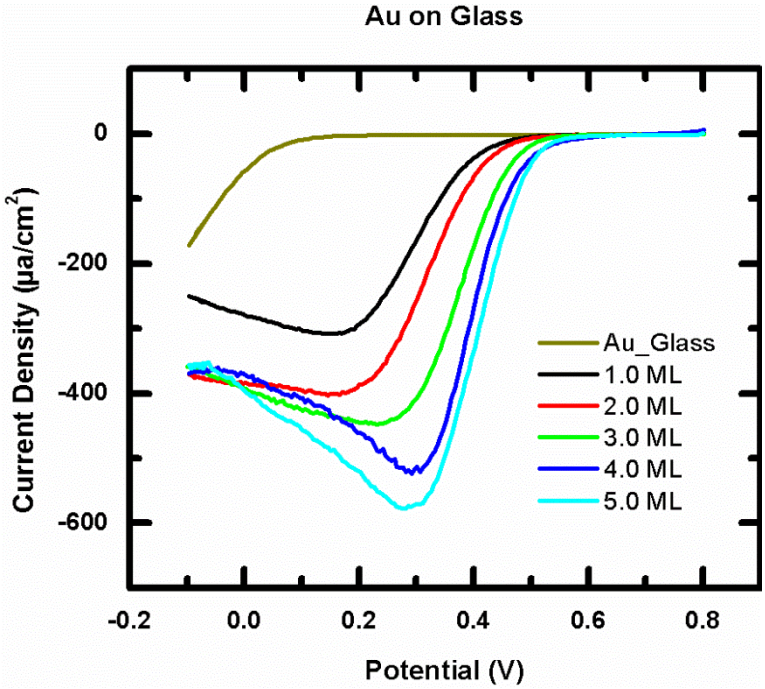

Figure 25: LSV sweeps for Pt/Au/Glass samples in O_2-saturated 0.1 M H_2SO_4. Referenced against Ag/AgCl.

When it comes to durability testing, samples were cycled long-term from 0.4 V to 0.75 V in oxygen-saturated 0.1 M H_2SO_4, with a total of 1000 cycles performed on each sample. A characterization CV curve from 0 V to 1.20 V was taken in N_2-saturated 0.1 M H_2SO_4, once before cycling and once after 1000 cycles in order to examine the changes in the Pt reduction shape. By measuring the integrated Pt reduction charge before and after cycling, an illustrative representation of the amount of surface coverage of Pt remaining

on these samples can be obtained. This is shown in Figure 26, where total Pt retention is displayed as a percentage its original integrated area.

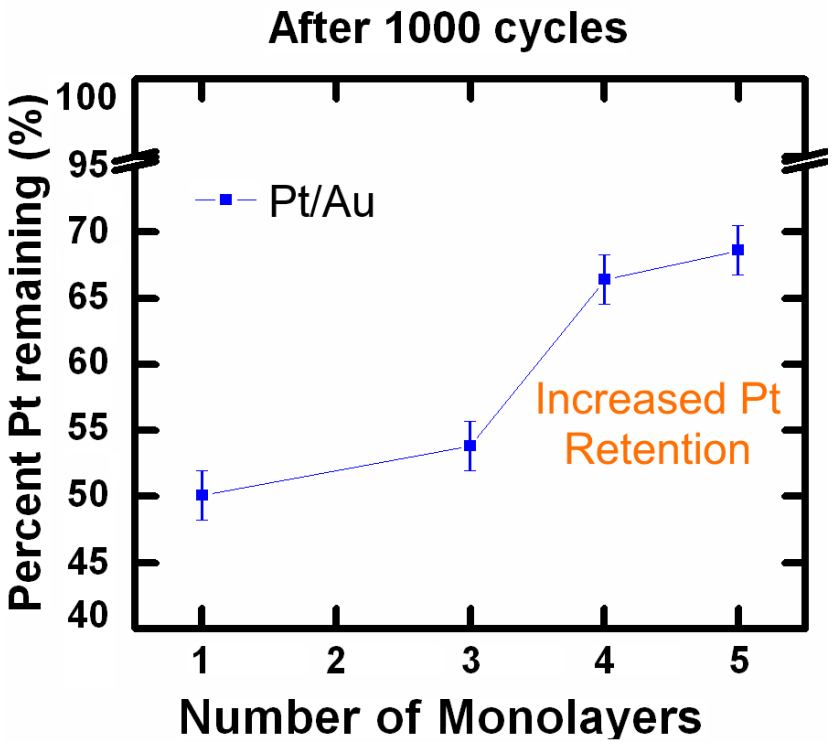

Figure 26: The percentage of surface Pt on Au-coated glass is calculated after 1000 cycles in acidic media. Cycles were performed from .4 V to .75 V in O_2-saturated H_2SO_4.

This voltage cycling experiment uses the potentials bordering the oxide formation and reduction regions for the ORR. By comparing the status of the Pt surface before and after cycling, it can describe how the reconstruction of the surface during potential-cycling in fuel cell operation can affect the stability of the surface. 4 and 5 ML Pt/Au samples showed improved Pt retention. The results indicate that loss of Pt is dictated mostly by bonding to other Pt atoms, and a significant increase in surface retention is achieved once several monolayers are grown.

4.2 XPS Characterization of Pt Monolayers on CFP

XPS analysis was employed to determine the oxidation state of the Pt, as well as the relative size of both the Pt and Au photoemissions. The Pt^0 4f photoemission exhibits a spin-orbit-split doublet, with two peaks ($4f_{7/2}$, $_{5/2}$) at binding energies around 71.25 eV and 74.5 eV, respectively, exhibiting a known spacing of about 3.25 eV. The Au^0 4f doublet lies about 12 eV higher, with binding energies ranging from ~84 eV to ~88 eV. XPS spectra of Pt and Au on CFP are shown in Figure 27 for Pt overlayer thickness from 1.0 ML to 5.0 ML.

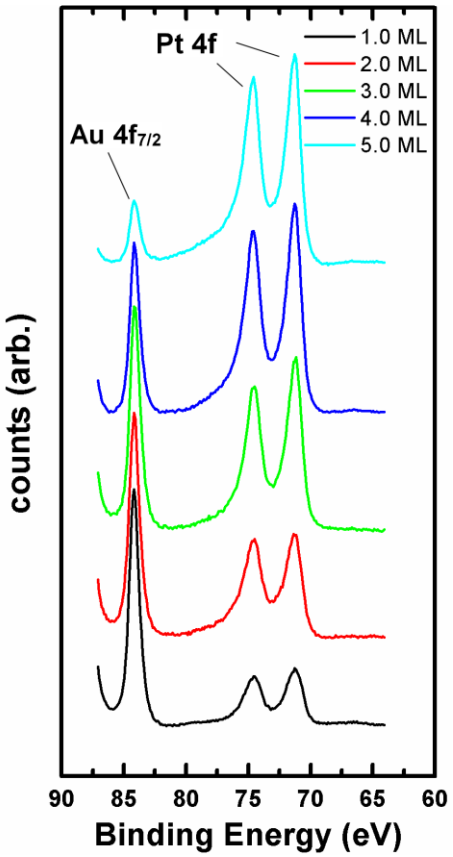

Figure 27: XPS spectra for Pt/Au/CFP samples from 1.0 to 5.0 MLs from an Al kα source.

Figure 27 shows how the Pt XPS photoemission increases in intensity relative to the Au signal as more layers of Pt are grown. Because the sample architecture is that of a layered structure, the relative photoemission intensity between Pt and Au can be used as a indicator of the thickness of the Pt overlayer as well as the overall wetting of Pt on Au. For Pt/Au/CFP samples, both these XPS measurements and CV data (Figure 18) exhibit Au signals up to 5.0 MLs, which indicates that Au may still be exposed on the CFP surface.

Using a tunable XPS system at a synchrotron facility, the chemical states of the Pt and Au can be examined as varying depths of the core-shell structure. By using photon energies much lower than what is possible at a typical laboratory Al kα source, these methods allows a case study sensitive enough to examine the very surface of core-shell structured samples and allow the analysis of the thickness-dependent structural features of both Pt overlayers and the underlying Au support. In addition, this study looks at the modifications at the core-shell structure of SLRR developed samples due to high temperature alloying of the samples.

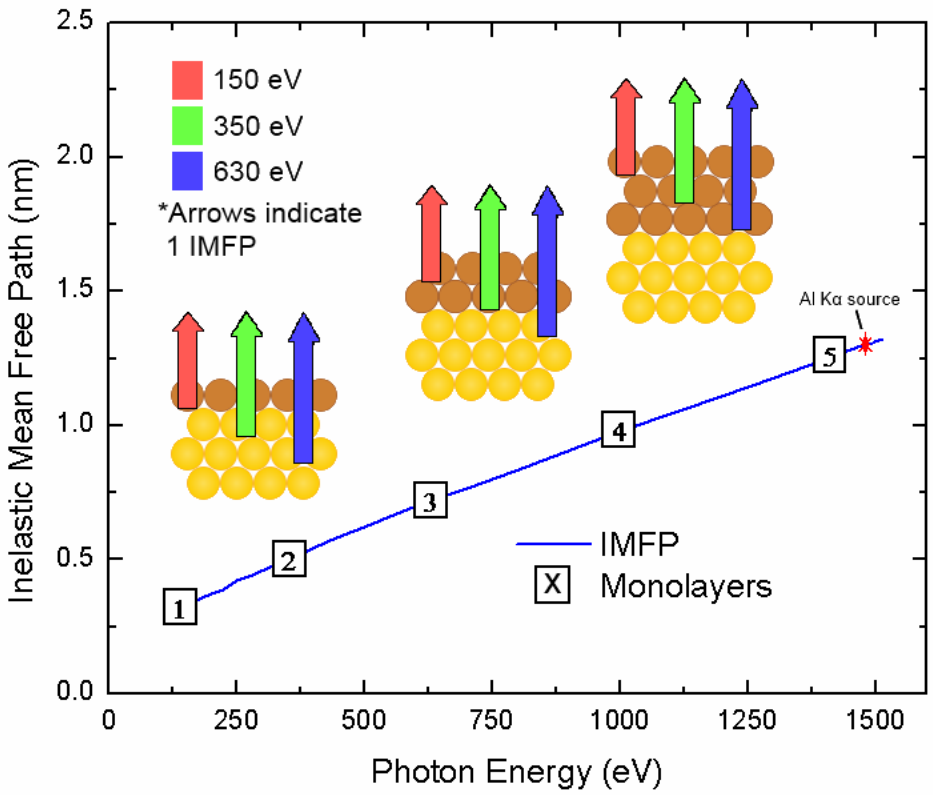

Figure 28: Plot indicating the information depth of an XPS experiment dependent on the incident photon energy. The inset images illustrate the effective information depth for a Pt/Au core shell sample with one, two, and three monolayers at 150 eV, 350 eV, and 630 eV for each. The information depths that correlate to one, two, and three monolayers are marked on the plot.

Figure 28 shows the basis for the depth penetration study of the sample set. Information depth values were obtained based on inelastic mean free path modeling functions by Cumpson and Seah.[211] Thicknesses of monolayers were estimated based on face-centered cubic stacking of platinum atoms. Each scatter-point indicates a particular photon energy utilized in the analysis of the sample set. The inset illustrations show a visualization of the information depth region by XPS for a variety of photon

energies on a 1.0, 2.0, and 3.0 monolayer thickness Pt/Au/CFP sample. One can determine that in order to penetrate more than 3 MLs of Pt effectively, a photon energy value greater than about 630 eV is required. Lower photon energy analysis leads to extremely surface sensitive information, where increasing photon energies allow further inspection of the deeper region of the samples. By varying the incident photon energies on a variety of samples, a comprehensive set of spectra can be obtained regarding the chemical state of the Pt and Au for core-shell style samples.

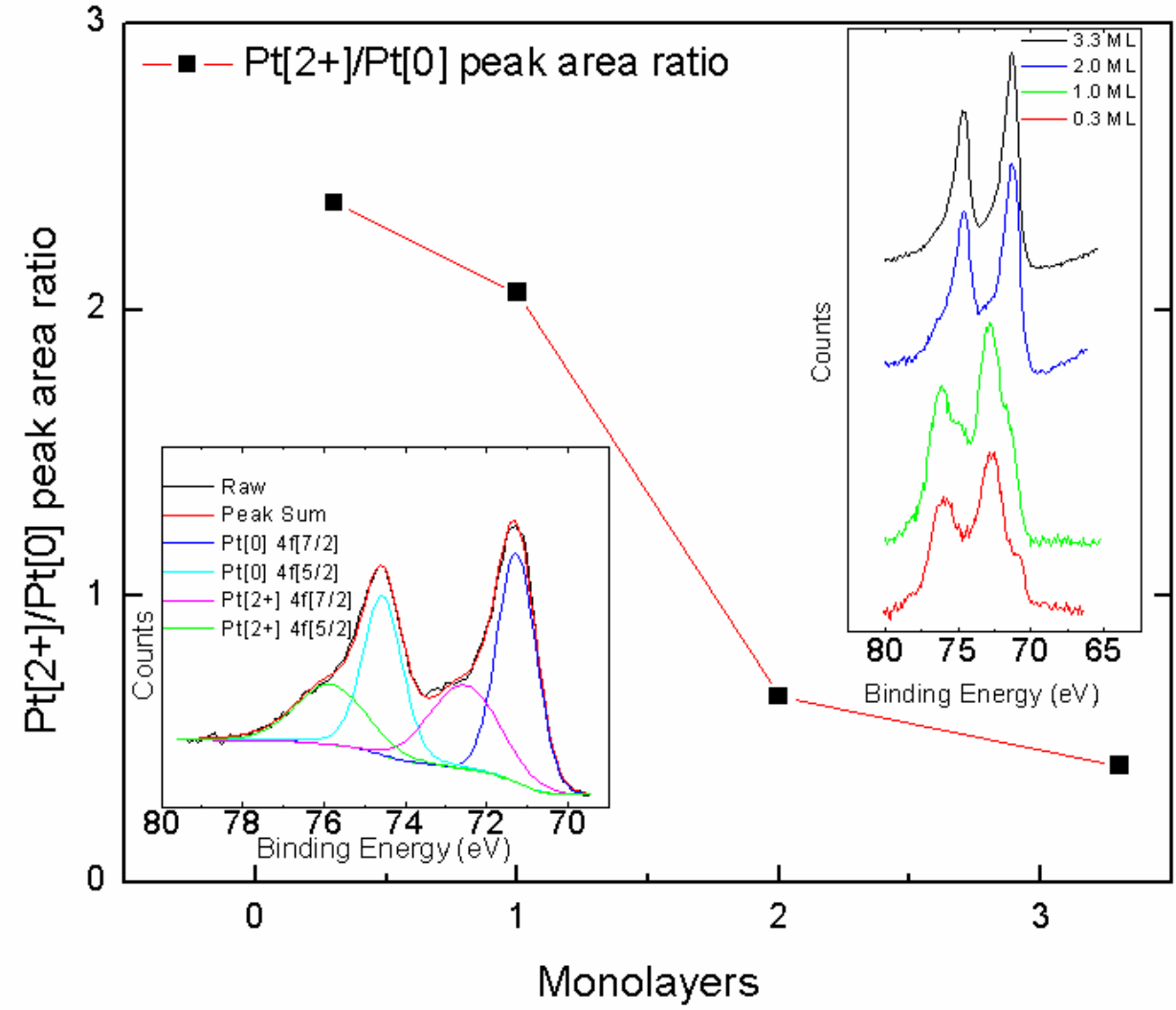

Figure 29: Thickness-dependent evolution of the chemical state of the Pt overlayer from 0.3 ML to 3.3 ML. The center plot shows the photoemission area ratio for the Pt^{2+} to Pt^{0} peaks as a function of monolayer with the red line acting as a guide to the eye. The left inset shows a typical fitting example for this type of spectra. The right inset shows the spectra comparison for the samples. All XPS showed are taken with incident photon energy of 180 eV, which correlates to an information depth of about .355 nm (Figure 28) – probing the very top layers of atoms.

Figure 29 shows the XPS photoemission spectra for Pt on samples up to 3.3 ML, noting that all samples had undergone a final electrochemical reduction step after fabrication. All spectra shown here were taken with incident photon energy of 180 eV, which corresponds to an information depth probing the very top layer of atoms as seen in Figure 28. The large scatter points show the area ratio of the Pt^{2+} to Pt^{0} photoemissions for these four samples, the upper right inset shows the Pt/Au XPS spectra for each of these four samples, and the lower left inset illustrates a typical fitting for the platinum photoemission. These XPS spectra indicate the presence of varying oxidation states for the Pt overlayer after fabrication. The peaks located at ~71.25 eV and ~74.50 eV are due to Pt^{0}, which is found to be the predominant species in Pt catalysts. The photoemissions of cationic Pt lay a few eV higher than their zero-valent state base.[68, 105] Features located at ~72.25 eV and ~76.00 eV are due to the Pt^{2+} oxidation state. Each pair of peaks (7/2, 5/2) has a similar full-width at half-maximum (FWHM) and a separation of about 3.3 eV. A relative decrease in the Pt^{2+} features are seen with a corresponding increase in Pt^{0} photoemissions as the number of Pt MLs increases. However, while the samples which higher than 2 ML show more metallic photoemissions, Pt^{2+} signal remains as a 'tail' enveloped by the cumulative photoemission.

These four samples underwent CV cycling in sulfuric acid before XPS analysis, which acts as a preliminary reduction step for the platinum overlayer. Regardless, it is clear that at 1 monolayer and lower, the dominant species on the surface remains Pt^{2+}. Samples that have at least 2 monolayers of Pt or more show a strong shift to metallic platinum as the Pt^{2+} photoemission becomes a shoulder in the spectra, and shrinks even more once a thickness of 3.3 monolayers is achieved, although it is notable that the

cationic presence does not seem to be fully eliminated. This is also illustrated by taking the area ratio of the fitted peaks (Figure 29) and a clear downward trend in this ratio is observed.

The XPS data presented here appears to indicate to that anionic species potentially incorporate themselves into the deposited Pt layer leading to incomplete reduction of the Pt species, even after achieving several monolayers in thickness, after a reduction cycling step. This result is in agreement with the literature, as Brankovic et al. have shown that anionic species, such as chlorine anions, may act as complexing agents during the SLRR process, also attributing to cationic Pt species.[197] The presence of the more metallic platinum surface achieved at 3.3 ML in thickness can also explain the improved durability seen in the aforementioned cycling experiments. It is worth noting that Pt^{4+} species are not prominent here for any sample, which is in agreement with previous studies done by this group for this type of fabrication.[68] In addition, this is also in agreement that an overlayer thickness of 2 monolayers can be considered a low-loading thickness limit for achieving a mostly metallic surface.

Samples that did not undergo an electrochemical reduction step prior to XPS analysis, however, displayed a significantly different XPS spectrum than the 3.3 ML sample shown in Figure 29. Instead of showing quite reduced photoemissions with a Pt^{2+} shoulder, both the Pt^{2+} and Pt^{4+} photoemissions are much larger, as seen in Figure 30.

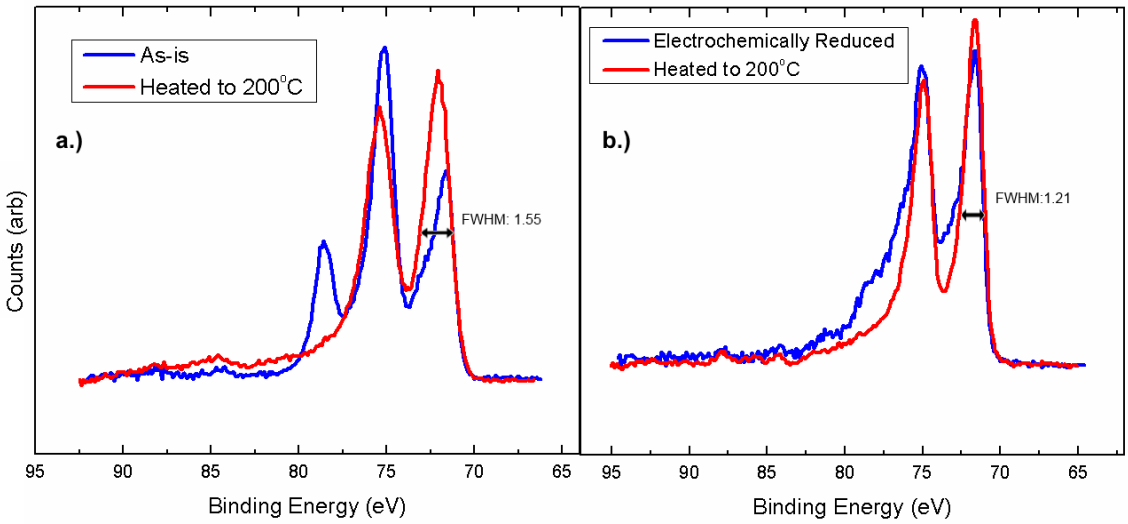

Figure 30: Comparison of XPS spectra for: a.) An as-is 5.0 ML sample and b.) an electrochemically reduced 5.0 ML sample. The blue lines are the photoemissions of the samples before heating, and the red lines are the photoemissions of the samples after heating to 200 °C for five minutes. FWHM values are given for the annealed sample Pt photoemissions. Incident photon energy was 525 eV.

The Pt photoemissions of the samples are dramatically changed depending on the sample fabrication route. As-is samples produced by SLRR, without electrochemical reduction, show significant photoemission peaks correlating to the 2+ and 4+ cationic Pt states. Figure 30 shows XPS spectra for a pair of samples with Pt overlayers 5.0 MLs in thickness, one as-is and one electrochemically reduced. The Pt^{4+} photoemission at ~78 eV is especially noticeable for the as-is sample. It is clear to see that in the cycle-reduced sample, the Pt^{4+} emission is no longer a distinct peak, but rather a small shoulder on the high binding energy side.

All the samples with overlayers thicker than 3 MLs showed similar results to this (not shown) indicating that cycling in sulfuric acid after fabrication helps to reduce the Pt content on the top surfaces of the samples. However, as aforementioned, it does not reduce the Pt completely. The galvanic replacement steps of SLRR followed by electrochemical reduction do not result in truly metallic Pt catalyst layers at the outermost surface. This is in agreement with prior results from the research group.[171] Literature suggests that a significant percentage of Pt oxides in such a catalyst architecture can play a detrimental role in catalytic performance.[212] Thus, it is of importance to ascertain methods to achieve more fully metallic Pt overlayers in Pt monolayer catalysts.

In attempt to further reduce the Pt layer, annealing was conducted on the samples in an effort to outgas any remaining anionic species that may be embedded in the surfaces. Figure 30 shows that after annealing the sample to 200 °C, the overlayer is even further reduced to be a primarily metallic photoemission. The Pt^{4+} peak or shoulder is almost fully eliminated and the Pt^{0} photoemission becomes sharper and more intense. As expected, samples having undergone both electrochemical reduction and annealing show sharper photoemissions than samples having undergone annealing alone, which is seen by comparison of the FWHM values. The shape of the platinum photoemissions of the as-is sample after annealing still presents a small shoulder and a larger FHWM value, indicative of presence of cationic Pt.

XPS was also used to examine the architecture of the SLRR-grown samples after modification by higher temperatures, having an alloying effect on the core-shell samples. It is known today, that Pt alloy catalytic activation is enhanced compared to pure Pt. The alloy catalyst is not only oftentimes more stable but also additionally more active due to

alloying modifying the electronic structure of platinum.[100] Literature has shown that alloying Pt with Au causes the ORR peak potential to shift indicating a change in electronic structure due to alloying.[99] A set of samples was taken to temperatures of 200 $^{\circ}$C and above inside the XPS chamber to not only reaffirm the reduction effects of annealing, but also to determine a temperature threshold at which the core-shell architecture is significantly altered. XPS was used to examine the resulting alloyed Pt/Au surface.

Samples that were brought to higher temperatures were done so inside the vacuum chamber at the beamline for a period of 5 minutes and then brought back to room temperature before XPS spectra were taken. This heating was done incrementally, first to 200 °C, then 300 °C, 350 °C, and finally 400 °C, taking the spectra data in between each heating step. As aforementioned, synchrotron XPS was then used to study the surface of the platinum overlayer with very precise control of the information depth, in order to gain insight on how the surface is modified and to examine the relative amounts of Au and Pt that exist on the surface.

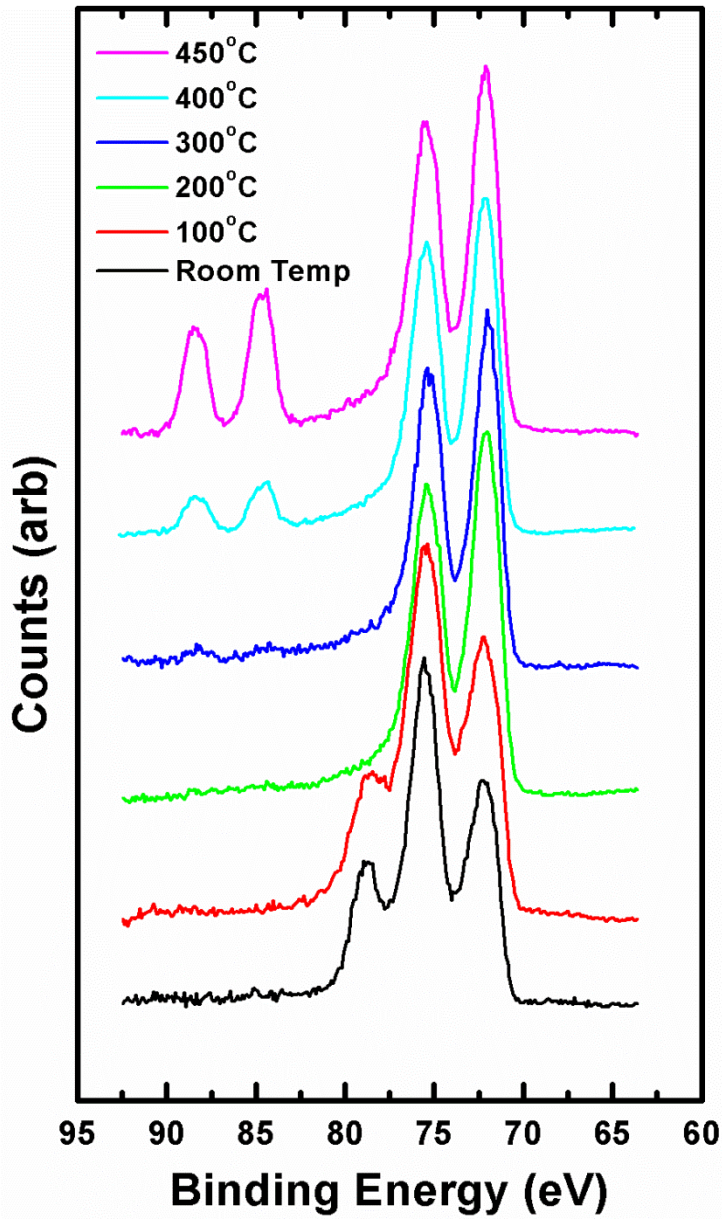

Figure 31: XPS Spectra of 6.0 ML sample after heating to 100, 200, 300, 400, and 450 °C for five minutes each. Incident photon energy for all spectra is 700 eV.

Samples around 10 SLRR iterations and above are expected to have a Pt overlayer thickness of at least 3 ML. Incident photons around 630 eV would not be able to penetrate the outer layer of platinum significantly for such samples as predicted in Figure

28. A set of such samples were heated to increasing temperatures with an XPS spectra taken after each heating step, examining the state of the Pt overlayer. Figure 31 shows XPS spectra for an as-is 6.0 ML sample after heating to several different temperatures for five minutes each. At room temperature, no Au photoemission can be seen at all, indicating a sufficiently thick layer of Pt on the sample. It is clear that much of the cationic Pt photoemission remain after heating the sample to 100 °C, and is only largely removed after heating to a temperature of 200 °C, giving us the familiar shape of the standard Pt 4f doublet with mostly metallic Pt. After heating the sample past 300 °C, to 400 °C and 450 °C, the emergence of the Au photoemission 4f doublet can be seen around 84 eV and 88 eV. This suggests that the core-shell structure is not significantly affected, at least for the time period used for annealing in this study, until a temperature past 300 °C degrees is achieved in vacuum. At this point, the Au photoemission grows in intensity relative to the Pt overlayer, indicating that the surface region is becoming more Au rich. This data suggests that heating the samples to 200 °C is a valid way to reduce much of the lingering cationic content on the sample surfaces without a significant alteration of the core shell structure. It is clear that this temperature is a good point to use for this because the cationic photoemissions are mostly removed, and that this is a safe temperature to heat to before significant modification of the core-shell structure occurs at temperatures beyond 300 °C.

The above XPS and durability (via CV) plots represent the types of characterizations that are being performed for the sample set, with comparisons made between catalyst supports, overlayer thickness, and other synthesis elements. The goal is to create a thorough understanding of Pt formation and properties for this catalyst architecture, including electronic transfer effects from various supporting cores. Further analysis is found in the next chapter.

CHAPTER 5: CORE-SHELL MONOLAYERS WITH GRAPHENE

Strain-based influences will be the key component for this chapter. In the case where ligand (substrate) effect is weak, the energy of the d-band center of metal overlayers is predominantly affected by the level of coherent strain.[213] Recent trends in catalyst design indicate that strain has to be appreciated as an important material's parameter which could be used to fine-tune catalyst activity and selectivity for particular reactions. Graphene is utilized in a variety of ways to alter the properties of Pt monolayers, both as an inducer of strain when used as a surface template, or as a protective barrier when used as an outer 'cage'.

The effects of alloying along the surface via core-shell interdiffusion are also examined, with property modifications arising from significant temperature effects. Both varying temperatures and varying annealing environments will be considered in examining alloying effects on the Pt-Au system. The goal is to examine how elevated temperatures can modify the architecture. The presence of oxygen, specifically, will also be one of the variables considered, due to known effects on metal interdiffusion.

5.1 Alloying and Interdiffusion

Alloying or layering Pt with Au has been shown to decrease the rate of catalyst poisoning and potentially increase the electrocatalytic activity for reactions like the ORR, as well as decrease the amount of Pt in the catalyst. [34, 98-106]. Surface Pt atoms deposited on properly chosen core metals could have enhanced intrinsic catalytic activity over those on the pure Pt surface, due to the so-called strain and ligand effects.[214] Au

is among the most stable metals shown to impede oxidative corrosion. However, for the electrocatalytic reduction of oxygen in acidic media, high Au compositions can lead to lower mass activities for the ORR.[98] In studies aimed at establishing the correlation between Pt/Au alloying and catalytic activities, a fundamental question is how the alloying and phase segregation can be controlled.[99, 215]

For PEMFCs, operation at temperatures 100 °C or higher can be desirable as it can lead to faster reaction kinetics, facilitate thermal and water management, and result in increased CO tolerance.[216, 217] However, elevated temperatures can lead to issues such as additional membrane and electrode resistance, as well as other electrode problems.[218] With such low loading limits for Pt monolayer catalysts, this study aims to examine the potential effects of temperatures of 100 °C and above on both the architecture of Pt-Au core shell as well as the effect on the activity towards the ORR. Determining how changes in these properties can affect the electrochemical performance is crucial if these architectures are going to be used in PEMFCs at elevated temperatures.

Due to its electronic and structural properties, graphene has been investigated for various catalysis applications.[33, 163, 219-221] Due to its high chemical and thermal stability, graphene has also been examined as a potential membrane for various applications, including selective ion passage,[221] standard gas barriers,[222] and filtration.[223] Graphene has also found success in the microelectronics industry as a diffusion barrier.[224-226] The strong C–C bonding and hexagonal atomic structure of graphene does not lend itself to substitutional atomic migration from many metallic alloys. With a ‘pore size’ of only 0.064 nm, if there is not sufficient thermal energy available, diffusing atoms will not penetrate the graphene barrier and any kinetic energy

will be converted to another form such as lattice phonons.[227] More specifically, single-layer graphene has been shown as a viable barrier to Cu diffusion in circuit technology around 500–900 °C. [224]

This study aims to investigate how elevated temperatures can modify synthesized Pt-Au core-shell architectures grown on both carbon fiber paper (CFP) and glass substrates. The presented study provides an examination of these annealing effects along with the contributions of single layer graphene placed at the core-shell interface, via spectroscopic and electrochemical characterization and ORR reaction probes.

5.1.1 Synchrotron-based XPS

In this study, the ultrathin Pt overlayers are prepared potentiostatically deposited Au on CFP via SLRR. The overlayer Pt atoms and the Au based substrate are first examined via XPS using a tunable light source, effectively allowing a depth profile study to be performed on the core-shell structured catalyst samples. Using a tunable XPS system with low energy incident photons, the chemical states of the Pt and Au can be examined as varying ‘information depths’ of the core-shell structure. This method enables a case study sensitive enough to examine the very surface of core-shell structured samples and allow for the analysis of the thickness-dependent structural features of both Pt overlayers and the underlying Au support. In addition, this study looks at the modifications at the core-shell structure of SLRR developed samples due to metal interdiffusion as a result of elevated temperatures. Heating in the analysis chamber was performed via a thermocouple connection on the sample stage in 15 minute intervals up to 400 °C.

By varying the incident photon energies between 400 and 650 eV on a variety of samples, a comprehensive set of spectra can be obtained regarding the chemical state of the Pt and Au for core-shell style samples as well as alloyed surfaces. A set including a 3, 4, and 5 ML sample were heated to increasing temperatures with an XPS spectra taken after each heating step, examining the state of the Pt overlayer. This annealing was done under vacuum conditions.

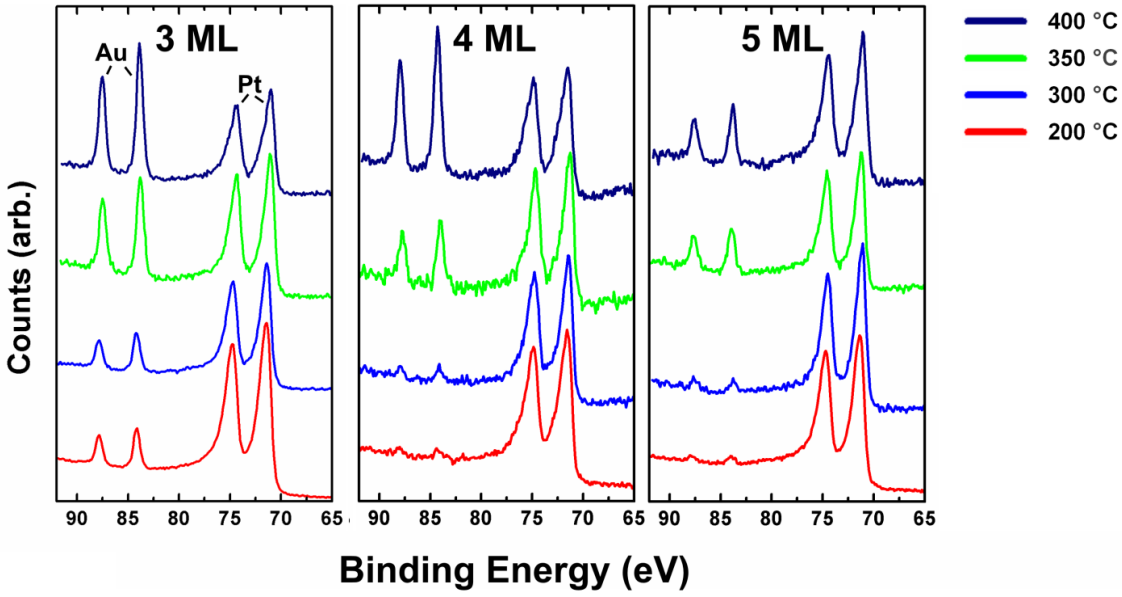

Figure 32: Synchrotron XPS spectra for three samples after each heating step with incident photon energy 400 eV at temperatures of 200 °C, 300 °C, 350°C, and 400 °C in vacuum. a) 3 ML sample b) 4 ML sample c) 5 ML sample

Figure 32 shows the XPS spectra for a 3, 4, and 5 ML samples on CFP taken after each individual heating step with incident photon energy of 400 eV. With regards to Au and Pt matrices, 400 eV corresponds to just slightly more than a half-nanometer of information depth, so the spectra are representative of the top half-nanometer of the sample. Pt is characterized as a 4f electron doublet ($4f_{7/2,5/2}$) at ~71 and ~74 eV, while the

Au 4f doublet is seen at ~84 and ~88 eV.[105] The first notable feature is that the Au photoemission is clearly visible for the 3 ML sample at lower annealing temperatures, whereas the 4 and 5 ML samples' Au photoemission is only marginally visible beyond the noise. This means, at 3 monolayers, selected incident photon energy of 400 eV is still able to penetrate past the deposited Pt overlayer into the Au substrate. However, for the 4 and 5 ML samples, photon energies this low can only provide information of the Pt overlayer; electrons from the underlying Au do not have enough energy to eject from the sample.

For the 4 and 5 ML samples, all Au detected at any temperature must be Au that has diffused into the half-nanometer region where the Pt overlayer resided before significant alteration by heating. However, for the 3 ML sample, it cannot easily be distinguished "bulk Au" to Au that has moved towards the surface, as the information depth proceeds through the Pt shell. However it is still clear by the increase in the Au photoemission that more Au has moved into the top few nanometers as the temperature is increased.

To better understand the Au diffusion, further XPS spectra were taken after the individual annealing steps at slightly higher incident photon energies to alter the information depths of the spectra. By altering the photon energy, it becomes possible to further determine the state of the top surface of these samples. It cannot be assumed that alloy formed at the surface by the in-situ heating is homogenous. Thus, lower energy photon energies can be used to determine the chemical state of the top-most layer of the alloyed surface while higher photon energies will incorporate chemical information slightly deeper into the overlayer.

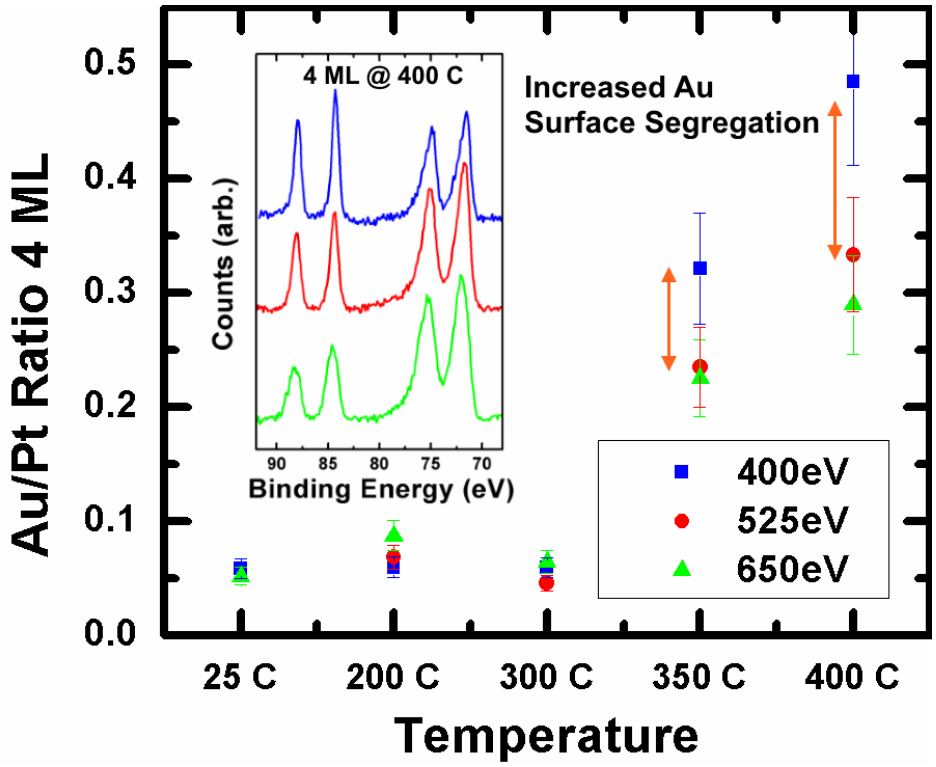

Figure 33: The ratio of the Au photoemission to the Pt XPS photoemission for a 4 ML sample, at 400, 525, and 650 eV. Inset: The XPS photoemission spectra of the 4 ML sample after heating to 400 °C in vacuum.

In Figure 33 the Au and Pt photoemissions for a 4 ML thick sample were fitted at 400, 525, and 650 eV, and the ratio of Au photoemission to Pt photoemission was calculated to quantify the level of diffusion of Au into the information depth region. The peak area comparisons were made via peak fitting using a Shirley background. At temperatures 300 °C and below, the sample's Au photoemission is very small, almost

indistinguishable from background, leading to a small ratio. This is consistent with inelastic mean free path calculations. Up to a temperature of 300 °C, these ratio values do not change significantly, showing that the layer-substrate structure of these samples are relatively unaffected after 15 minutes of heating. The Au/Pt ratio is largely unaffected by higher photon energies in this temperature, as the Au signal is still only barely noticeable even with increased information depths. However, once the samples are heated to 350 °C, the spectra exhibit a significant increase in the Au photoemission, leading to an increased value to the ratio. This shows that the sample now has more Au near the XPS-sensitive surface region. Heating to 400 °C only substantiates this trend, as the surface becomes even more Au rich.

By also examining energies of 525 eV and 650 eV, it can be seen that after heating past 300 °C, these ratios are significantly affected for the 4 ML sample. The 400 eV spectra show a relatively higher amount of Au than the 525 eV spectra which in turn shows a relatively higher amount of Au than the 650 eV spectra. As incident photons of 400 eV are the most surface sensitive, this indicates is that the Au is now largely sitting close to the top of the sample with the former Pt shell now sitting underneath it, at least partially. As higher photon energy results in higher inelastic mean free paths for the emitted electrons, this shows that relatively less Au is being detected at deeper information depths, or inversely, that the surface is especially Au rich. The Au has segregated itself to the top of the sample, making the outer surface of the sample Au-rich. This results warrants further investigation as now the once fully Pt surface has been replaced by a surface of Au.

From the XPS spectra in Figure 33 inset, it is apparent that the Au/Pt ratio is highest at the lowest photon energy and decreases with increasing photon energy. The Au peak doublet is most prominent at low photon energy and its shape decreases as the incident photon energy is increased. This is especially interesting considering at room temperature; very little Au could be detected on the surface at any of these photon energies.

One important thing to note regarding the synchrotron experiments is that the temperature control and measurement was performed only via a thermocouple connection on the sample stage in the beamline sample chamber. While the temperatures listed in Figure 32 and Figure 33 represent the temperatures measured on the stage, they may not accurately reflect the actual temperature the CFP samples experienced inside the vacuum environment. In order to investigate this temperature and atmosphere dependence on these effects more closely, further experiments were performed in non-synchrotron environments, using laboratory XPS and electrochemical characterization.

5.1.2 X-ray Spectroscopic and Electrochemical Characterization

Pt-Au core-shell samples grown on CFP were also heated in both open atmosphere and under Ar in a tube furnace. Examining the effects of elevated temperatures on the core-shell architecture in varying annealing environments is important not only to verify temperature thresholds for diffusion effects, but also because the presence of various atmospheric gases can affect the extent to which diffusion can occur at any given temperature. The presence of oxygen in an annealing atmosphere is noted to facilitate atom transport steps in two-phase boundary reactions.[228] XPS

spectra were obtained for a sample sets consisting of 1, 2, 3, 4, and 5 ML thick Pt overlayers before and after heating. The Au/Pt photoemission ratios are shown in Figure 34.

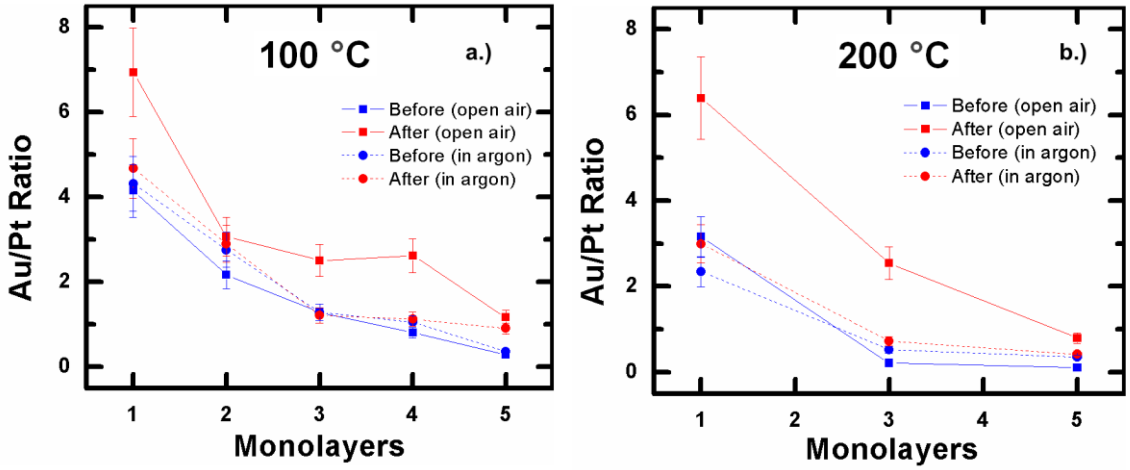

Figure 34: The ratio of Au to Pt of XPS photoemissions of Pt-Au-CFP samples before and after heating for 15 minutes in open air and under Ar at temperatures: A.) 1, 2, 3, 4, and 5 ML at 100 °C B.) 1,3, and 5 ML at 200 °C

Figure 34 shows the Au/Pt photoemission ratios for CFP based samples heated to 100 °C and 200 °C in both open atmosphere and under Ar for 15 minutes. A higher Au/Pt ratio indicates a higher presence of Au seen in the XPS spectra along the surface of the Pt monolayer catalyst. Figure 34a shows how in an open environment, the presence of Au in the monolayer shell notably increases even when only heated to 100 °C, which was not seen in the vacuum studies in Figure 32 and Figure 33. Removing oxygen from the annealing atmosphere, by heating under Ar, shows that the Au/Pt ratio remains more intact. At 200 °C, as seen in Figure 34b, the Au/Pt ratio is even further increased, with samples heated in Ar also showing diffusion of substrate Au into the Pt overlayer.

To further investigate the catalyst surface, the Pt coverage of samples was also examined via CV. Similar to experiments in the previous chapter, voltammograms were conducted in N_2-saturated 0.1 M H_2SO_4 by sweeping from -0.2 to 1.5 V at a scan rate of 20 mV/s. The results for the 4 and 5 MLs can be seen in Figure 35. CV is a surface-sensitive technique where the currents seen are generated from reactions at the metal−electrolyte interface. Changes in Pt surface area can be tracked by either the Pt oxide reduction feature near 0.45 V or the hydrogen adsorption/desorption curve from -0.2 to 0.0 V against an Ag/AgCl reference electrode. Similarly, the presence of a small Au reduction feature at 0.9 V indicates Au along the surface of the CFP-based samples. These methods of tracking Pt coverage on Au have often been employed.[33, 68, 179, 206]

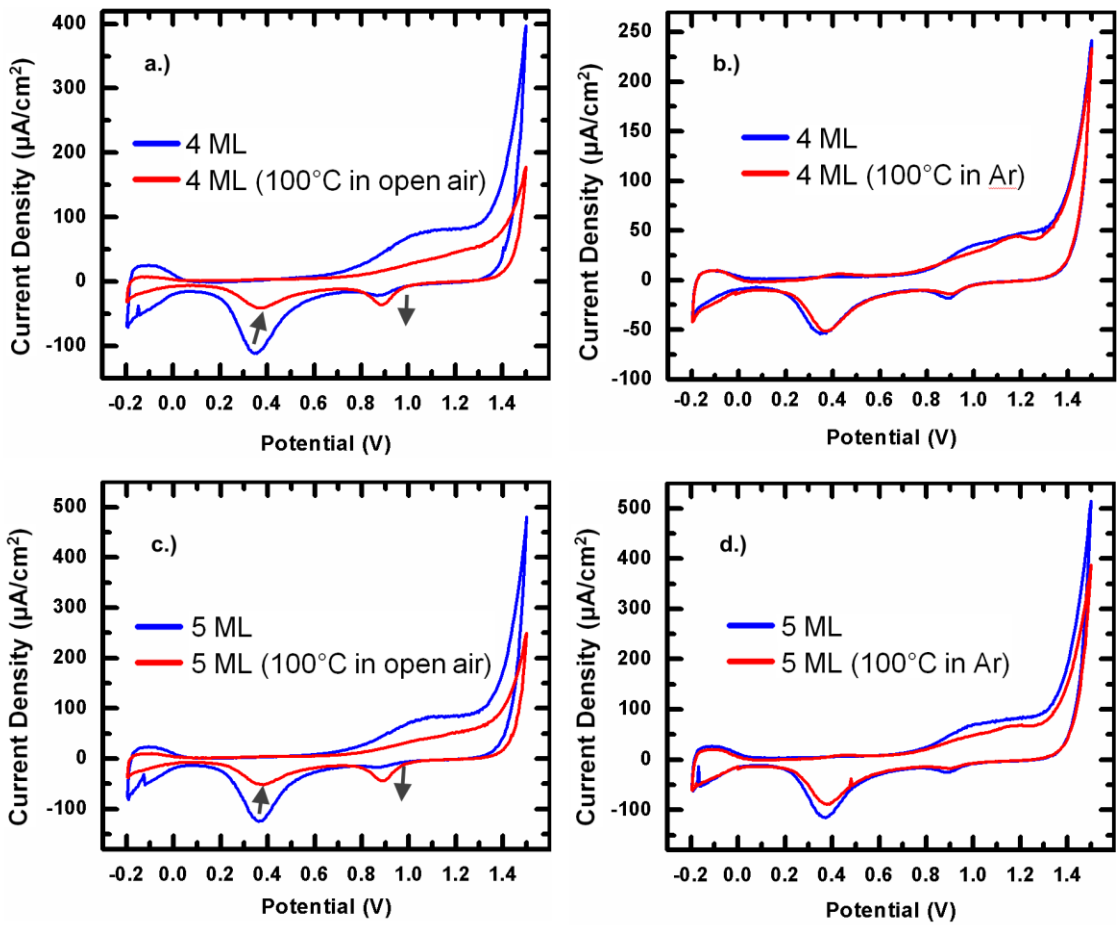

Figure 35: Cyclic voltammograms comparing a 4 and 5 ML sample heated to 100 °C in both open atmosphere and Ar. The surface presence of Pt can be examined by the Pt oxide reduction current at .45 V or the H adsorption curve at -.2 V. Potentials are measured against an Ag/AgCl reference electrode. a.) 4 ML in open air b.) 4 ML in Ar c.) 5 ML in open air d.) 5 ML in Ar

The CV voltammograms show results that agree with the XPS data shown in Figure 34. In an open environment, the Pt features both diminish dramatically after heating to 100 °C. This Pt decrease is accompanied by an increase in the Au reduction feature, once again showing presence of Au closer to the surface of the samples after exposure to higher temperatures. When heated under Ar, the Pt-Au architecture is able to

mostly maintain itself at 100 °C. At 200 °C, the Pt loss in open air is even more apparent. While samples heated under Ar were still able to retain some Pt when heated to 200 °C, CVs indicate a slight amount of catalyst loss (not shown).

When it comes to catalyst performance, the ORR at fuel cell cathodes is a key reaction to investigate. This study aims to see not only how the effects of annealing can modify sample core-shell architecture, but also how raised temperatures affects achieved catalytic currents. ORR performance in acidic electrolyte is highly dependent on the ratio of Au and Pt on the electrode surface. It has been shown that the presence of Au can have a negative effect on catalytic currents in acidic media.[98] In order to investigate this trend with respect to the effect of annealing temperatures, electrocatalytic activity tests were conducted by performing LSV in oxygen-saturated 0.1 M H_2SO_4 at room temperature, from 0.8 to −0.1 V, in order to analyze the catalytic activity towards the ORR.[180]. The current densities of the generated ORR were measured at -0.1 V and recorded in Figure 36.

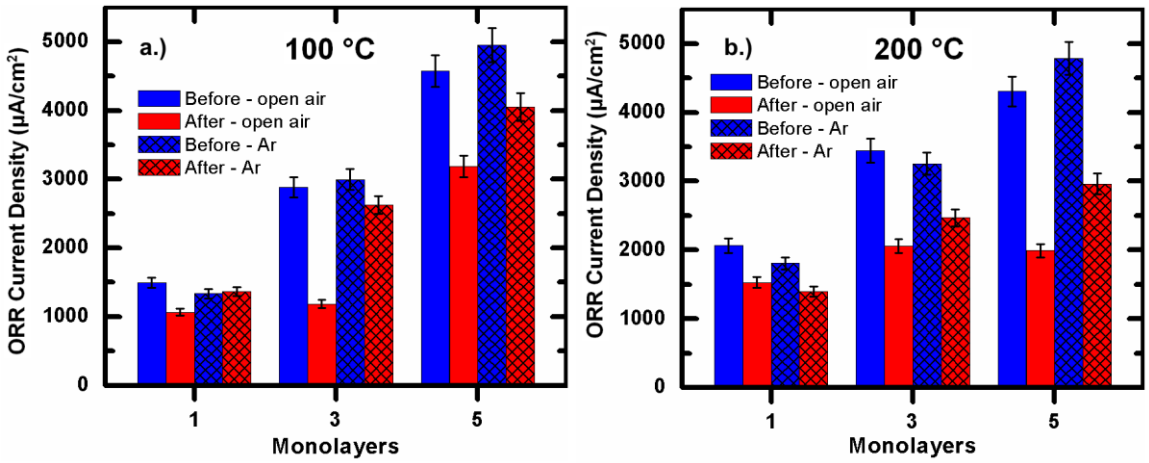

Figure 36: The ORR current densities measured at -0.1 V (vs Ag/AgCl) for Pt-Au core-shell samples on CFP before and after annealing in open air and Ar at a.) 100 °C and b.) 200 °C

Figure 36 shows the ORR currents achieved during LSV experiments for CFP based catalysts heated to 100 °C and 200 °C in both open air and Ar. As seen in Figure 36a, reaching temperatures of 100 °C in air has shown to have dramatic effect in lowering the ORR current as seen in the solid-filled bars. Samples annealed in Ar, despite showing little change in XPS and CV characterizations as seen in Figure 34 and Figure 35 respectively, also show a decrease in ORR currents after annealing. At 200 °C, as seen in Figure 36b, all samples show a significant decrease in ORR current density regardless of annealing atmosphere. As an example, the 5 ML sample annealed in Ar showed about a 40% decrease in ORR current density.

Finally, local atomic structure around an average Pt atom was investigated using EXAFS synchrotron methods for the Pt shell, both as-prepared and annealed. In Figure 37, the R-space spectra for Pt-Au-CFP samples with a 3 ML thick Pt surface can be seen with three annealing conditions: as-prepared, annealed to 200 °C in open air, and annealed to 400 °C in open air. The y-axis in the plot is proportional to a weighted partial radial distribution function around an average Pt atom. Pt foil is known to exhibit an apparent nearest neighbor (*nn*) distance of about 2.2 Å, which is actually at a Pt-Pt bond distance of 2.78 Å when corrected for the phase shifts of the electron waves in XAS.[33]

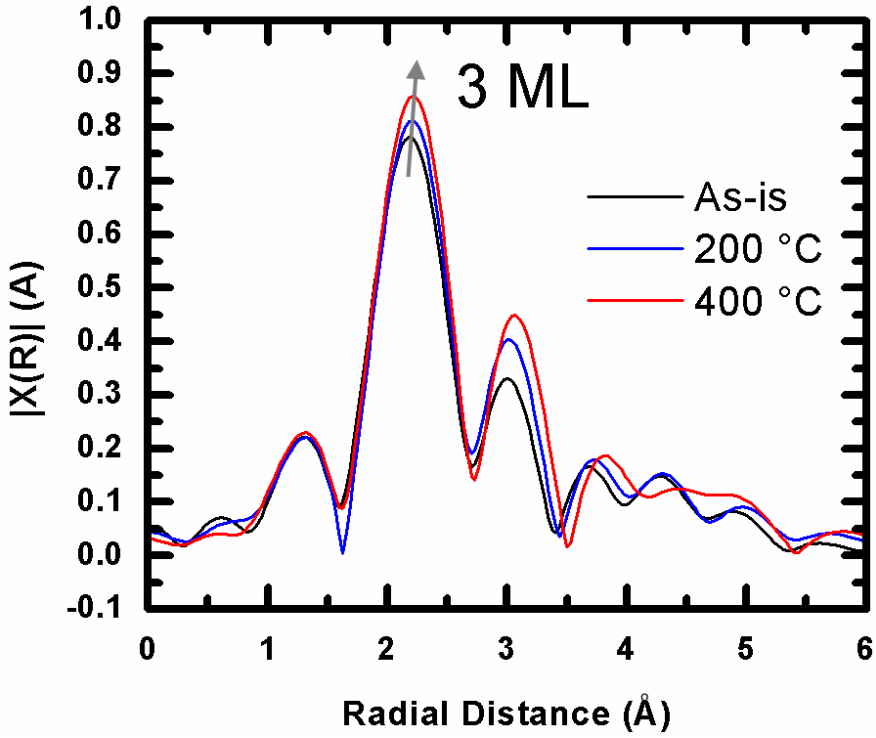

Figure 37: EXAFS spectra of 3 ML Pt-Au-CFP samples as-is, annealed at 200 °C, and annealed at 400°C in open air.

One key result can be seen in Figure 37. The *nn* peak shifts from its original position to higher radial distance as a function of temperature. This can be attributed to Au diffusing into the Pt regime of the core-shell architecture, where Pt can be expected to no longer be only bonding with other Pt atoms, but with Au atoms as well. The Pt-Pt bond is known to be 2.78 Å while a Au-Au bond is slightly larger at 2.88 Å.[229] The positive shift of the *nn* peak can be explained by multiple Pt-Au bonds being made in the Pt overlayer, confirming the expected diffusion of Au as also indicated by both XPS and CV methods.

5.1.3 Graphene as a Diffusion Barrier

XPS, CV, and EXAFS results on CFP based samples all show how Pt monolayer catalysts exhibit Pt/Au interdiffusion at temperatures less than 200 °C, especially when annealed in normal atmosphere. ORR data shows how this mixing of Pt and Au has detrimental effect on the ORR activity of the catalyst system, perhaps due to loss of the beneficial ligand effect when the architecture is modified away from a core-shell configuration.[91, 123] In attempt to mitigate such effects caused by elevated temperatures, this study synthesized catalyst architectures incorporating single layer graphene at the Pt-Au interface in order to examine its effectiveness as a barrier. Diffusion in 3d metals occurs largely by substitutional diffusion, which is dominated by the concentration of vacancies. Strong C–C bonds and the hexagonal atomic structure of graphene does not lend itself to substitutional atomic migration from the large atomic diameter metallic alloys used in many technologies, including microelectronics.[227]

Two Pt/GR/Au samples on glass were synthesized, one with a Pt overlayer thickness of 4 ML and a second with an overlayer thickness of 6 ML. The Au/Pt photoemission ratios were taken via XPS and the results are shown in Figure 38.

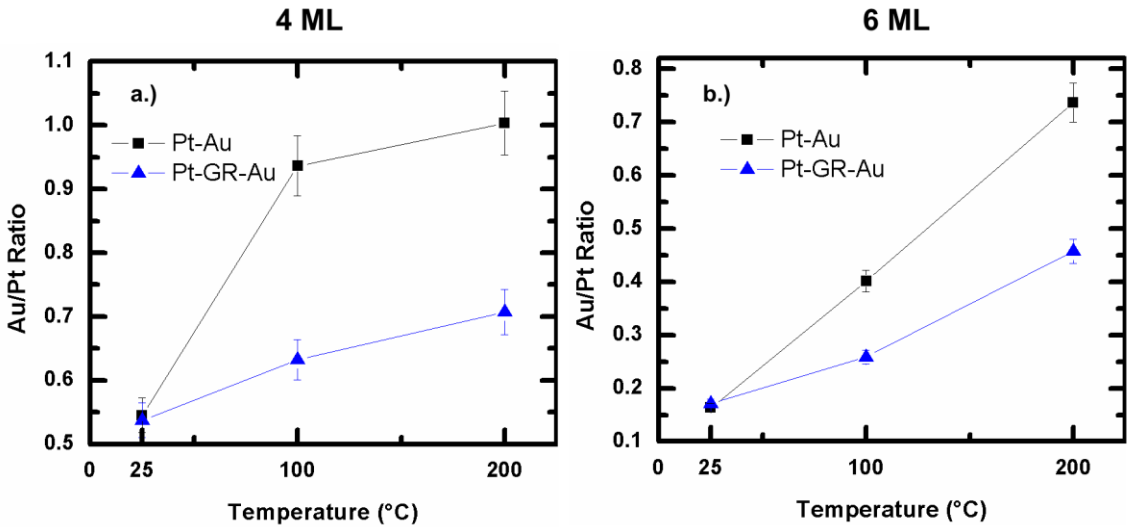

Figure 38: Au/Pt XPS photoemission ratios at 25 °C, 100 °C, and 200 °C in open air for Pt/GR/Au samples a.) 4 ML b.) 6 ML

Figure 38a and Figure 38b show the Au/Pt photoemission ratios as a function of annealing temperature for Pt-GR-Au samples with a 4 ML thick surface and a 6 ML surface, respectively. The presence of graphene at the Pt-Au interface clearly displays a lower Au/Pt ratio, given by the blue triangles in the figure, indicating a reduced amount of Au diffusion into the Pt shell. While a single layer of graphene does not prevent diffusion completely, it is shown to be effective is mitigating Au transport.

The extent to which single-layer graphene may be able to successfully prevent diffusion has been shown to be dependent on its average grain size, where larger grains are more effective as a barrier than smaller grains.[224] With more careful selection of larger grain sizes in graphene, it's likely the amount of diffusion seen would be lowered even moreso than what has been shown.

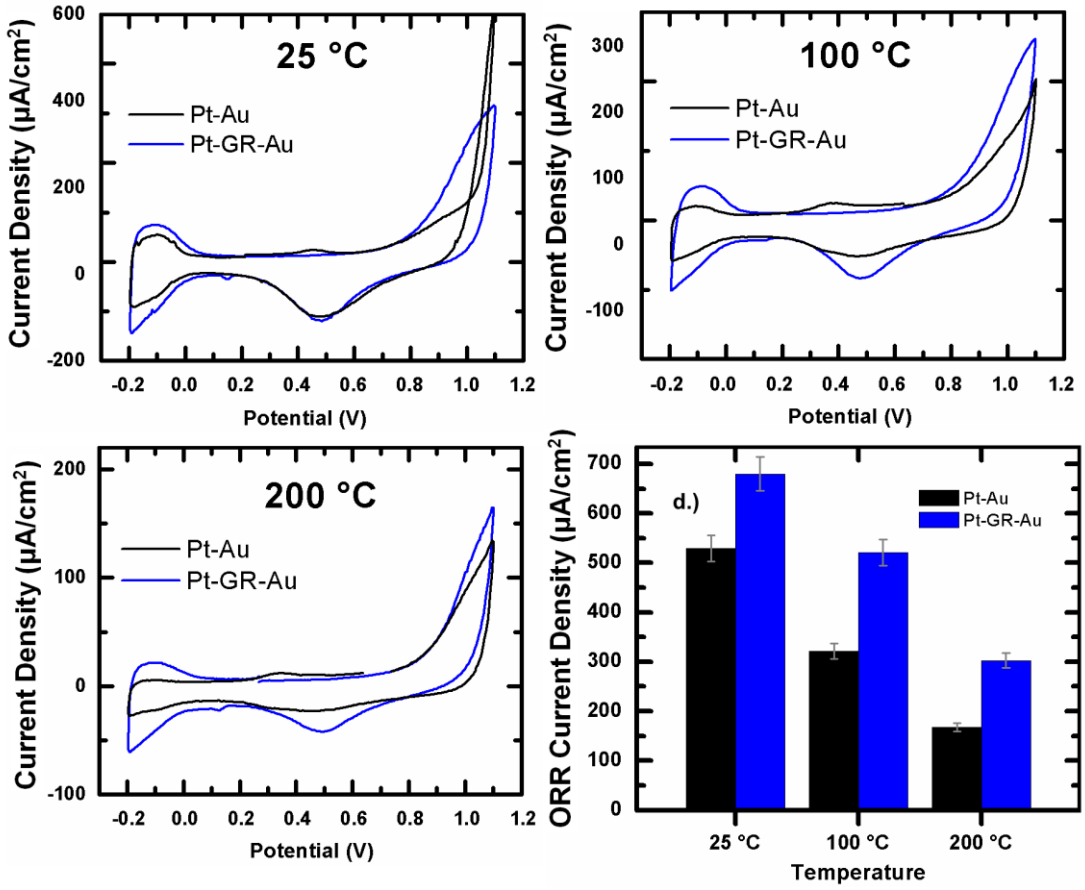

Figure 39: CV comparing Pt-Au and Pt-GR-Au voltammograms at room temperature, 100 °C, and 200 °C respectively. d.) ORR current densities achieved by LSV measured at 0.3 V.

Electrochemical techniques were also used to evaluate the Pt/GR/Au samples. Figure 39a-c show CV experiments conducted in N_2-saturated 0.1 M H_2SO_4 from -0.2 to 1.1 V at a scan rate of 20 mV/s. When comparing the size and shape of the Pt oxide reduction feature at ~.45 V and the H adsorption shape at -0.2 V at room temperature, it can be seen that Pt/Au and Pt/GR/Au samples show similar voltammograms. At 100 °C and 200 °C, both Pt related currents are diminished for Pt-Au samples in comparison to

Pt/GR/Au catalyst architectures. Figure 39d shows the achieved ORR current densities for Pt-GR-Au samples, measured at 0.3 V during LSV sweeps in O_2-saturated 0.1 M H_2SO_4. Before any annealing is done, Pt-GR-Au architectures show higher achievable current densities, a result that aligns with previous research done by this group.[33] However, the ORR currents diminish after annealing in both cases, indicating other annealing effects can alter the surface activity other than significant alteration of the catalyst architecture. It's possible that elevated temperatures can lead to coalescence or island formation of the Pt shell, lowering its surface area and subsequently reducing its activity towards catalyzing the ORR, even if Au diffusion itself has been mitigated.

This study presents careful characterization of surface alloyed nanostructures with respect to the relative core/shell compositions and activity towards the ORR, using electrochemical and x-ray spectroscopic methods. At operating temperatures of 100°C and above, there is potential for interdiffusion to occur between the primary and support metals of bimetallic core-shell catalyst systems. Single-layer graphene sheets have the potential to transform these architectures and prevent unwanted surface alloying between layered metals. The results shows that by incorporating graphene at metal-metal interfaces, diffusion effects of metal catalyst constituents can be reduced and is worth further exploration.

5.2 Graphene-Templated Pt Monolayers

The study also embodies a systematic examination on the effects of graphene when incorporated into core−shell Pt monolayer catalysts, and explores the dimensional

aspect of structure-driven surface properties of metal monolayers grown on a graphene/Au template.

5.2.1 Sample Preparation

In this study, Pt monolayers are synthesized on Au (111) thin films supported on glass substrates. In order to examine the effects of graphene, two sample sets were synthesized. The first sample set had Pt overlayers directly deposited via SLRR on top of the Au. The second set consists of having monolayer graphene first transferred onto the Au/glass followed by the SLRR growth of Pt overlayers. These sets will be referred to as 'Pt/Au' and 'Pt/GR/Au' samples, respectively. A schematic of these designs are shown in Figure 40.

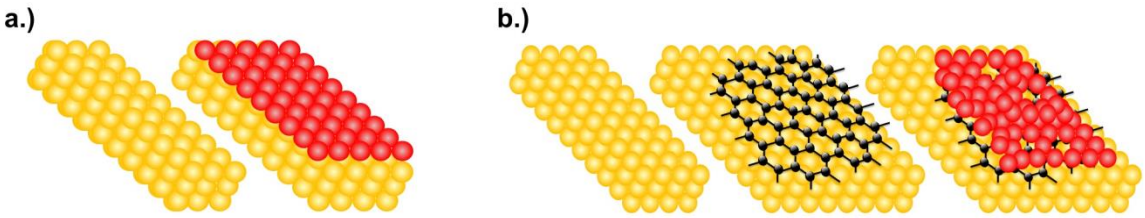

Figure 40: a.) Represents Pt/Au samples, where Pt is grown directly on a bare Au substrate by SLRR. b.) Represents Pt/GR/Au samples, where graphene is first transferred on top of the Au substrate before Pt deposition by SLRR.

Pt monolayers were grown by SLRR using UPD Cu as a sacrificial metal - a method supported by several fundamental studies.[196, 197] This growth method not only greatly reduces the Pt loading as compared to bulk potentiostatic Pt growth but also provides high dispersion of Pt. For Pt/GR/Au samples, Cu is expected to form relatively

large separated clusters with low island density.[164] A total of ten sample configurations were prepared for this study: 1, 2, 3, 4, and 5 monolayer (ML) thick surfaces for both Pt/GR/Au samples and Pt/Au samples. Although the sample synthesis method is the same for each sample type, for samples on graphene specifically, as full Pt wetting cannot be assumed at all times. In order to denote differences in assumed overlayer formation between the sample sets, these Pt/GR/Au samples will be referred to as 'monolayer equivalent' (ML-eq) rather than pure monolayers.

5.1.2 XPS and CV Characterization

The Pt surface coverage of samples was examined via CV. Voltammograms were conducted in N_2-saturated 0.1 M H_2SO_4 by sweeping from 0 V to 1.2 V at a scan rate of 20 mV/s. The results for 2, 3, 4, and 5 MLs for both sample sets can be seen in Figure 41. The presence of a small Au reduction feature at 0.9 V indicates when Pt deposits are not fully masking the underlying Au.[68, 179, 206]

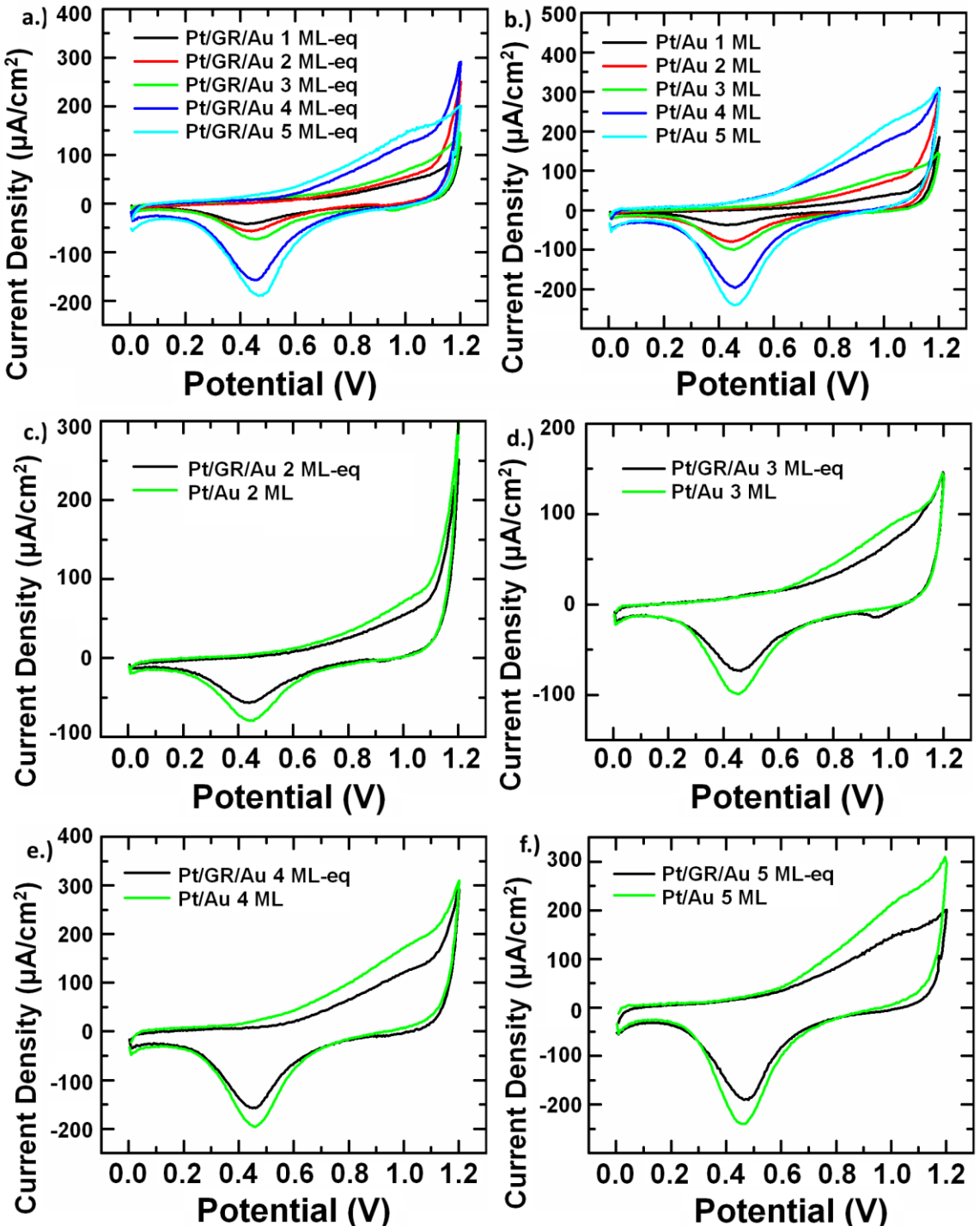

Figure 41: Cyclic Voltammograms for a.) Pt/Au samples b.) Pt/GR/Au samples, c-f.) 2, 3, 4, 5 ML samples respectively, comparing samples with graphene to those without. CVs were performed in N^2-saturated 0.1 M H_2SO_4. Voltages are referenced to a Ag/AgCl electrode.

From Figure 41a and Figure 41b, it is clear that the total surface coverage of Pt increases with SLRR iterations in both sample cases. Figure 41c-f shows that Pt/GR/Au consistently exhibit a smaller Pt oxide reduction current density when compared to Pt/Au. A small Au reduction peak is seen around 0.95 V for 2 ML-eq and 3 ML-eq Pt/GR/Au samples. This is likely due to the sacrificial Cu layer clustering upon initial deposition and leaving exposed Au in patches on the surface, as mentioned by Liu *et al*.[164] For the Pt/GR/Au samples, a slight increase in the Au feature is seen from 2 ML-eq to 3 ML-eq despite a larger Pt reduction feature. This indicates a further tendency of contraction or clustering of Pt atoms rather than its wetting over Au. Beginning at 4 ML-eq in the Pt/GR/Au case, the Au reduction peak disappears in CV, which indicates an eventual total coverage of Pt over graphene. This observation proves that an ultra-thin layer of Pt at 4 ML-eq (1-2 nm thick) was able to fully mask the graphene/Au substrate. To this study's knowledge, this is the first reported full coverage of a metal on graphene at such low dimension over macroscopic surfaces areas. Pt/Au do not exhibit a Au reduction peak in CV even at 1 ML, which indicates that the Au must be fully masked by a wetted Pt layer by the first monolayer.

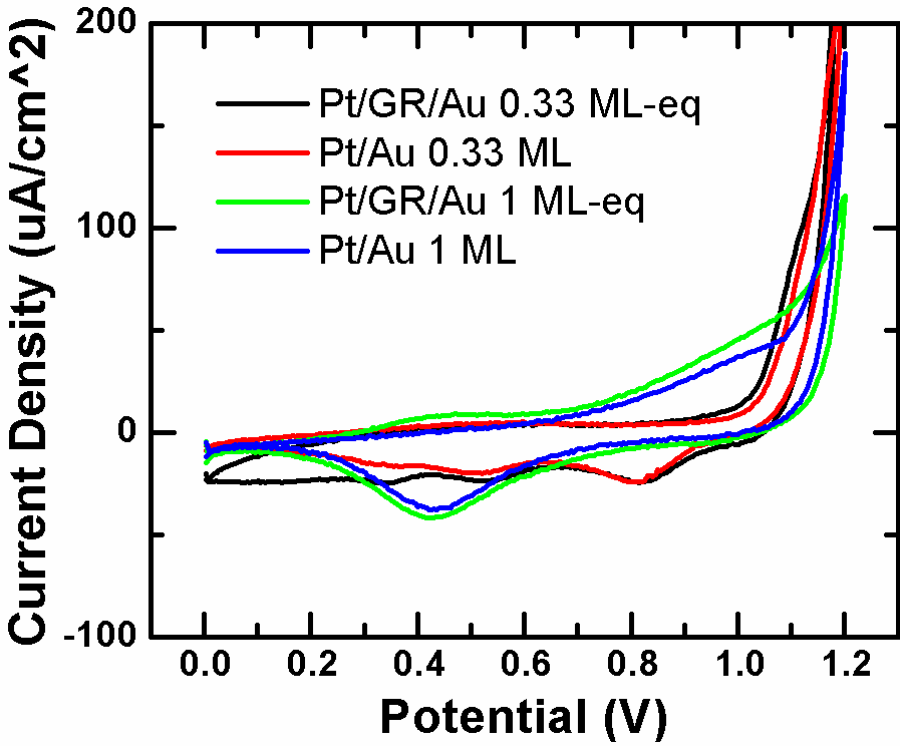

Figure 42: Cyclic Voltammograms for 0.33 ML and 1.0 ML coverages for Pt/Au and Pt/GR/Au samples. CVs were performed in N^2-saturated 0.1 M H_2SO_4. Voltages are referenced to a Ag/AgCl electrode.

CVs of submonolayer coverages of Pt were also taken for each sample case, and can be seen in Figure 42. For both Pt/Au and Pt/GR/Au, having undergone only a single SLRR iteration (nominally 0.33 MLs of Pt), a clear Au reduction feature can be seen. This shows that the Pt overlayer insufficiently covers the surface of the substrate and that the presence of Au can be seen when exposed to solution. There is verification, therefore, that the absence of a Au reduction feature is indicative of a fully wetted Pt overlayer at 1 ML coverage.

In addition to characterization by cyclic voltammetry, synthesized samples were also examined using XPS in order to determine the chemical state of the overlayer. In

Figure 43, Pt is represented as a 4f electron doublet ($4f_{7/2,\ 5/2}$) at ~71 eV and ~74 eV, while the Au $4f_{7/2}$ photoemission is seen at ~84 eV.[105] Due to the surface sensitive nature of electron photoemissions, the relative peak size of the Pt $4f_{7/2}$ photoemission to that of the Au $4f_{7/2}$ photoemission is related to the average thickness of the surface shell. Figure 43 shows that, for both sample cases, Pt $4f_{7/2}$ grows in intensity relative to the Au $4f_{7/2}$ when more Pt monolayers are deposited on the surface.

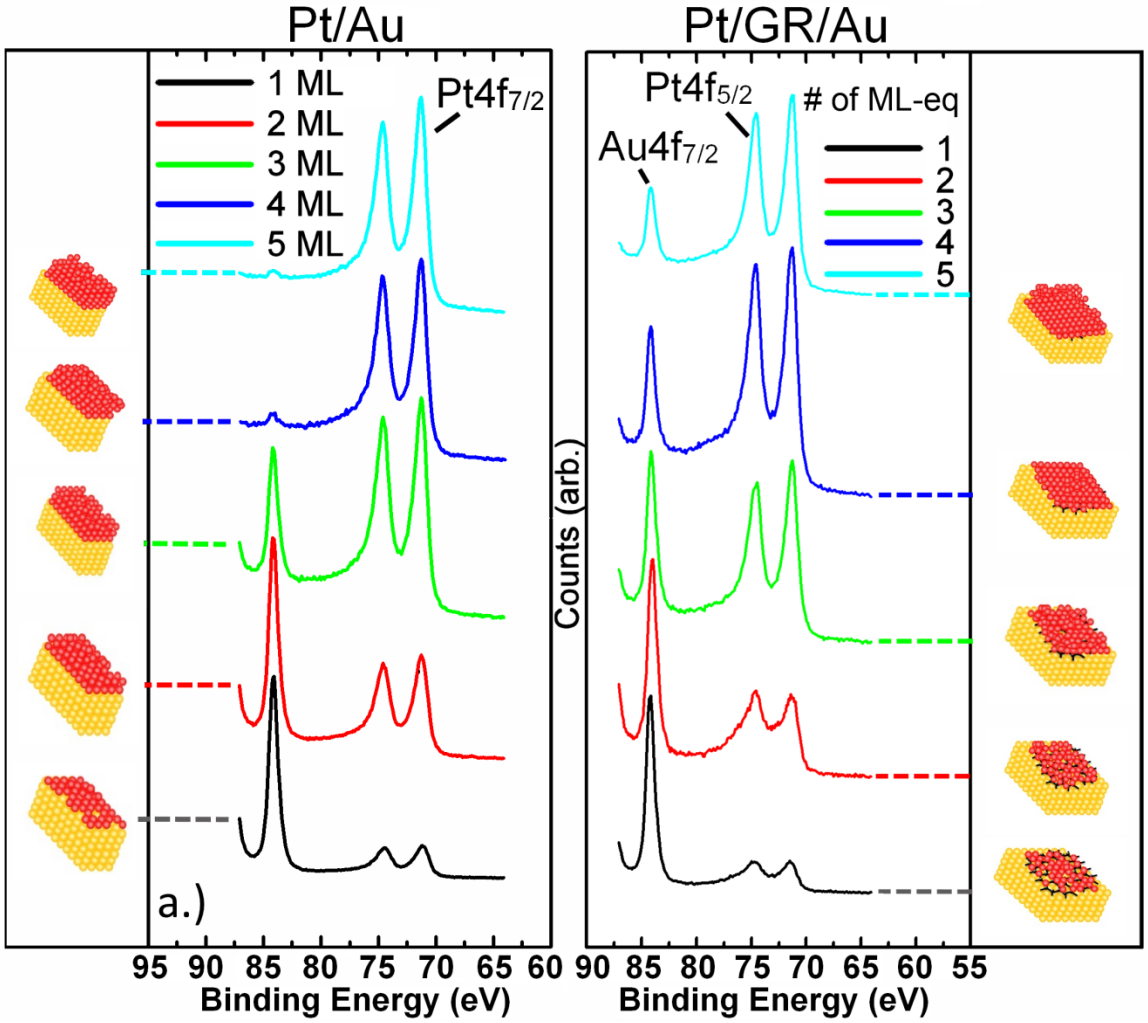

Figure 43: X-Ray Photoelectron Spectra of Pt $4f_{7/2}$, Pt $4f_{5/2}$ and Au $4f_{7/2}$, sequentially shown from low to high binding energy, for a.)1, 2, 3, 4, and 5 ML Pt/Au samples and b.)1, 2, 3, 4, and 5 ML-eq Pt/GR/Au samples. Sidebars show expected sample architecture of grown Pt overlayers.

However, the intensity increase is not growing at the same rate between the two sample sets. When comparing the 4 ML and 5 ML samples, the Au photoemission is almost completely masked for Pt/Au. This indicates that there are very few core electrons from Au that are emitted beyond the top few nanometers of the surface. For the Pt/GR/Au samples, the Au photoemission is not fully diminished even at 5 ML-eq. This indicates that more Au is near the surface allowing its bound electrons to be detected. This could be due to a relatively thinner Pt overlayer in some regions that allow more Au 4f electrons through than in the graphene-free case. The peak area between Pt and Au comparisons were made via peak fitting using a Shirley background, and are shown in Figure 44.

Both the CV and XPS results show that growth process is not identical between the two sample cases. Cyclic voltammograms (Figure 41) show exposed Au on the surface for low monolayer Pt/GR/Au samples. XPS results cannot give an indication of surface wetting, but the data shows lower average Pt thickness in the core-shell structure for the Pt/GR/Au samples as evidenced by a less intense Pt photoemission relative to Au. This supports the findings made by Liu *et al*, which expected Cu to form more clustered structures on top of graphene, as SLRR in this case was by depositing Cu first which was replaced galvanically afterwards by Pt. The sidebars on Figure 43 represent the expected surface architecture for the sample set. This study surmises these representations for the samples based on the data achieved and the conclusions made by Liu *et al*. and Dai *et al*.[164, 165]

Figure 44 represents the Pt $4f_{7/2}$ peak area normalized to the Au $4f_{7/2}$ peak areas. It can be seen that Pt/Au samples exhibit a larger relative Pt area and that the difference becomes more pronounced at 4 and 5 MLs. The deviation can be explained in the following way: at 3 ML-eq, the Pt/GR/Au sample undergoes Pt redistribution such that the Au substrate is re-exposed. At 4 ML-eq, the subsequent Pt deposited covers the exposed Au. Thus, while the Pt in Pt/Au continues iterative growth that results in a pseudo-linear increase the ratio of Pt to Au peaks in XPS between 3 and 4 ML, the Pt in Pt/GR/Au deviates from this linearity because of the exposure and subsequent masking of Au from 3 to 4 ML-eq. The re-exposure of Au between 2 and 4 ML-eq in Pt/GR/Au necessarily implies clustering of Pt. In Figure 44 this region is denoted as the "island growth mode" for Pt/GR/Au. Only once the islands reach a threshold size at 4 ML-eq is a fully wetted layer achieved again, evidenced by lack of a Au oxide reduction peak in CV (Figure 41).

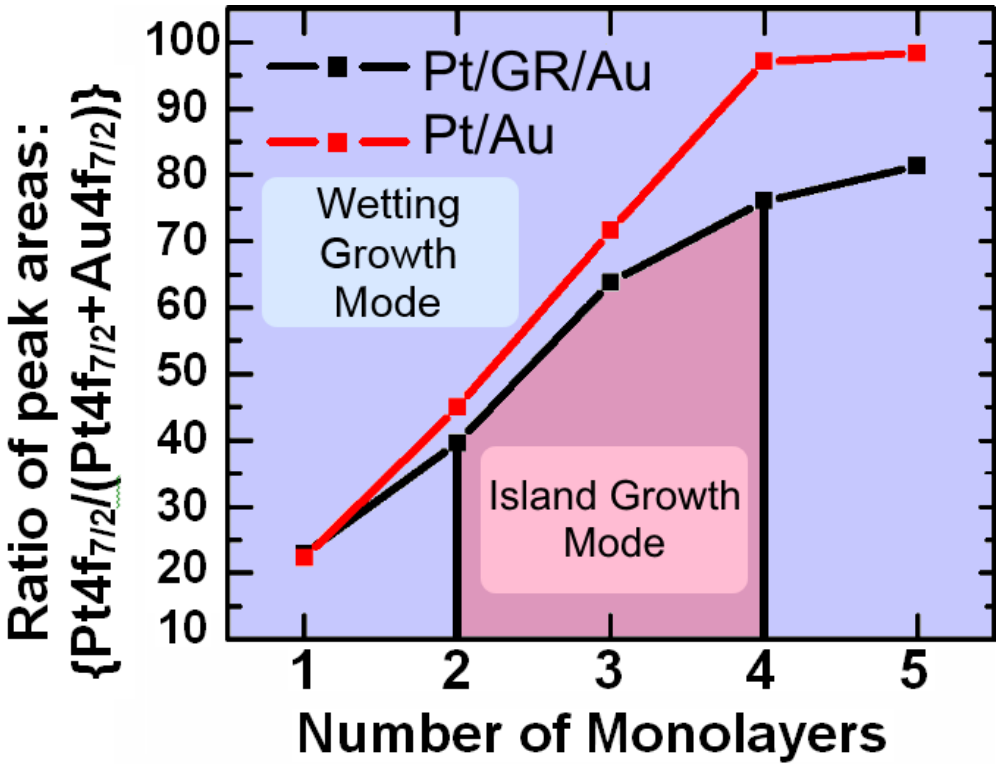

Figure 44: Representation of Pt to Au ratio by comparing the $4f_{7/2}$ peak area of Pt to the total $4f_{7/2}$ peak area of both Pt and Au as a percentage.

5.1.3 X-ray Absorption Spectroscopy of Strained Pt Monolayers

The local atomic structure around an average Pt atom was investigated using EXAFS for Pt adlayers in a subset of the Pt/GR/Au samples. In Figure 45a, the R-space spectra for Pt/GR/Au samples can be seen, as well as spectra for Pt foil. The y-axis in the plot is proportional to a weighted partial radial distribution function around an average Pt atom. Bulk Pt (Pt foil) exhibits an apparent nearest neighbor (nn) distance of about 2.2 Å, consistent with previous work,[68] which is actually at a Pt-Pt bond distance of 2.78 Å when corrected for the phase shifts of the electron waves in XAS. In Figure 45a it can be seen that the 1 ML-eq sample exhibits the nn distance of bulk Pt. This is interesting when considering the preference of Pt to adsorb onto the bridge sites of graphene.[165, 167] A flat, close-packed, Pt layer arrived at by populating every other bridge site with a Pt atom (Figure 45b), would exhibit a Pt-Pt nn distance of 2.14 Å instead of the 2.78 Å (phase shift corrected) nn distance observed. At a 2.14 Å nn distance, the 1 ML-eq Pt film would under a large compressive strain (Figure 45b). One could argue, instead, that this 1 ML-eq Pt film utilizes its degrees of freedom normal to the film plane to buckle, alternately adjusting the Pt-bridge distances and arriving at the 2.78 Å nn average bond length for Pt-Pt (schematically shown in Figure 45a).

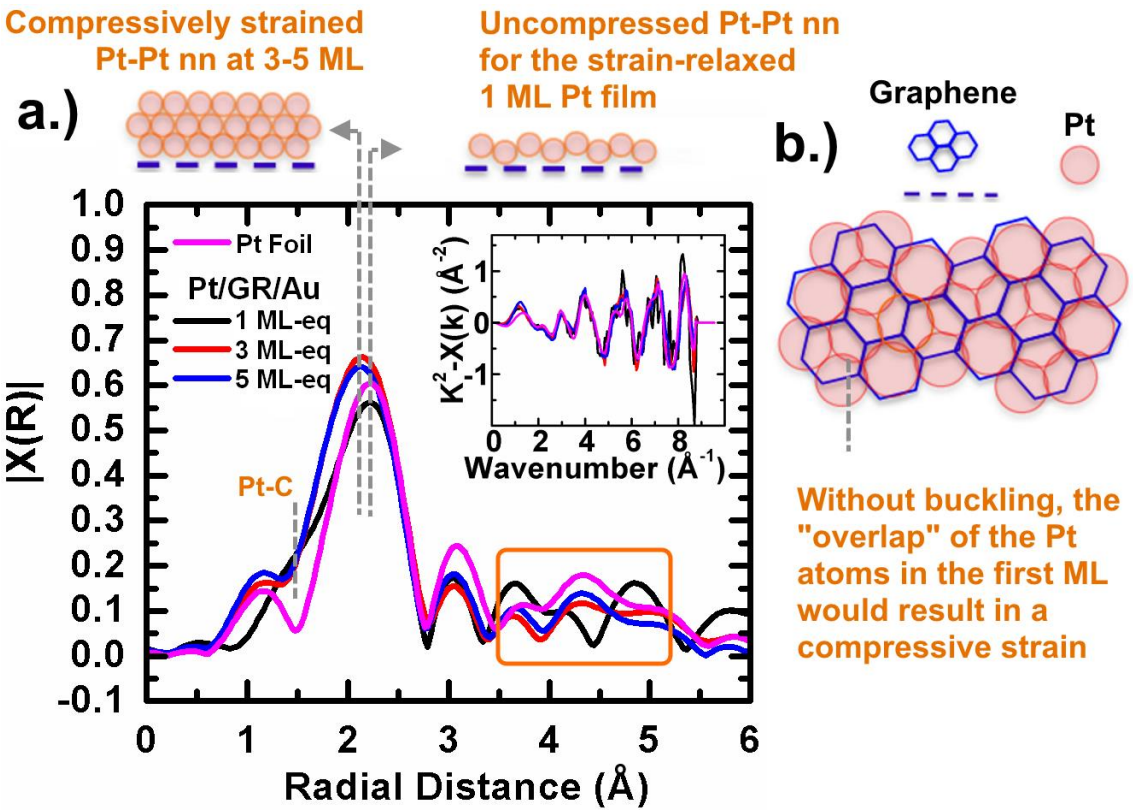

Figure 45: a.) EXAFS spectra for Pt/GR/Au samples of 1, 3, and 5 ML-eq and a Pt foil reference. Inset: The corresponding k-space data. b.) Schematic of Pt atoms on graphene.

The structural similarity between the buckled 1 ML-eq Pt/GR/Au Pt film and the bulk 3D structure of Pt foil is mainly restricted to the Pt-Pt nn bond. The 1 ML-eq Pt film shows a Pt-C peak shoulder at about 1.5 Å, due to its bond with graphene, which is obviously absent in the Pt foil. Furthermore, the long range order of bonding is quite different in comparison, highlighted by the window in the observed 3.5 to 5.5 Å range (Figure 45a). In this R range, the spectra for the reference foil, the nominally 3 ML-eq, and 5 ML-eq samples all line up peak for peak, but the 1 ML-eq case shows a variant long-range order. With only a single layer of Pt atoms, 1 ML-eq film does not have an evolved long range structure resembling that of bulk Pt.

When the Pt overlayer is several monolayers thick and distanced from the underlying graphene sheet, the atoms reject the buckled template of the 1 ML-eq film and instead choose a strained face centered cubic (FCC) structure. While the 3 ML-eq and 5 ML-eq samples exhibit Pt FCC configuration, they however show a ~ 0.1 Å (or about 3.5%) compressive strain in the nn bond. This aligns with previous observations in CV where the Au reduction peak increased at 3 ML-eq. Pt atoms were subjected to more compressive stresses, increasing the exposed Au surface as a consequence. Beyond 3 ML-eq, further addition of Pt retains the compressive stress achieved at the 3 ML-eq stage, but additional Pt begin to fill in the exposed Au spots and maintain a full mask of Pt over graphene, as indicated by CV in Figure 41.

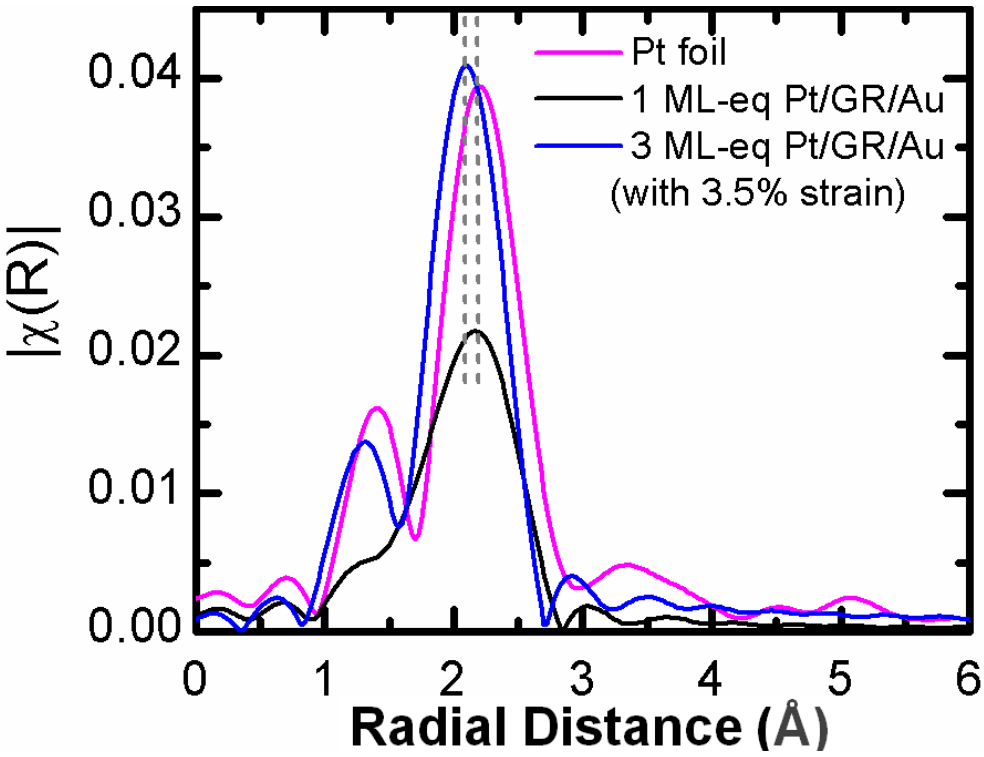

Figure 46: Modeled EXAFs spectra for a 1 ML Pt/GR structure, a 3 ML Pt/GR structure, and bulk Pt foil

Figure 46 shows preliminary modeling for Pt atoms on a graphene support. Simple models were made for 1 ML Pt on graphene, 3 ML Pt on graphene, and bulk Pt. The 1 ML Pt/GR model is unstrained and exhibits 6-fold Pt-Pt coordination and 3-fold Pt-C coordination, representing the average Pt environment for this case. The 3 ML Pt/GR structure incorporates 3.5% compressive strain to the Pt-Pt bond, and Pt-Pt coordination is adjusted to account for the undercoordinated top and bottom layers while Pt-C coordination is added to the bottom layer. A bulk Pt model (12-fold coordination, without strain) is also placed for comparison. This study observes that the positions of the peaks in the models correspond well to the trends observed experimentally, validating the earlier conclusions on the observed compressive strain.

By introducing graphene as a sandwich layer, therefore, the study has effectively created a new Pt-based species, one that has the electronic configuration and atomic structure of bulk Pt, but with higher electron density than due to its inherent compressive strain.

5.2.4 Pt/GR/Au Catalyst Performance

When one looks closer at the Pt photoemission binding energies in XPS, opposing trends emerging between the two sample sets can be seen, shown in Figure 47.

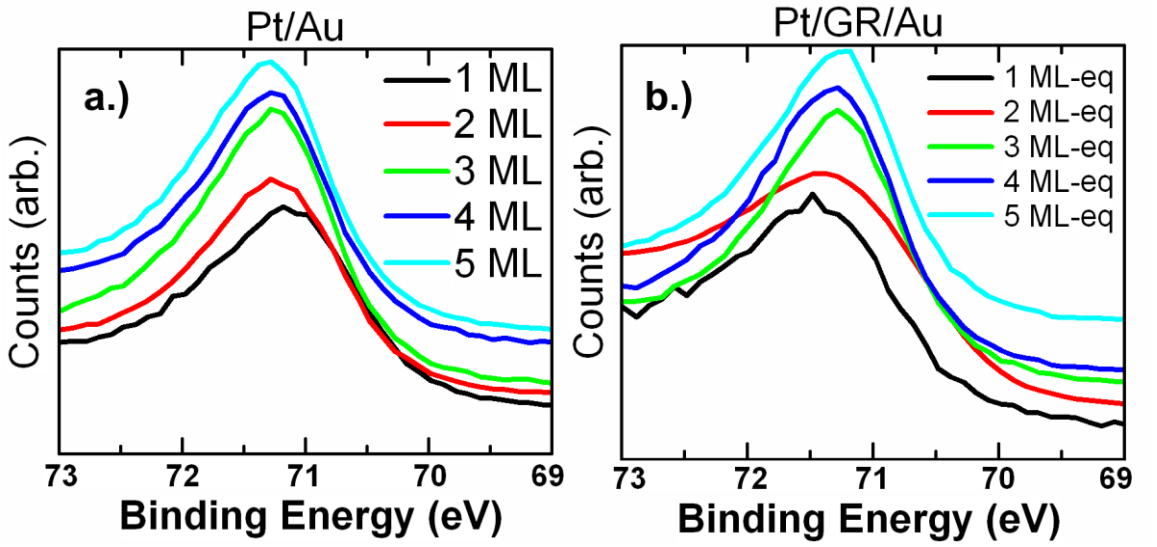

Figure 47: Pt 4f7/2 photoemission from XPS for a.) Pt/Au samples b.) Pt/GR/Au

For Pt/Au samples, the binding energy shifts higher, from ~71.1 eV to 71.3 eV, with increasing overlayer thickness. This trend has been attributed to low-dimensional electron transfer effects from Au.[82] The Au substrate transfers charge to the adsorbed Pt, an effect which diminishes with increasing Pt overlayer thickness. Pt/GR/Au samples instead show a shift to lower binding energy, from 71.3 eV to 71.2 eV. These results are also shown in Figure 49. This study explores next whether these observed shifts in electron binding energy directly influences catalyst performance.

Electrocatalytic activity tests were conducted by performing LSV in oxygen-saturated 0.1 M H_2SO_4 at room temperature, from 0.8 V to -0.1 V, in order to analyze the ORR.[180] The experimental results for each sample are shown in Figure 48. By following the first derivative peak of the ORR polarization curves, the overpotential needed to catalyze the reaction can be measured. Because sweeps are performed in a negative direction, a higher reported potential denotes a lower required overpotential for the ORR. Those results are shown in Figure 48, with potentials reported against Ag/AgCl

reference electrodes. These results compare favorably to other studies utilizing a similar method of evaluation.[230]

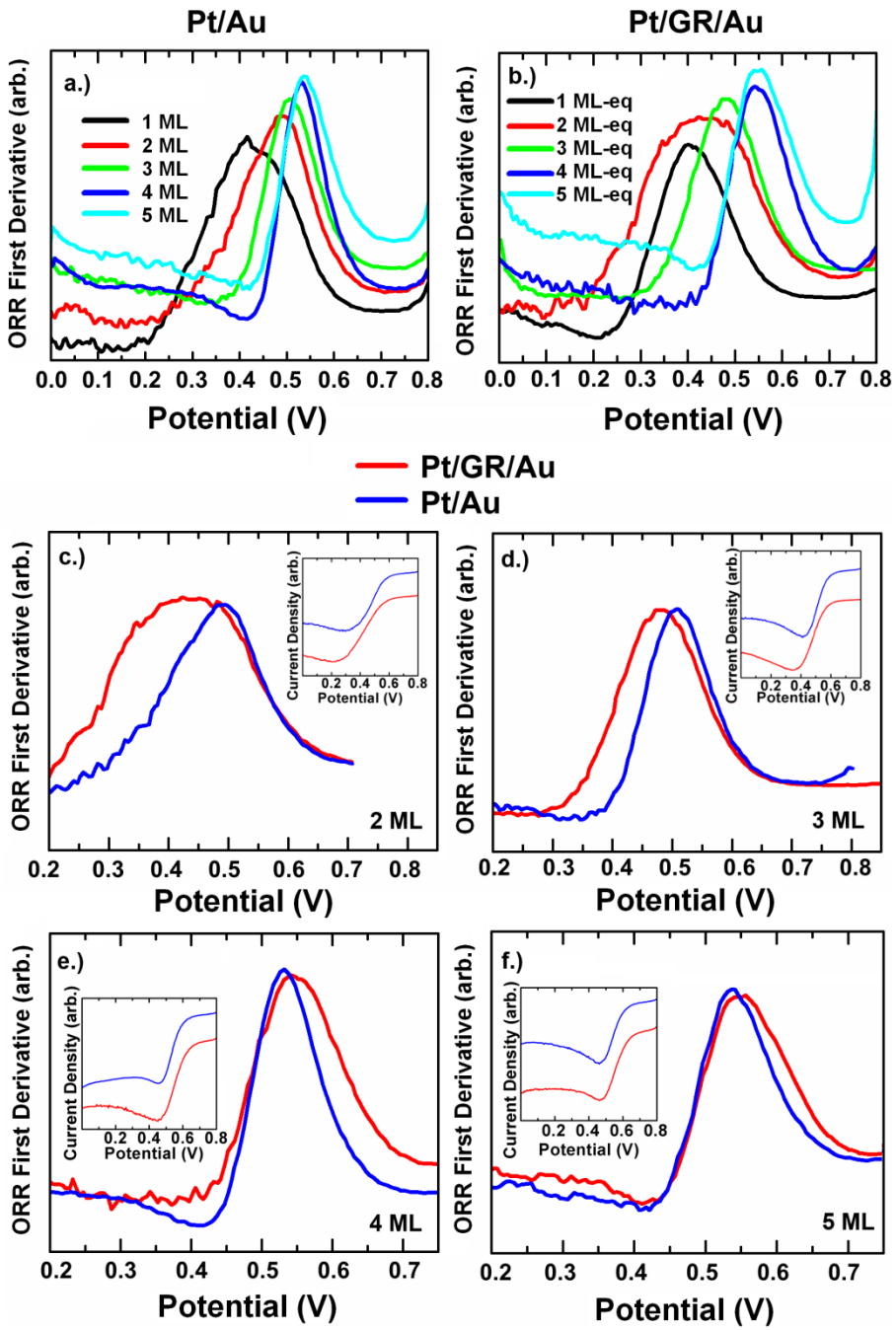

Figure 48: First derivative of oxygen reduction reaction polarization curves (against a Ag/AgCl reference electrode) obtained by linear sweep voltammetry in O_2-saturated 0.1 M H_2SO_4. a.) Pt/Au samples. b.) Pt/GR/Au samples. c-f.) 2, 3, 4, and 5 ML respectively. Insets) ORR polarization curves for each sample pair. The sweep rate is 20 mV/s.

Figure 48 shows that for both sample cases, increasing the number of Pt monolayers results in higher potential values for the inflection point. For the 2 and 3 ML cases, the Pt/Au showed a notably higher ORR potential compared to Pt/GR/Au samples. However, for the 4 and 5 ML cases, the inverse is observed, where Pt/GR/Au samples show higher potentials when compared to Pt/Au samples. In terms of overpotential, the Pt/GR/Au samples demonstrate appreciably lower overpotential required once a sufficient amount of Pt is achieved on the surface. This correlates well with the binding energy values recorded, and a comparison between these experiments can be seen in Figure 49.

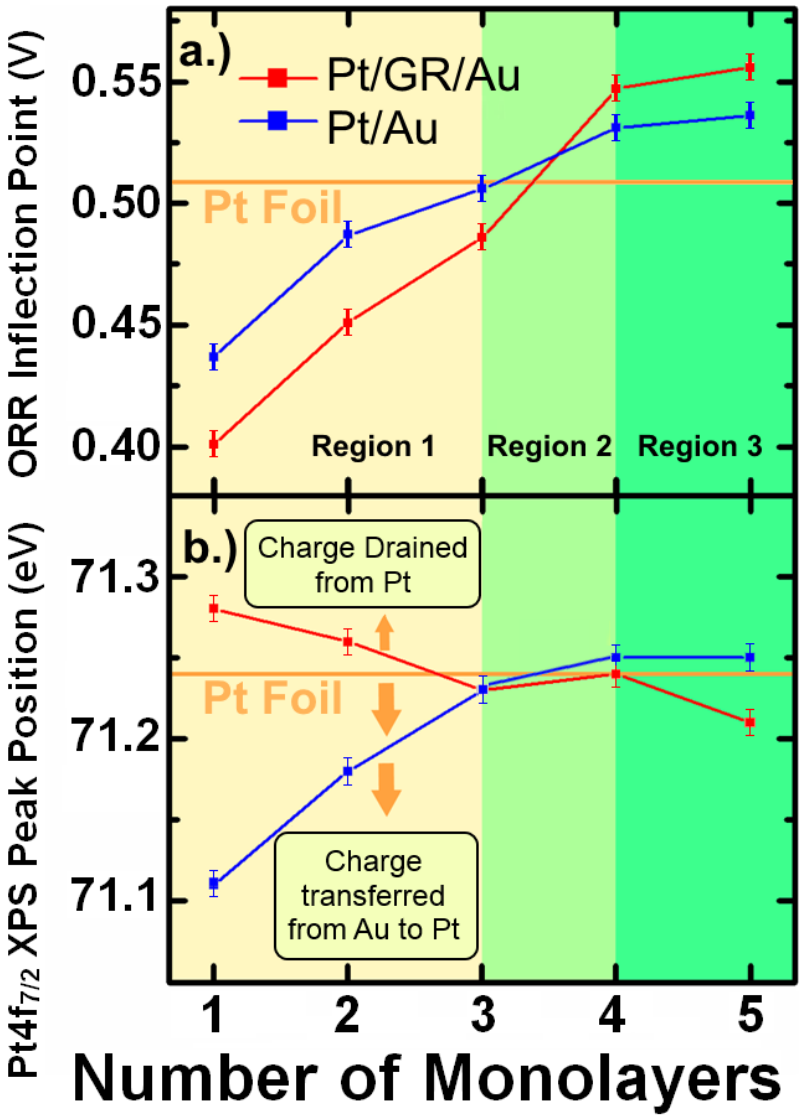

Figure 49: a.) The inflection point of the ORR polarization curves and b.) the Pt $4f_{7/2}$ photoemission binding energy for each sample case. A horizontal line is used to reference the binding energy of bulk Pt foil. Region 1 is explained by charge transfer mechanisms, from Au to Pt in the case of Pt/Au samples, and from Pt to graphene in the Pt/GR/Au case. Region 2 shows where charge transfer mechanisms have significantly diminished into Region 3, where graphene interfacial strain is lowering the binding energy of the Pt overlayer and ORR overpotential surpasses that of bulk Pt.

A convergence and eventual crossover of the ORR potential is seen, as indicated by the polarization curve inflection points. This is represented in Figure 49a. Additionally, as seen earlier in Figure 47, opposite trends in binding energy between the two sample cases can be seen(Figure 49b). In Pt/Au samples, the low-dimensionality of the Pt overlayer allows charge transfer from the underlying Au, causing a negative shift of the core electron binding energy of the Pt monolayers. The data shows a correlation between a negatively shifted binding energy and a diminished ORR potential for these samples. This correlation can be explained by the adsorption of OH- groups on Pt surface. Adzic *et al*. have reported how desorption of OH- species from the catalyst surface is a crucial process in allowing completion of the electronic reduction of O_2 to H_2O.[63] Previous research has shown that OH- species on the surface of a Pt shell less than two MLs thick require more energy to be removed than from a bulk Pt surface.[82] This supports the ORR observations here for the present sample set, where the ORR potential is lowered due to an increased Pt-OH adsorption. This conclusion also matches well with other studies done with similar Pt catalysts.[179] As the overlayer thickness grows, this low-dimensional effect diminishes, resulting in a binding energy which increases to that of bulk Pt as the net charge transfer approaches zero.

In Pt/GR/Au samples, Pt overlayers of low ML thickness exhibit increased binding energies in comparison to Pt/Au. This is seen in Region 1 of Figure 49. This binding energy increase can be explained by surface charge calculations for noble metals adsorbed on graphene. Thermodynamically, Pt favors adsorbing on the graphene at the bridge site between two C atoms, as mentioned earlier when discussing the EXAFS data. A Pt atom forms a polarized covalent bond with the C atoms underneath, and pushes

them to move apart from one another. This bonding has been calculated to lower the charge of the adsorbed Pt by 0.108 electrons.[231] With this diminished surface charge, the binding energy of Pt photoemissions in XPS can be expected to be slightly increased as the data shows.

The XPS data indicates that this electron donation from Pt to graphene is diminished with increasing monolayer thickness, and the binding energy decreases to that of bulk Pt foil. Assuming that the unoccupied densities of states in graphene is already saturated by the available electron density from 1 ML of Pt, any additional Pt deposited will diminish the share of electron density transferred to graphene per Pt adatom. Thus, for the Pt/GR/Au sample set, the binding energy of Pt electrons diminishes as the overlayer thickness grows. The binding energies of the two sample sets converge at 3 ML. The plot also shows the convergence of the overpotential point between 3 and 4 ML. These two phenomena are represented by the Region 2. The Pt is no longer donating any electron density once it achieves 4 ML-eq in thickness but is still affected by partially strained early monolayers, which causes a lattice mismatch resulting in increasing the ORR potential.

The 4 and 5 ML samples for both Pt/GR/Au and Pt/Au cases show lower ORR overpotential than bulk Pt foil, as observed in Region 3. The monolayer-scale platinum surface exhibits a higher percentage of close-packed Pt in comparison to that of bulk polycrystalline Pt, resulting from pseudo-epitaxial growth over the respective Au (111) and graphene substrates. The lower the amount of imperfections and the more ordered the Pt surface, the better it can be active towards ORR due to weaker OH- binding. Both the monolayer architectures can be expected to be more ordered and more defect free than Pt

foil. Thanks to a compressed overlayer, as inferred from EXAFS data, it is also clear that 4 & 5 ML-eq Pt/GR/Au samples achieve an additional boost in catalytic aptitude. This strain, caused by the graphene, will cause a decrease of the Pt–OH adsorption energy, further reducing the coverage of OH- species on the surface that inhibit the oxygen reduction.[69]

5.2.5 Catalyst Durability

One of the major requirements for an effective catalyst is its durability. Earlier efforts looked to using carbon support materials, such as carbon black, in order to enhance Pt retention.[232] While some improvement of catalytic activity was achieved, the durability of Pt catalysts remains a critical issue. Graphene has already been shown to improve catalyst durability in a variety of configurations.[21, 233, 234] This study investigated the durability of the synthesized graphene supported Pt ML catalysts by cycling in acidic media.

Samples were cycled long-term from 0.4 V to 0.75 V in oxygen-saturated 0.1 M H_2SO_4, with a total of 1000 cycles performed on each sample. A characterization CV curve from 0 V to 1.20 V was taken in nitrogen-saturated 0.1 M H_2SO_4, once before cycling and once after 1000 cycles in order to examine the changes in the Pt reduction shape. By measuring the integrated Pt reduction charge before and after cycling, an illustrative representation of the amount of surface coverage of Pt remaining on these samples can be obtained. This is shown in Figure 50, where total Pt retention is displayed as a percentage its original integrated area. For the 1 ML-eq Pt/GR/Au sample, the Pt reduction curve reduces more than 50% after 1000 cycles, showing low durability for the

overlayer and is consistent with previous Pt monolayer experiments. This could be due to the unevolved metallic bonding of the 1 ML Pt film. The 3, 4, and 5 ML-eq Pt/GR/Au samples retain Pt much more strongly than 1 ML-eq, although there is still about a ~25% loss in electrochemically active surface area after 1000 cycles.

Pt/Au samples were examined in the same fashion. The 1 ML sample showed improved retention over its Pt/GR/Au counterpart, although it achieves only 50% retention after 1000 cycles. The advantage could be due to better wetting of the initial overlayer. 1 ML Pt/Gr/Au is buckled and should have poorer adherence to GR/Au than its 1 ML Pt/Au counterpart. 4 and 5 ML Pt/Au samples showed improved Pt retention, but remain lower than the corresponding Pt/GR/Au samples. For the 4 and 5 ML cases, Pt/GR/Au showed improved Pt retention relative to Pt/Au with the largest difference (of about 20%) for the 3ML case. The results indicate that loss of Pt is dictated mostly by bonding to other Pt atoms, an effect which is seemingly amplified on the graphene templated Pt due to the compressive strain.

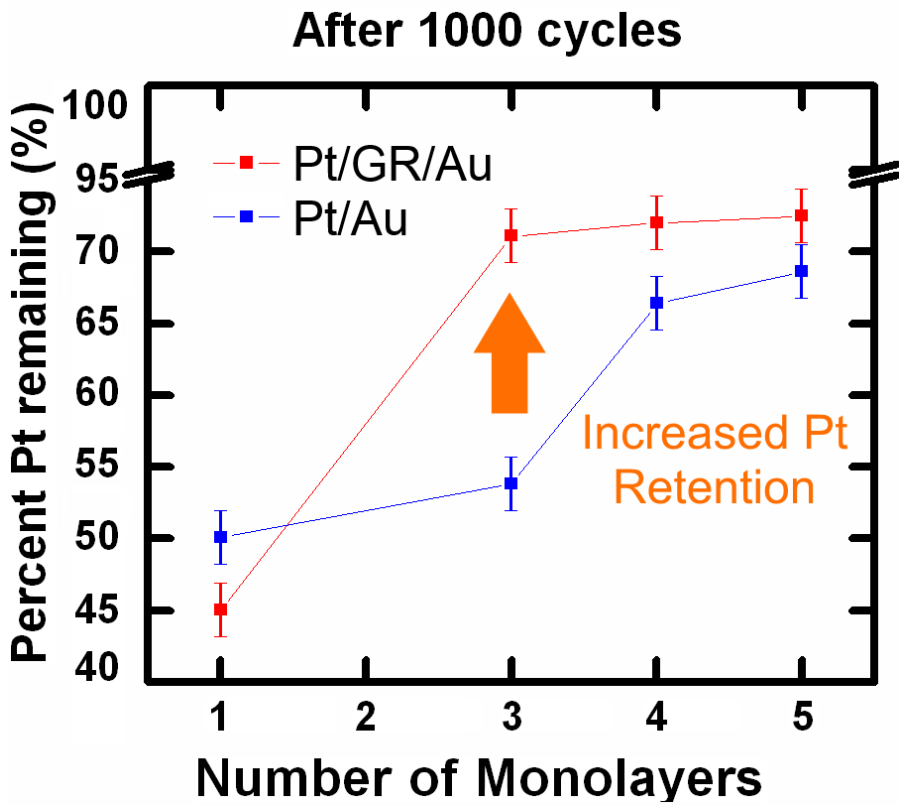

Figure 50: Using the Pt reduction shape in CV, the percentage of surface Pt is calculated after 1000 cycles in acidic media. Cycles were performed from .4 V to .75 V in O_2-saturated H_2SO_4.

5.3 Graphene-Capped Pt Monolayers

A characteristic nature of low-dimensional catalysts materials is an unfortunate activity-stability dilemma. With an increased proportion of surface atoms, lower dimensions increase the density of active sites that, however, are also responsible for decreased stability through transport (loss of active catalyst surface from corrosion and ripening). This study demonstrates a graphene-capped monolayer platinum catalyst (GR/Pt/Au) architecture that transcends this activity-stability compromise by simultaneously exhibiting enhanced activity due to a graphene-induced compressive

strain at theoretical limits of catalyst utilization, while also retaining its full activity beyond 1000 catalytic cycles for the oxygen reduction reaction (ORR). While catalyst surfaces protected by a semi-permeable barrier have been reported in the literature, these reported architectures layers inevitably reduce the activity for critical reactions due to obstruction. Using x-ray photoelectron/absorption spectroscopy (XPS/XAS), Raman and electrochemical methods, this study shows that due to intimate graphene-Pt contact, the GR/Pt/Au hybrids are able to catalyze the oxygen reduction reaction (ORR) through the graphene without any additional energy barrier to the reaction. These results open the door to using a graphene cap on catalysts more broadly as a method to improve catalyst lifetime across a wide range of catalytic reactions.

In a fuel cell, the electrode performance degradation is largely due to electrochemical surface area (ESA) loss, which can either result from catalyst nanoparticles detaching and dissolving into the electrolyte.[20] Another source of performance degradation can stem from poor durability of the carbon-based support.[235] More generally, ESA can also be lost through catalyst particle growth that proceeds through atomic migration between individual particles (Ostwald ripening)[236] and by the subsequent coalescence of particles. While there have been schemes to reduce the particle growth problem by alloying in a higher-melting point metal,[237] and by increasing the metal–support interaction energy by choosing specific oxides supports,[238] these approaches are not generally applicable because they restrict the catalyst chemical composition and therefore function. Prevention of these contributing factors is the key aspect to improving the durability of catalysts.

Recently, various groups have investigated using semipermeable exterior materials as a barrier against catalyst erosion. For example, a carbon coating material was found to be effective in protecting Pt nanoparticles from direct exposure to corrosive environments.[239] Others have found that the degradation of metal surfaces can be inhibited with layers of a porous inorganic oxide such as zirconia.[240] However, these architectures layers inevitably reduce the activity for critical reactions, such as the oxygen reduction reaction (ORR), due to obstruction.

Conceptually speaking, single-layer graphene, being only an atom thick, is at the low-dimensional end of any candidate corrosion-barrier material. Therefore, as a barrier, it should only reduce the catalytic activity minimally. Due to its electronic configuration and structural properties, graphene has already been investigated for various catalysis applications.[163, 219-221] While several groups have investigated using graphene as a support material, incorporating graphene as a protective barrier has not been thoroughly studied. A part of the reason may be the fact that graphene, as a membrane, is practically impermeable to atomic transport of most standard molecules.[222] However, this logic holds only in the case where reactant species must first transport fully through the graphene in order to access the catalyst.

This study posits that the inherent strength of graphene's sp^2 bonding should not only provide structural integrity against chemical corrosion (such as in the oxidative environment of a fuel cell cathode) but, when presented as an atomically intimate cover over the catalyst, it should also act as a barrier to prevent catalyst loss. In the context of a fuel cell cathode, due to graphene's honeycomb nature and the atomic vicinity to the Pt catalyst, the oxygen reduction reaction (ORR) can take place without compromise to

activity but with significantly improved Pt retention. In the present work, this study investigated these phenomena using monolayers of Pt supported by a Au substrate either with or without a single-layer graphene cap. The stability of the catalytic surface and the electrochemical activity toward the ORR were investigated as a function of the dimensional evolution of the atomic and electronic structure of the Pt film and as a function of the presence/absence of the graphene cap. Surface coverage, catalytic activity, electronic and atomic structure were measured with a complementary suite of electrochemical and x-ray spectroscopic methods.

Using single-layer graphene as an intimate capping sheet, the open honeycomb nature allows the surface to participate in catalysis while preventing surface dissolution of electrode metals into the electrolyte, without adversely affecting activity towards ORR. The graphene overlayer also has the potential to mitigate surface poisoning effects from larger species such as CO. These properties should not only allow a graphene to act as a cap to prevent dissolution of the platinum surface, it has the propensity to maintain itself during potential cycling.

In order to evaluate the effect of single-layer graphene covering Pt overlayers, two sample sets were synthesized. The first sample set consists of Pt monolayers of varying thicknesses capped by single-layer graphene (GR/Pt/Au). Samples with Pt overlayer thicknesses of 1, 2, 3, 4, and 5 monolayers (MLs) were created via SLRR and the graphene was adhered through an annealing process. A second sample set (Pt/Au) was synthesized in identical fashion including the same annealing process, but without graphene. This allowed a one-to-one comparison between sample sets where the effects of the presence of graphene can be easily identified. The reason for controlling the

(GR/Pt/Au) architecture with the monolayer level control of the Pt, is to investigate the dimensional component of the activity and durability of Pt with and without graphene capping.

5.3.1 ORR Activity and Relation to Electronic Structure

The results for linear sweep ORR probe experiments are shown in Figure 51. By taking the first derivative of the ORR polarization curves, the peak position represents the inflection point of the current reaction curve and can be used to evaluate the required overpotential needed to catalyze the ORR. [180, 230] Since a negative potential sweep was used to probe the ORR, the higher the reported potential values are for the first derivative peak position, the lower the required overpotential is for the ORR to take place.

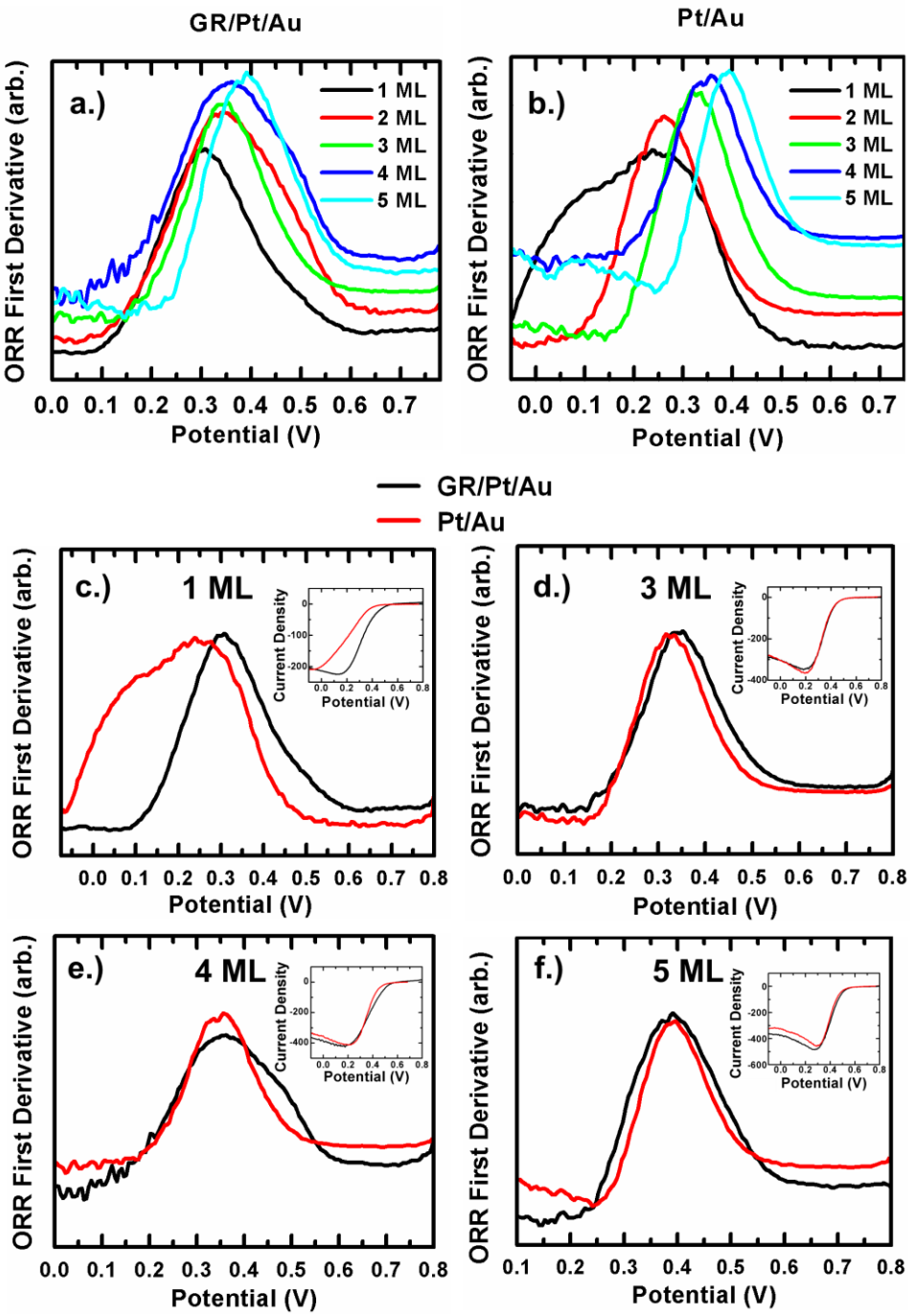

Figure 51: First derivative of oxygen reduction reaction polarization curves (against a Ag/AgCl reference electrode) obtained by linear sweep voltammetry in O_2-saturated 0.1 M H_2SO_4. a.) GR/Pt/Au samples. b.) Pt/Au samples. c-f.) 1, 3, 4, and 5 ML respectively. Insets) ORR polarization curves for each sample pair. The sweep rate is 20 mV/s. Current densities units are μA/cm2.

For GR/Pt/Au samples, despite the Pt overlayer surface being fully capped by graphene, it is able to generate catalytic performance towards the ORR. In both the GR/Pt/Au and Pt/Au cases, the peak potential increases as the number of Pt monolayers increases, which is equivalent to a lower overpotential required to catalyze the ORR. For 1 and 3 Pt MLs, the peak overpotential value of the GR/Pt/Au samples lies at a higher potential than corresponding Pt/Au samples. At 5 MLs, the two samples share the same potential value. This indicates that the presence of graphene at the surface of the Pt has either a beneficial or no effect on lowering the required overpotential towards catalyzing the ORR. The current densities achieved for GR/Pt/Au and Pt/Au samples were consistently similar.

In order to further investigate the surface components of the monolayer catalysts, XPS was used as the primary characterization tool in evaluating the electronic state of the sample surfaces. Significant shifts can be seen in the binding energy of the Pt $4f_{7/2}$ photoemission for GR/Pt/Au samples in Figure 52. The Pt/Au samples showed a slight shift towards lower binding energies with increasing Pt loading, flattening out around 71.15 eV. Research has previously shown a correlation between a negatively shifted binding energy and a diminished ORR potential for these samples.[33] This correlation can be explained by the adsorption of OH^- groups on Pt surface. Previous research has also shown that OH^- species on the surface of a Pt shell less than two MLs thick require more energy to be removed than from a bulk Pt surface.[33] Thus, for Pt/Au, a slightly decreased ORR overpotential is expected until the Pt overlayer grows to past two MLs in thickness.

On the other hand, GR/Pt/Au samples showed a more significant negative shift in binding energy. Low thickness samples exhibit binding energies as low as ~70.95 eV - with a shift towards higher binding energies with more addition of Pt. Graphene-Pt bonds have been a calculated to lower the charge of the Pt atom[231], which should subsequently raise the binding energy of Pt bound electrons. Despite this, the ORR curves for samples 3 ML and less in thickness show a slight advantage for GR/Pt/Au samples. When considering electron energies for GR/Pt/Au architecture, electron transfer to and from the Au substrate, transfer effects from the overlaying graphene, and lateral interactions with coexisting Pt all must be considered

Graphene has a tendency to donate electrons towards Au,[231] and when only a few monolayers of Pt are placed on top of 50 nm of Au, a majority of electron transfer can be expected to be directed toward the substrate. Such a transfer would be expected to accompanied by a slightly negative binding energy shift for Au 4f electrons, which is in fact seen in XPS by about .1 eV (not shown). Electron donation from graphene to Au is believed to take place through the Pt monolayers, also lowering the binding energies of Pt. When only a single Pt layer is present, this negative shift is most significant as seen in Figure 52c. As the Pt layer grows in thickness, the cumulative effect of this electronic transfer is diminished but not entirely. Increasing the Pt layer thickness leads to increasing the binding energy of Pt atoms, as the interaction between Au and graphene becomes less influential. Referring back to the ORR results, these lowered binding energies, especially at low Pt MLs, can explain the increased activity of the catalyst that is observed.

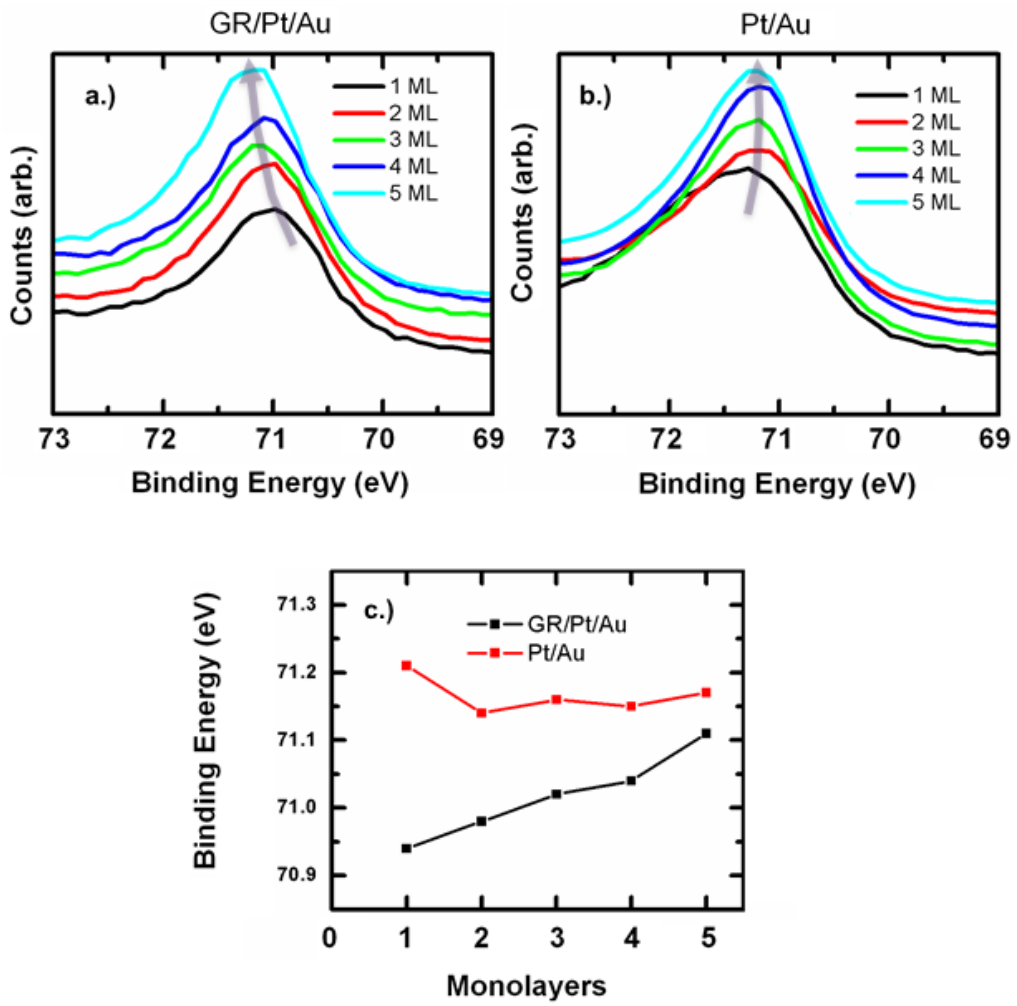

Figure 52: Pt $4f_{7/2}$ photoemission for a) GR/Pt/Au and b) Pt/Au samples. c) The binding energy trends for the sample set.

The ORR pathway includes several intermediate species, including O^- and OH^-, both of which require access to the catalyst surface in order for the reduction to take place.[241-243] It is widely accepted that adsorbed OH^- acts as an intermediate species for the ORR on metal surfaces.[244] Since adsorption of oxygen species plays a major role in determining the kinetics of oxygen reduction at Pt electrodes, maintaining an open interface with the electrolyte is necessary. The nature of graphene allows the catalyst

surface to remain in sufficiently intimate contact with the incoming ORR intermediates while preventing Pt dissolution into the electrolyte. The underlying Pt is thus still available to catalyze oxygen at no overpotential disadvantage when compared to a pure platinum surface. Figure 53 shows a hypothetical schematic of the ORR taking place at the surface of a GR/Pt electrode, emulating what would be seen at the cathode of a fuel cell. The ORR intermediates, such as hydroxyl, can adsorb to the Pt surface within the open spaces allowed by graphene. It is also possible that the capping graphene layer can act as a shield against electrochemical poisons with large molecular sizes relative to OH^-, such as CO.

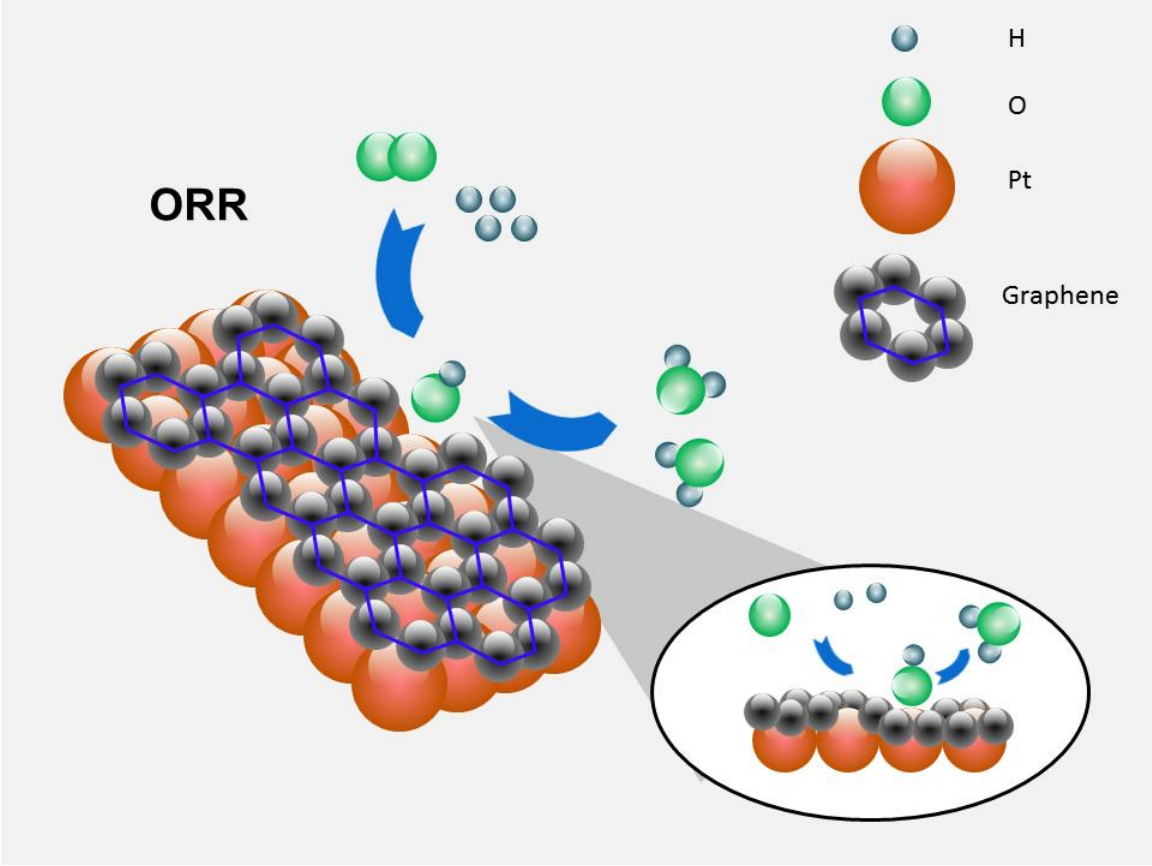

Figure 53: Illustration of the oxygen reduction reaction taking place through the graphene layer.

The local atomic coordination around Pt atoms was investigated using EXAFS for Pt adlayers for a subset of samples. In Figure 54, the R-space spectra for these samples is presented, as well as a reference Pt foil, with the y-axis representing a weighted partial radial distribution function around an average Pt atom. Bulk Pt (Pt foil) exhibits an apparent nearest neighbor (*nn*) distance of about 2.2 Å, consistent with previous work, [68] which as aforementioned, is actually at a Pt-Pt bond distance of 2.78 Å when phase-shift corrected. For the GR/Pt/Au samples in Figure 54a, the *nn* peak for the 5 ML case shows both a shift towards lower values and a widening of the peak. This may be indicating that Pt is also bonding to the overlying graphene carbon at many points along the surface of the electrode, and can be attributed to a compressive strain effect induced by the graphene.[33] The long range structure past the *nn* peak is, however, still very similar to that of Pt foil, meaning that the Pt overlayer not largely disordered. For Pt/Au samples of sufficient thickness in Figure 54b, the EXAFS spectra is very similar to that of the Pt reference, as all intensity features line up peak-for-peak.

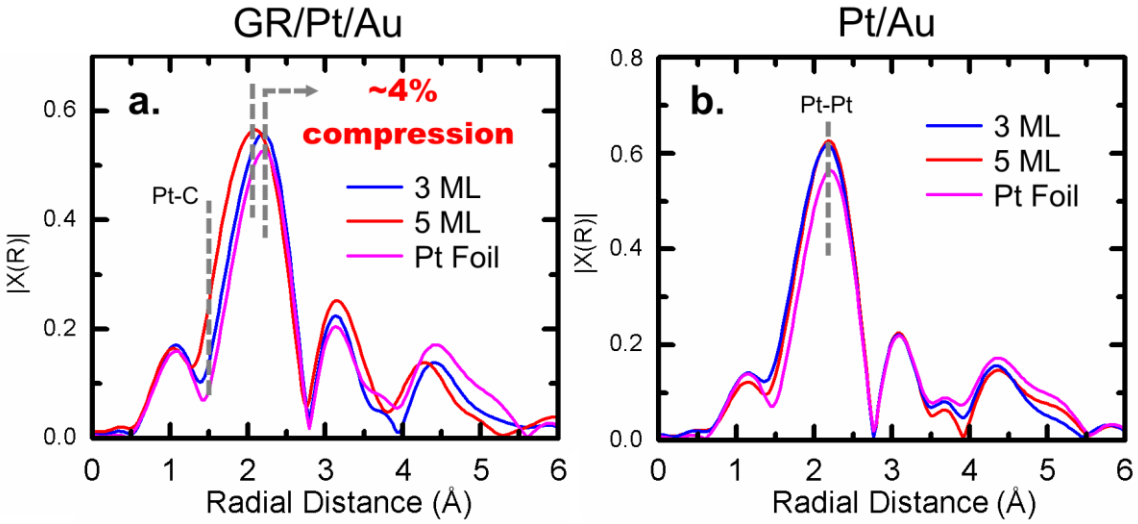

Figure 54: EXAFS spectra for 3 and 5 GR/Pt/Au ML samples.

The Pt overlayer is in intimate contact with the graphene, and maintains an FCC type structure underneath the graphene sheet. When it comes to the catalysis of the ORR, the GR/Pt surface is essentially identical to that of an uncovered Pt overlayer, and the graphene provides no barriers to reaction. Surface Pt atoms might in fact be slightly compressively strained from the overlying graphene sheet, which in the past has been shown to positively affect the surface activity towards ORR catalysis.[33]

5.3.2 Durability of GR/Pt/Au

The ORR probe and EXAFS spectra show that graphene-capped samples remain as effective in catalysis as samples without graphene. To investigate how graphene affects the durability of the surface over time, a subset samples were cycled from 400 mV to 750 mV (vs. Ag/AgCl) in oxygen-saturated 0.1 M H_2SO_4 for 1000 cycles, which repeatedly forces surface oxidation/reduction cycles of Pt.[21]

Furthermore, XPS spectra of the samples before and after 1000 cycles were taken to evaluate the surface architecture of each sample. Because the sample architecture is that of a Pt-Au core-shell, by comparing the relative photoemission intensity of the Pt overlayer to the underlying Au photoemission, the relative average thickness of the Pt shell can be determined. Figure 55 displays the Pt and Au XPS spectra for 1, 2, 3, and 4 ML sample cases, both before and after cycling experiment. After 1000 cycles, the XPS spectra for the GR/Pt/Au samples are almost identical to their spectra prior to cycling, as the peak intensity for the Pt 4f photoemissions is unchanged relative to the Au 4f photoemission. On the other hand, Pt/Au samples without graphene clearly showed dramatic reduction in Pt peak intensity relative to Au. This indicates that the Pt overlayer

is much thinner and a large amount of erosion of Pt has occurred from the ORR cycling. The spectra or GR/Pt_ML/Au samples show that the Pt surface does not undergo either Pt surface dissolution or agglomeration through Ostwald ripening. The results here clearly show that the graphene cap works to effectively lock the Pt ML surface in place and dramatically improves the retention of Pt at a variety of monolayer thicknesses.

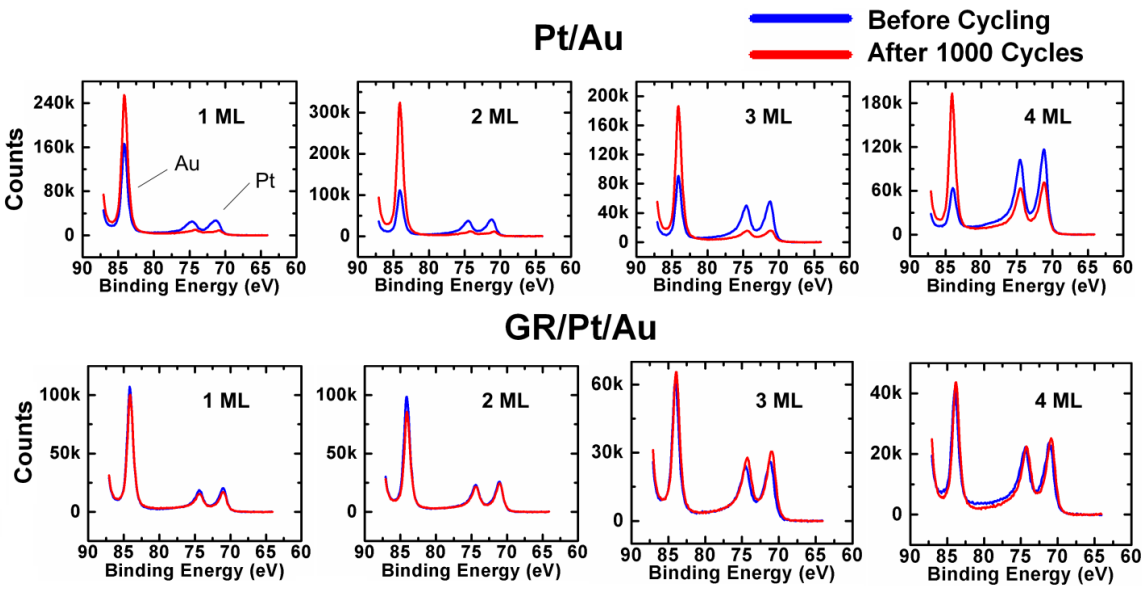

Figure 55: The Pt 4f7/2, 5/2 pair and the Au 4f7/2 XPS spectra for GR/Pt/Au samples and Pt/Au samples are shown before and after ORR cycling.

Cyclic voltammetry was also used to evaluate the surface composition of the samples during long-term cycling. A characterization CV curve was performed before cycling, after 500 cycles, and after 1000 cycles in order to examine the changes in the Pt reduction shape on the reverse sweep. Results for the 4 ML sample are shown in Figure 56a and Figure 56b. GR/Pt/Au samples showed that the reduction peak of Pt was maintained during cycling, as shown in Figure 56a. However, Pt/Au samples showed

significant decrease in the platinum reduction feature at 0.45 V after 500 cycles in oxygen-saturated H_2SO_4, indicating a significant amount of ESA loss along the surface of the sample due to dissolution into the electrolyte.

Linear potential sweeps investigating the ORR also showed about a 30% decrease in current for the 4 ML Pt/Au samples after cycling, while GR/Pt/Au counterpart maintained its ORR current as seen in Figure 56d. The reduced current of the Pt/Au sample after cycling is similar to what was achieved for a 3 ML sample as seen in Figure 51. In corroboration with the XPS results shown in Figure 55, it is clear that the graphene acting as a cap over top of the platinum monolayer is an effective barrier to prevent dissolution effects during potential cycling.

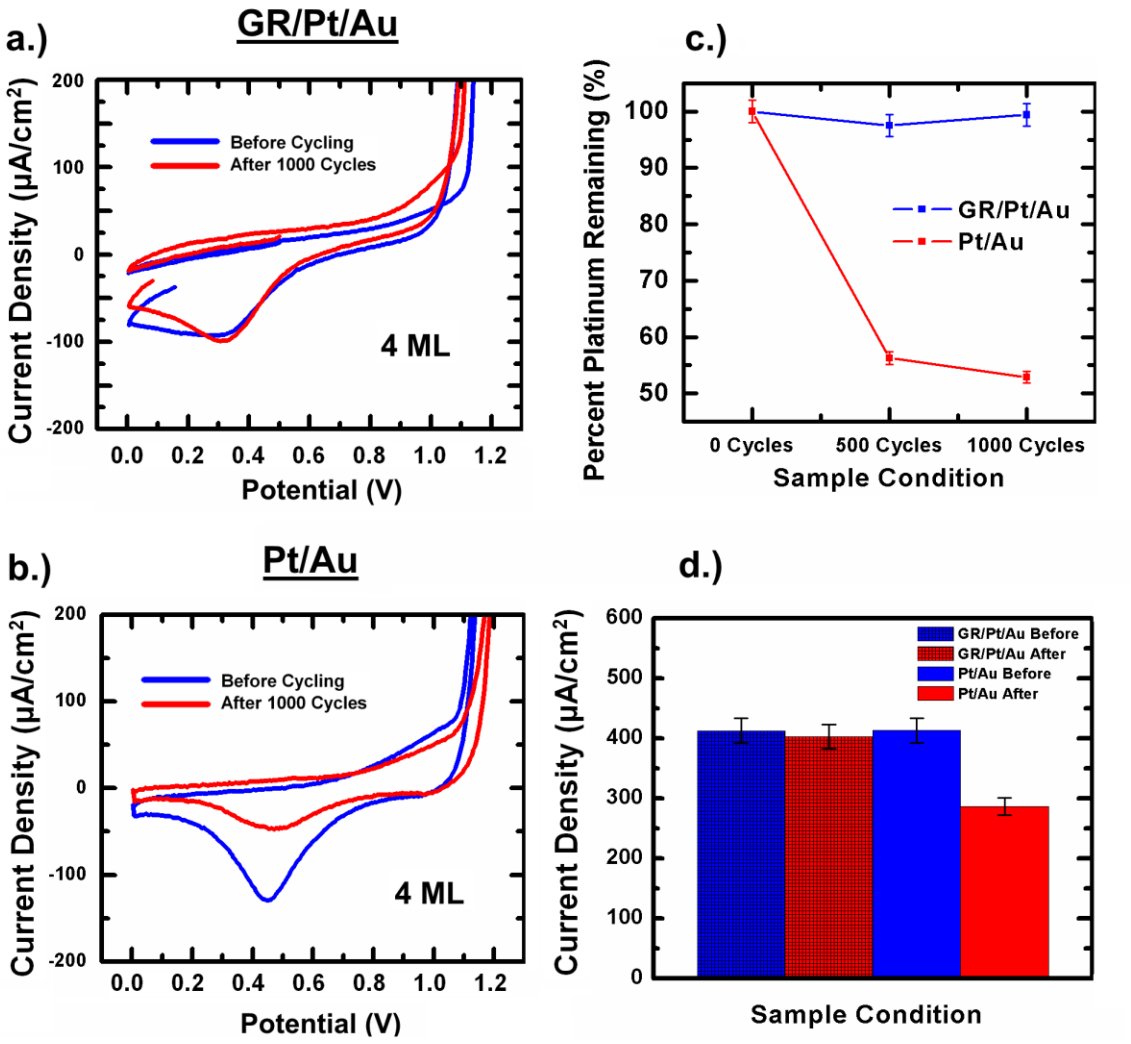

Figure 56: Cyclic Voltammograms during cyclic experiments before and after cycling for a.) 4 ML GR/Pt/Au sample, and b.) 4 ML Pt/Au sample. c.) The size of the platinum shape as a percentage of the initial charge during cycling. d.) The ORR current reached at .2 V vs. Ag/AgCl.

Raman spectroscopy was used to verify the state of the graphene, and these results are shown in Figure 57, which compares a fresh graphene deposit on an Au substrate to that of a Pt sample after cycling experiments. The 2D resonance peak at 2700 cm^{-1} is widely used as a simple and efficient way to confirm the presence of single-layer

graphene which is the most intense signal for a pristine graphene. Raman spectra after 1000 cycles for the GR/Pt/Au sample showed slightly more multilayer graphene, indicated by a sharp intensity at G band 1600 cm^{-1} than the starting single layer case, which originates from in-plane vibration of sp^2 carbon atoms. [245, 246] However, the 2D band remains intense after 1000 cycles. This is consistent with earlier results found by this group, where graphene acting as a support (rather than a cap) improved catalyst retention. [33] These combined results show much promise for incorporating graphene as a template at various catalyst interfaces as a surface resistant to potential cycling environments, potentially preventing both catalyst and support corrosion.

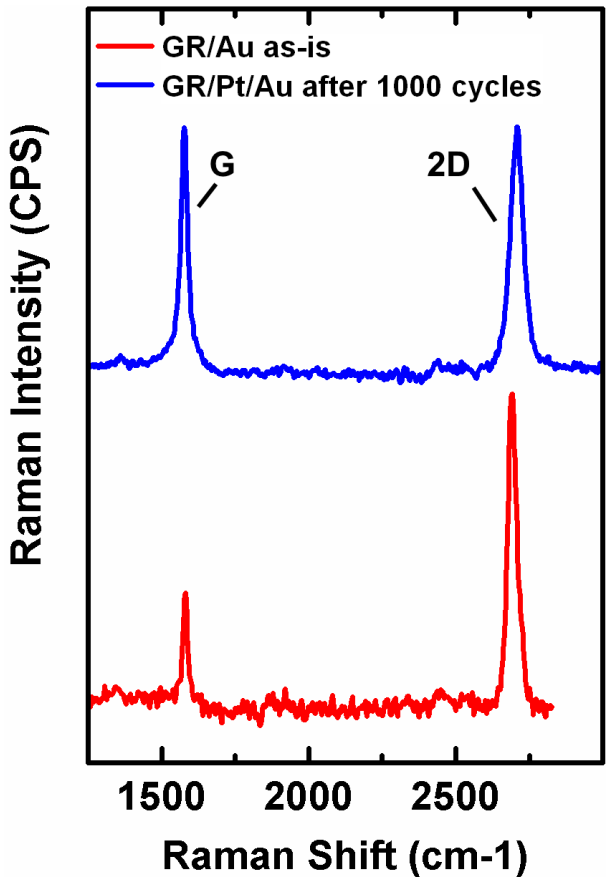

Figure 57: Raman shift spectra for the 3 ML GR/Pt/Au sample

This study has successfully created a robust graphene-covered, Au-supported Pt monolayer catalysts system (GR/Pt_ML/Au). Due to the open honeycomb structure of the graphene and its intimate contact with the Pt atoms below, and due to the compressive strain imposed by the graphene on topmost Pt layer, the GR/Pt_ML hybrids were able to catalyze the ORR through the graphene layer without any additional energy barrier to the reaction. Furthermore, the addition of graphene was found to lower the required overpotential at thinner Pt loading (less than 4ML), in correlation with lowering the Pt $4f_{7/2}$ binding energies. XPS and CV measurements show a substantial improvement in ESA retention due to robustness of graphene against harsh electrochemical working conditions, where both Pt erosion and agglomeration through Ostwald ripening after 1000 potential cycles significantly lowered. This data shows that using a graphene cap effectively works to lock the Pt surface in place, and as a method to improve catalyst lifetime is effective and an avenue of research worth further investigation.

CHAPTER 6: CONCLUSIONS

This study has focused on the structure-property relationships of Pt monolayer architectures grown on Au. It presents a careful analysis of surface nanostructures with respect to the relative core/shell compositions, as well as an examination of activity towards the ORR for the synthesized electrodes, using electrochemical and x-ray spectroscopic methods. Additionally, this study has reported activity and retention testing of a variety of graphene modified systems to investigate the potential of new catalyst architectures. A comprehensive array of experimental techniques, including X-ray photoelectron spectroscopy (XPS), cyclic voltammetry (CV), linear sweep ORR probing, extended X-ray absorption fine structure (EXAFS), and long-term potential cycling durability tests all have provided a broad range of information concerning chemical state, surface stability, catalytic aptitude, and bonding tendencies.

The completed research demonstrates fundamental knowledge regarding atomic structure, material properties, and catalytic aptitude for core-shell catalysts on a variety of support materials. A series of Pt-Au-CFP and Pt-Au-glass catalysts were prepared by Cu UPD and subsequent redox replacement by Pt ions, allowing for high precision Pt growth. In addition to metallic Pt, Pt^{2+} and Pt^{4+} surface cationic species have been reconfirmed in low-energy XPS spectra generated by a synchrotron source. This study has identified a low-loading limits of 2 monolayers below which a Pt film exhibits decreased metallic Pt-Pt bonding and lessened ORR activity, and a limit around 3 monolayers where a significant increase in surface durability can be seen. Dramatically different atomic states where detected for samples grown as-is via SLRR or after and electrochemical reduction step.

Pt ML samples that were annealed showed considerably more metallic XPS photoemissions, and higher temperature annealing also has been shown to lead to an alloying of the Pt overlayer and Au substrate. Higher temperatures and times lead to an alloyed surface which was observed to have gold-rich surfaces. At operating temperatures of 100 °C and above, there is potential for interdiffusion to occur between the primary and support metals of bimetallic core-shell catalyst systems. The study has exhibited that single-layer graphene sheets have the potential to transform these architectures and prevent unwanted surface alloying between layered metals. This study presents preliminary findings regarding the use of graphene as a barrier to diffusion. The research shows that by incorporating graphene at metal-metal interfaces, diffusion effects of metal catalyst constituents can be reduced and is worth further exploration.

This research also embodies a systematic examination on the structural effects of graphene when incorporated into core-shell Pt monolayer catalysts. This study has grown a fully wetted ultra-thin layer of Pt metal over graphene that is nominally 4 monolayers (less than 2 nm) thick. At such low dimensions, the theoretical limits of Pt loading are meat, thereby significantly increasing the activity per Pt atom. Moreover, due to a compressive strain of the Pt surface of about 3.5%, an observable increase of the catalytic activity of this low-dimensional Pt is seen relative to its bulk counterpart due its graphene templated growth. In addition, samples seated on graphene have shown a higher Pt retention than those without when subjected to long-term cycling experiments. The ability to induce strain on ultrathin Pt deposits, regardless of the nature of the substrate underneath, is an important new paradigm. New research opportunities can be explored in strain-tuned surface electronic properties by incorporating graphene as a template.

Finally, this report has successfully covered outer Pt monolayers grown over Au with single layer graphene. Due to the open honeycomb structure, Pt atoms have been shown to be able to catalyze the ORR through the graphene layer with no significant change to the required overpotential. XPS and CV measurements show a substantial improvement in ESA retention where Pt erosion after 1000 potential cycles was almost negligible. This data shows that using a graphene cap as a method to improve catalyst lifetime is effective and an avenue of research worth pursuing.

Thus this work has provided both continued fundamental understanding of Pt monolayer catalyst, as well as a foundation for novel architectures, through an innovative use of high-precision electrochemical synthesis and graphene incorporation. More work is needed in taking what has been learned and translating that knowledge to more practical and applied applications for real-world catalysts in fuel cell energy devices.

REFERENCES

[1] Y. Wang, K. S. Chen, J. Mishler, S. C. Cho, and X. C. Adroher, "A review of polymer electrolyte membrane fuel cells: Technology, applications, and needs on fundamental research," *Applied Energy*, vol. 88, pp. 981-1007, Apr 2011.

[2] S. Zhang, Y. Y. Shao, G. P. Yin, and Y. H. Lin, "Recent progress in nanostructured electrocatalysts for PEM fuel cells," *Journal of Materials Chemistry A*, vol. 1, pp. 4631-4641, 2013.

[3] M. K. Debe, "Electrocatalyst approaches and challenges for automotive fuel cells," *Nature*, vol. 486, pp. 43-51, Jun 2012.

[4] Y. Qiao and C. M. Li, "Nanostructured catalysts in fuel cells," *Journal of Materials Chemistry*, vol. 21, pp. 4027-4036, 2011.

[5] A. Rabis, P. Rodriguez, and T. J. Schmidt, "Electrocatalysis for Polymer Electrolyte Fuel Cells: Recent Achievements and Future Challenges," *Acs Catalysis*, vol. 2, pp. 864-890, May 2012.

[6] C. Natl Res, *Catalysis for Energy: Fundamental Science and Long-Term Impacts of the U.S. Department of Energy Basic Energy Sciences Catalysis Science Program*. Washington: Natl Academies Press, 2009.

[7] J. Greeley, I. E. L. Stephens, A. S. Bondarenko, T. P. Johansson, H. A. Hansen, T. F. Jaramillo, J. Rossmeisl, I. Chorkendorff, and J. K. Norskov, "Alloys of platinum and early transition metals as oxygen reduction electrocatalysts," *Nature Chemistry*, vol. 1, pp. 552-556, Oct 2009.

[8] J. B. Wu and H. Yang, "Platinum-Based Oxygen Reduction Electrocatalysts," *Accounts of Chemical Research*, vol. 46, pp. 1848-1857, Aug 2013.

[9] Y. Y. Shao, S. Park, J. Xiao, J. G. Zhang, Y. Wang, and J. Liu, "Electrocatalysts for Nonaqueous Lithium-Air Batteries: Status, Challenges, and Perspective," *Acs Catalysis*, vol. 2, pp. 844-857, May 2012.

[10] Y. C. Lu, Z. C. Xu, H. A. Gasteiger, S. Chen, K. Hamad-Schifferli, and Y. Shao-Horn, "Platinum-Gold Nanoparticles: A Highly Active Bifunctional Electrocatalyst for Rechargeable Lithium-Air Batteries,"

Journal of the American Chemical Society, vol. 132, pp. 12170-12171, Sep 2010.
[11] Z. L. Wang, D. Xu, J. J. Xu, and X. B. Zhang, "Oxygen electrocatalysts in metal-air batteries: from aqueous to nonaqueous electrolytes," *Chemical Society Reviews*, vol. 43, pp. 7746-7786, Nov 2014.
[12] C. C. L. McCrory, S. H. Jung, J. C. Peters, and T. F. Jaramillo, "Benchmarking Heterogeneous Electrocatalysts for the Oxygen Evolution Reaction," *Journal of the American Chemical Society*, vol. 135, pp. 16977-16987, Nov 2013.
[13] M. Gong, Y. G. Li, H. L. Wang, Y. Y. Liang, J. Z. Wu, J. G. Zhou, J. Wang, T. Regier, F. Wei, and H. J. Dai, "An Advanced Ni-Fe Layered Double Hydroxide Electrocatalyst for Water Oxidation," *Journal of the American Chemical Society*, vol. 135, pp. 8452-8455, Jun 2013.
[14] E. A. Wargo, C. R. Dennison, and E. C. Kumbur, "Chapter 1 - Durability of Polymer Electrolyte Fuel Cells: Status and Targets," in *Polymer Electrolyte Fuel Cell Degradation*, ed Boston: Academic Press, 2012, pp. 1-14.
[15] Y. L. Sun, M. Delucchi, and J. Ogden, "The impact of widespread deployment of fuel cell vehicles on platinum demand and price," *International Journal of Hydrogen Energy*, vol. 36, pp. 11116-11127, Aug 2011.
[16] W. D. Maier, S. J. Barnes, V. Gartz, and G. Andrews, "Pt-Pd reefs in magnetitites of the Stella layered intrusion, South Africa: A world of new exploration opportunities for platinum group elements," *Geology*, vol. 31, pp. 885-888, Oct 2003.
[17] Johnson Matthey Plc, "PGM Market Report May 2015: Summary of Platinum Supply & Demand in 2014," 2015.
[18] V. R. Stamenkovic, B. S. Mun, M. Arenz, K. J. J. Mayrhofer, C. A. Lucas, G. F. Wang, P. N. Ross, and N. M. Markovic, "Trends in electrocatalysis on extended and nanoscale Pt-bimetallic alloy surfaces," *Nature Materials*, vol. 6, pp. 241-247, Mar 2007.
[19] J. R. Yu, T. Matsuura, Y. Yoshikawa, M. N. Islam, and M. Hori, "In situ analysis of performance degradation of a PEMFC under nonsaturated humidification," *Electrochemical and Solid State Letters*, vol. 8, pp. A156-A158, 2005.
[20] Y. Y. Shao, G. P. Yin, and Y. Z. Gao, "Understanding and approaches for the durability issues of Pt-based catalysts for PEM fuel cell," *Journal of Power Sources*, vol. 171, pp. 558-566, Sep 2007.

[21] C. M. Wang, L. Ma, L. W. Liao, S. Bai, R. Long, M. Zuo, and Y. J. Xiong, "A unique platinum-graphene hybrid structure for high activity and durability in oxygen reduction reaction," *Scientific Reports*, vol. 3, Sep 2013.
[22] A. C. Chen and P. Holt-Hindle, "Platinum-Based Nanostructured Materials: Synthesis, Properties, and Applications," *Chemical Reviews*, vol. 110, pp. 3767-3804, Jun 2010.
[23] M. M. Liu, R. Z. Zhang, and W. Chen, "Graphene-Supported Nanoelectrocatalysts for Fuel Cells: Synthesis, Properties, and Applications," *Chemical Reviews*, vol. 114, pp. 5117-5160, May 2014.
[24] Y. Z. Lu and W. Chen, "One-pot synthesis of heterostructured Pt-Ru nanocrystals for catalytic formic acid oxidation," *Chemical Communications*, vol. 47, pp. 2541-2543, 2011.
[25] W. Chen, L. P. Xu, and S. W. Chen, "Enhanced electrocatalytic oxidation of formic acid by platinum deposition on ruthenium nanoparticle surfaces," *Journal of Electroanalytical Chemistry*, vol. 631, pp. 36-42, Jun 2009.
[26] W. Chen, J. M. Kim, S. H. Sun, and S. W. Chen, "Electrocatalytic reduction of oxygen by FePt alloy nanoparticles," *Journal of Physical Chemistry C*, vol. 112, pp. 3891-3898, Mar 2008.
[27] J. Zhang, H. Z. Yang, K. K. Yang, J. Fang, S. Z. Zou, Z. P. Luo, H. Wang, I. T. Bae, and D. Y. Jung, "Monodisperse Pt3Fe Nanocubes: Synthesis, Characterization, Self-Assembly, and Electrocatalytic Activity," *Advanced Functional Materials*, vol. 20, pp. 3727-3733, Nov 2010.
[28] V. R. Stamenkovic, B. Fowler, B. S. Mun, G. F. Wang, P. N. Ross, C. A. Lucas, and N. M. Markovic, "Improved oxygen reduction activity on Pt3Ni(111) via increased surface site availability," *Science*, vol. 315, pp. 493-497, Jan 2007.
[29] B. Y. Xia, H. B. Wu, X. Wang, and X. W. Lou, "One-Pot Synthesis of Cubic PtCu3 Nanocages with Enhanced Electrocatalytic Activity for the Methanol Oxidation Reaction," *Journal of the American Chemical Society*, vol. 134, pp. 13934-13937, Aug 2012.
[30] H. Z. Yang, J. Zhang, K. Sun, S. Z. Zou, and J. Y. Fang, "Enhancing by Weakening: Electrooxidation of Methanol on Pt3Co and Pt Nanocubes," *Angewandte Chemie-International Edition*, vol. 49, pp. 6848-6851, 2010.

[31] Y. J. Kang and C. B. Murray, "Synthesis and Electrocatalytic Properties of Cubic Mn-Pt Nanocrystals (Nanocubes)," *Journal of the American Chemical Society,* vol. 132, pp. 7568-+, Jun 2010.
[32] W. Chen and S. W. Chen, "Iridium-platinum alloy nanoparticles: Composition-dependent electrocatalytic activity for formic acid oxidation," *Journal of Materials Chemistry,* vol. 21, pp. 9169-9178, 2011.
[33] A. Abdelhafiz, A. Vitale, C. Joiner, E. Vogel, and F. M. Alamgir, "Layer-by-Layer Evolution of Structure, Strain, and Activity for the Oxygen Evolution Reaction in Graphene-Templated Pt Monolayers," *Acs Applied Materials & Interfaces,* vol. 7, pp. 6180-8, 2015 Mar 25 (Epub 2015 Mar 2015.
[34] M. H. Shao, A. Peles, K. Shoemaker, M. Gummalla, P. N. Njoki, J. Luo, and C. J. Zhong, "Enhanced Oxygen Reduction Activity of Platinum Monolayer on Gold Nanoparticles," *Journal of Physical Chemistry Letters,* vol. 2, pp. 67-72, Jan 2011.
[35] H. Zhang, M. S. Jin, and Y. N. Xia, "Enhancing the catalytic and electrocatalytic properties of Pt-based catalysts by forming bimetallic nanocrystals with Pd," *Chemical Society Reviews,* vol. 41, pp. 8035-8049, 2012.
[36] C. H. Bartholomew and R. J. Farrauto, *Fundamentals of Industrial Catalytic Processes, 2nd Edition*. Oxford: Blackwell Science Publ, 2006.
[37] J. Zhang, K. Sasaki, E. Sutter, and R. R. Adzic, "Stabilization of platinum oxygen-reduction electrocatalysts using gold clusters," *Science,* vol. 315, pp. 220-222, Jan 2007.
[38] J. G. Chen, C. A. Menning, and M. B. Zellner, "Monolayer bimetallic surfaces: Experimental and theoretical studies of trends in electronic and chemical properties," *Surface Science Reports,* vol. 63, pp. 201-254, May 2008.
[39] M. J. Janik, C. D. Taylor, and M. Neurock, "First principles analysis of the electrocatalytic oxidation of methanol and carbon monoxide," *Topics in Catalysis,* vol. 46, pp. 306-319, Dec 2007.
[40] N. M. Markovic, T. J. Schmidt, V. Stamenkovic, and P. N. Ross, "Oxygen Reduction Reaction on Pt and Pt Bimetallic Surfaces: A Selective Review," *Fuel Cells,* vol. 1, pp. 105-116, Jul 2001.
[41] Z. Jusys and R. J. Behm, "Methanol oxidation on a carbon-supported Pt fuel cell catalyst - A kinetic and mechanistic study by differential electrochemical mass spectrometry," *Journal of Physical Chemistry B,* vol. 105, pp. 10874-10883, Nov 2001.

[42] R. Dillon, S. Srinivasan, A. S. Arico, and V. Antonucci, "International activities in DMFC R&D: status of technologies and potential applications," *Journal of Power Sources,* vol. 127, pp. 112-126, Mar 2004.
[43] A. S. Arico, S. Srinivasan, and V. Antonucci, "DMFCs: From Fundamental Aspects to Technology Development," *Fuel Cells,* vol. 1, pp. 133-161, Jul 2001.
[44] S. G. Chalk and J. E. Miller, "Key challenges and recent progress in batteries, fuel cells, and hydrogen storage for clean energy systems," *Journal of Power Sources,* vol. 159, pp. 73-80, Sep 2006.
[45] W. Schmittinger and A. Vahidi, "A review of the main parameters influencing long-term performance and durability of PEM fuel cells," *Journal of Power Sources,* vol. 180, pp. 1-14, May 2008.
[46] R. Borup, J. Meyers, B. Pivovar, Y. S. Kim, R. Mukundan, N. Garland, D. Myers, M. Wilson, F. Garzon, D. Wood, P. Zelenay, K. More, K. Stroh, T. Zawodzinski, J. Boncella, J. E. McGrath, M. Inaba, K. Miyatake, M. Hori, K. Ota, Z. Ogumi, S. Miyata, A. Nishikata, Z. Siroma, Y. Uchimoto, K. Yasuda, K. I. Kimijima, and N. Iwashita, "Scientific aspects of polymer electrolyte fuel cell durability and degradation," *Chemical Reviews,* vol. 107, pp. 3904-3951, Oct 2007.
[47] J. Xie, D. L. Wood, K. L. More, P. Atanassov, and R. L. Borup, "Microstructural changes of membrane electrode assemblies during PEFC durability testing at high humidity conditions," *Journal of the Electrochemical Society,* vol. 152, pp. A1011-A1020, 2005.
[48] E. Guilminot, A. Corcella, F. Charlot, F. Maillard, and M. Chatenet, "Detection of Ptz+ ions and Pt nanoparticles inside the membrane of a used PEMFC," *Journal of the Electrochemical Society,* vol. 154, pp. B96-B105, 2007.
[49] P. J. Ferreira, G. J. la O, Y. Shao-Horn, D. Morgan, R. Makharia, S. Kocha, and H. A. Gasteiger, "Instability of Pt/C electrocatalysts in proton exchange membrane fuel cells - A mechanistic investigation," *Journal of the Electrochemical Society,* vol. 152, pp. A2256-A2271, 2005.
[50] R. L. Borup, J. R. Davey, F. H. Garzon, D. L. Wood, and M. A. Inbody, "PEM fuel cell electrocatalyst durability measurements," *Journal of Power Sources,* vol. 163, pp. 76-81, Dec 2006.
[51] K. Yasuda, A. Taniguchi, T. Akita, T. Ioroi, and Z. Siroma, "Platinum dissolution and deposition in the polymer electrolyte membrane of a PEM fuel cell as studied by potential cycling," *Physical Chemistry Chemical Physics,* vol. 8, pp. 746-752, Feb 2006.

[52] B. J. Eastwood, P. A. Christensen, R. D. Armstrong, and N. R. Bates, "Electrochemical oxidation of a carbon black loaded polymer electrode in aqueous electrolytes," *Journal of Solid State Electrochemistry*, vol. 3, pp. 179-186, May 1999.
[53] D. A. Stevens and J. R. Dahn, "Thermal degradation of the support in carbon-supported platinum electrocatalysts for PEM fuel cells," *Carbon*, vol. 43, pp. 179-188, 2005.
[54] N. Zamel and X. G. Li, "Transient analysis of carbon monoxide poisoning and oxygen bleeding in a PEM fuel cell anode catalyst layer," *International Journal of Hydrogen Energy*, vol. 33, pp. 1335-1344, Feb 2008.
[55] A. A. Franco, M. Guinard, B. Barthe, and O. Lemaire, "Impact of carbon monoxide on PEFC catalyst carbon support degradation under current-cycled operating conditions," *Electrochimica Acta*, vol. 54, pp. 5267-5279, Sep 2009.
[56] R. J. Bellows, E. P. MarucchiSoos, and D. T. Buckley, "Analysis of reaction kinetics for carbon monoxide and carbon dioxide on polycrystalline platinum relative to fuel cell operation," *Industrial & Engineering Chemistry Research*, vol. 35, pp. 1235-1242, Apr 1996.
[57] J. Divisek, H. F. Oetjen, V. Peinecke, V. M. Schmidt, and U. Stimming, "Components for PEM fuel cell systems using hydrogen and CO containing fuels," *Electrochimica Acta*, vol. 43, pp. 3811-3815, 1998.
[58] J. J. Baschuk and X. G. Li, "Carbon monoxide poisoning of proton exchange membrane fuel cells," *International Journal of Energy Research*, vol. 25, pp. 695-713, Jun 2001.
[59] A. A. Shah, P. C. Sui, G. S. Kim, and S. Ye, "A transient PEMFC model with CO poisoning and mitigation by O-2 bleeding and Ru-containing catalyst," *Journal of Power Sources*, vol. 166, pp. 1-21, Mar 2007.
[60] Y. A. Tang, Z. X. Yang, and X. Q. Dai, "A theoretical simulation on the catalytic oxidation of CO on Pt/graphene," *Physical Chemistry Chemical Physics*, vol. 14, pp. 16566-16572, 2012.
[61] D. E. Curtin, R. D. Lousenberg, T. J. Henry, P. C. Tangeman, and M. E. Tisack, "Advanced materials for improved PEMFC performance and life," *Journal of Power Sources*, vol. 131, pp. 41-48, May 2004.
[62] S. Mukerjee, S. Srinivasan, M. P. Soriaga, and J. McBreen, "ROLE OF STRUCTURAL AND ELECTRONIC-PROPERTIES OF PT AND PT ALLOYS ON ELECTROCATALYSIS OF OXYGEN REDUCTION - AN IN-SITU XANES AND EXAFS

INVESTIGATION," *Journal of the Electrochemical Society,* vol. 142, pp. 1409-1422, May 1995.

[63] R. R. Adzic, J. Zhang, K. Sasaki, M. B. Vukmirovic, M. Shao, J. X. Wang, A. U. Nilekar, M. Mavrikakis, J. A. Valerio, and F. Uribe, "Platinum monolayer fuel cell electrocatalysts," *Topics in Catalysis,* vol. 46, pp. 249-262, Dec 2007.

[64] S. Martin, P. L. Garcia-Ybarra, and J. L. Castillo, "High platinum utilization in ultra-low Pt loaded PEM fuel cell cathodes prepared by electrospraying," *International Journal of Hydrogen Energy,* vol. 35, pp. 10446-10451, Oct 2010.

[65] N. Tsiouvaras, M. A. Pena, J. L. G. Fierro, E. Pastor, and M. V. Martinez-Huerta, "The effect of the Mo precursor on the nanostructure and activity of PtRuMo electrocatalysts for proton exchange membrane fuel cells," *Catalysis Today,* vol. 158, pp. 12-21, Dec 2010.

[66] R. E. Rettew, J. W. Guthrie, and F. M. Alamgir, "Layer-by-Layer Pt Growth on Polycrystalline Au: Surface-Limited Redox Replacement of Overpotentially Deposited Ni Monolayers," *Journal of the Electrochemical Society,* vol. 156, pp. D513-D516, 2009.

[67] B. I. Podlovchenko, T. D. Gladysheva, A. Y. Filatov, and L. V. Yashina, "The Use of Galvanic Displacement in Synthesizing Pt(Cu) Catalysts with the Core-Shell Structure," *Russian Journal of Electrochemistry,* vol. 46, pp. 1189-1197, Oct 2010.

[68] S. Cheng, R. E. Rettew, M. Sauerbrey, and F. M. Alamgir, "Architecture-Dependent Surface Chemistry for Pt Monolayers on Carbon-Supported Au," *Acs Applied Materials & Interfaces,* vol. 3, pp. 3948-3956, Oct 2011.

[69] R. Adzic, "Platinum Monolayer Electrocatalysts: Tunable Activity, Stability, and Self-Healing Properties," *Electrocatalysis,* vol. 3, pp. 163-169, Dec 2012.

[70] M. Fayette, Y. Liu, D. Bertrand, J. Nutariya, N. Vasiljevic, and N. Dimitrov, "From Au to Pt via Surface Limited Redox Replacement of Pb UPD in One-Cell Configuration," *Langmuir,* vol. 27, pp. 5650-5658, May 3 2011.

[71] S. Morin, A. Lachenwitzer, F. A. Moller, O. M. Magnussen, and R. J. Behm, "Comparative in situ STM studies on the electrodeposition of ultrathin nickel films on Ag(111) and Au(111) electrodes," *Journal of the Electrochemical Society,* vol. 146, pp. 1013-1018, Mar 1999.

[72] K. Kim, J. Y. Choi, T. Kim, S. H. Cho, and H. J. Chung, "A role for graphene in silicon-based semiconductor devices," *Nature,* vol. 479, pp. 338-344, Nov 2011.

[73] A. Venugopal, L. Colombo, and E. M. Vogel, "Contact resistance in few and multilayer graphene devices," *Applied Physics Letters*, vol. 96, Jan 2010.
[74] E. J. H. Lee, K. Balasubramanian, R. T. Weitz, M. Burghard, and K. Kern, "Contact and edge effects in graphene devices," *Nature Nanotechnology*, vol. 3, pp. 486-490, 2008.
[75] D. Wang, H. L. Xin, R. Hovden, H. Wang, Y. Yu, D. A. Muller, F. J. DiSalvo, and H. D. Abruña, "Structurally ordered intermetallic platinum-cobalt core-shell nanoparticles with enhanced activity and stability as oxygen reduction electrocatalysts," *Nature Materials*, vol. 12, pp. 81-87, 2013.
[76] W. Gong, W. Zhang, C. Ren, X. Ke, S. Wang, P. Huai, W. Zhang, and Z. Zhu, "Strain-controlled interface engineering of binding and charge doping at metal-graphene contacts," *Applied Physics Letters*, vol. 103, p. 143107, 2013.
[77] M. Mavrikakis, B. Hammer, and J. K. Norskov, "Effect of strain on the reactivity of metal surfaces," *Physical Review Letters*, vol. 81, pp. 2819-2822, Sep 1998.
[78] C. Gong, D. Hinojos, W. C. Wang, N. Nijem, B. Shan, R. M. Wallace, K. J. Cho, and Y. J. Chabal, "Metal-Graphene-Metal Sandwich Contacts for Enhanced Interface Bonding and Work Function Control," *Acs Nano*, vol. 6, pp. 5381-5387, Jun 2012.
[79] Y. M. Li, L. H. Tang, and J. H. Li, "Preparation and electrochemical performance for methanol oxidation of pt/graphene nanocomposites," *Electrochemistry Communications*, vol. 11, pp. 846-849, Apr 2009.
[80] N. G. Shang, P. Papakonstantinou, P. Wang, S. Ravi, and P. Silva, "Platinum Integrated Graphene for Methanol Fuel Cells," *Journal of Physical Chemistry C*, vol. 114, pp. 15837-15841, Sep 2010.
[81] S. S. Zhang, X. Z. Yuan, J. N. C. Hin, H. J. Wang, K. A. Friedrich, and M. Schulze, "A review of platinum-based catalyst layer degradation in proton exchange membrane fuel cells," *Journal of Power Sources*, vol. 194, pp. 588-600, Dec 2009.
[82] R. E. Rettew, C. S., M. Sauerbrey, M. T., D. Sholl, D. Fischer, and F. M. Alamgir, "Near Surface Phase Transition of Solute Derived Pt Monolayers," *Topics in Catalysis*, vol. 56, p. 8, 2013.
[83] B. Lindstrom and L. J. Pettersson, "A brief history of catalysis," *Cattech*, vol. 7, pp. 130-138, Aug 2003.
[84] A. Robertson, "The Early History of Catalysis," *Platinum Metals Rev.*, vol. 19, pp. 64-69, 1975.

[85] J. N. Armor, "A history of industrial catalysis," *Catalysis Today*, vol. 163, pp. 3-9, Apr 2011.
[86] K. Mori and H. Yamashita, "Progress in design and architecture of metal nanoparticles for catalytic applications," *Physical Chemistry Chemical Physics*, vol. 12, pp. 14420-14432, Nov 2010.
[87] M. A. Neouze, "Nanoparticle assemblies: main synthesis pathways and brief overview on some important applications," *Journal of Materials Science*, vol. 48, pp. 7321-7349, Nov 2013.
[88] D. Bera, S. C. Kuiry, and S. Seal, "Synthesis of nanostructured materials using template-assisted electrodeposition," *Jom*, vol. 56, pp. 49-53, Jan 2004.
[89] J. H. Sinfelt, "CATALYSIS BY ALLOYS AND BIMETALLIC CLUSTERS," *Accounts of Chemical Research*, vol. 10, pp. 15-20, 1977.
[90] W. T. Yu, M. D. Porosoff, and J. G. G. Chen, "Review of Pt-Based Bimetallic Catalysis: From Model Surfaces to Supported Catalysts," *Chemical Reviews*, vol. 112, pp. 5780-5817, Nov 2012.
[91] H. Igarashi, T. Fujino, Y. M. Zhu, H. Uchida, and M. Watanabe, "CO Tolerance of Pt alloy electrocatalysts for polymer electrolyte fuel cells and the detoxification mechanism," *Physical Chemistry Chemical Physics*, vol. 3, pp. 306-314, 2001.
[92] S. R. Brankovic, J. X. Wang, Y. Zhu, R. Sabatini, J. McBreen, and R. R. Adzic, "Electrosorption and catalytic properties of bare and Pt modified single crystal and nanostructured Ru surfaces," *Journal of Electroanalytical Chemistry*, vol. 524, pp. 231-241, May 2002.
[93] J. Souza-Garcia, E. Herrero, and J. M. Feliu, "Breaking the C-C Bond in the Ethanol Oxidation Reaction on Platinum Electrodes: Effect of Steps and Ruthenium Adatoms," *Chemphyschem*, vol. 11, pp. 1391-1394, May 2010.
[94] A. Q. Wang, C. M. Chang, and C. Y. Mou, "Evolution of catalytic activity of Au-Ag bimetallic nanoparticles on mesoporous support for CO oxidation," *Journal of Physical Chemistry B*, vol. 109, pp. 18860-18867, Oct 2005.
[95] D. Wang, A. Villa, F. Porta, L. Prati, and D. S. Su, "Bimetallic gold/palladium catalysts: Correlation between nanostructure and synergistic effects," *Journal of Physical Chemistry C*, vol. 112, pp. 8617-8622, Jun 2008.
[96] J. K. Edwards and G. J. Hutchings, "Palladium and Gold-Palladium Catalysts for the Direct Synthesis of Hydrogen Peroxide,"

Angewandte Chemie-International Edition, vol. 47, pp. 9192-9198, 2008.

[97] R. E. Rettew, A. Meyer, S. D. Senanayake, T. L. Chen, C. Petersburg, J. I. Flege, J. Falta, and F. M. Alamgir, "Interactions of oxygen and ethylene with submonolayer Ag films supported on Ni(111)," *Physical Chemistry Chemical Physics*, vol. 13, pp. 11034-11044, 2011.

[98] J. Luo, P. N. Njoki, Y. Lin, L. Y. Wang, and C. J. Zhong, "Activity-composition correlation of AuPt alloy nanoparticle catalysts in electrocatalytic reduction of oxygen," *Electrochemistry Communications*, vol. 8, pp. 581-587, Apr 2006.

[99] B. Brown, S. D. Wolter, B. R. Stoner, and J. T. Glass, "Alloying effects of cosputtered gold-platinum thin films on the oxygen reduction reaction in acidic electrolyte," *Journal of the Electrochemical Society*, vol. 155, pp. B852-B859, 2008.

[100] H. Wendt, E. V. Spinace, A. O. Neto, and M. Linardi, "Electrocatalysis and electrocatalysts for low temperature fuel cells: fundamentals, state of the art, research and development," *Quimica Nova*, vol. 28, pp. 1066-1075, Nov-Dec 2005.

[101] M. M. Maye, N. N. Kariuki, J. Luo, L. Han, P. Njoki, L. Y. Wang, Y. Lin, H. R. Naslund, and C. J. Zhong, "Electrocatalytic reduction of oxygen: Gold and gold-platinum nanoparticle catalysts prepared by two-phase protocol," *Gold Bulletin*, vol. 37, pp. 217-+, 2004.

[102] J. Luo, M. M. Maye, V. Petkov, N. N. Kariuki, L. Y. Wang, P. Njoki, D. Mott, Y. Lln, and C. J. Zhong, "Phase properties of carbon-supported gold-platinum nanoparticles with different bimetallic compositions," *Chemistry of Materials*, vol. 17, pp. 3086-3091, Jun 2005.

[103] D. Mott, J. Luo, P. N. Njoki, Y. Lin, L. Y. Wang, and C. J. Zhong, "Synergistic activity of gold-platinum alloy nanoparticle catalysts," *Catalysis Today*, vol. 122, pp. 378-385, Apr 2007.

[104] M. Van Brussel, G. Kokkinidis, A. Hubin, and C. Buess-Herman, "Oxygen reduction at platinum modified gold electrodes," *Electrochimica Acta*, vol. 48, pp. 3909-3919, Nov 15 2003.

[105] G. Selvarani, S. V. Selvaganesh, S. Krishnamurthy, G. V. M. Kiruthika, P. Sridhar, S. Pitchumani, and A. K. Shukla, "A Methanol-Tolerant Carbon-Supported Pt-Au Alloy Cathode Catalyst for Direct Methanol Fuel Cells and Its Evaluation by DFT," *Journal of Physical Chemistry C*, vol. 113, pp. 7461-7468, Apr 30 2009.

[106] A. U. Nilekar, K. Sasaki, C. A. Farberow, R. R. Adzic, and M. Mavrikakis, "Mixed-Metal Pt Mono layer Electrocatalysts with Improved CO Tolerance," *Journal of the American Chemical Society*, vol. 133, pp. 18574-18576, Nov 23 2011.
[107] E. Antolini, "Formation of carbon-supported PtM alloys for low temperature fuel cells: a review," *Materials Chemistry and Physics*, vol. 78, pp. 563-573, Feb 2003.
[108] H. A. Gasteiger, S. S. Kocha, B. Sompalli, and F. T. Wagner, "Activity benchmarks and requirements for Pt, Pt-alloy, and non-Pt oxygen reduction catalysts for PEMFCs," *Applied Catalysis B-Environmental*, vol. 56, pp. 9-35, Mar 2005.
[109] J. H. Wee and K. Y. Lee, "Overview of the development of CO-tolerant anode electrocatalysts for proton-exchange membrane fuel cells," *Journal of Power Sources*, vol. 157, pp. 128-135, Jun 2006.
[110] H. Inoue, S. R. Brankovic, J. X. Wang, and R. R. Adzic, "Oxygen reduction on bare and Pt monolayer-modified Ru(0001), Ru(1010) and Ru nanostructured surfaces," *Electrochimica Acta*, vol. 47, pp. 3777-3785, Aug 2002.
[111] P. Strasser, S. Koh, T. Anniyev, J. Greeley, K. More, C. F. Yu, Z. C. Liu, S. Kaya, D. Nordlund, H. Ogasawara, M. F. Toney, and A. Nilsson, "Lattice-strain control of the activity in dealloyed core-shell fuel cell catalysts," *Nature Chemistry*, vol. 2, pp. 454-460, Jun 2010.
[112] P. Hernandez-Fernandez, S. Rojas, P. Ocon, A. de Frutos, J. M. Figueroa, P. Terreros, M. A. Pena, and J. L. G. Fierro, "Relevance of the nature of bimetallic PtAu nanoparticles as electrocatalysts for the oxygen reduction reaction in the presence of methanol," *Journal of Power Sources*, vol. 177, pp. 9-16, Feb 2008.
[113] C. Wang, D. van der Vliet, K. L. More, N. J. Zaluzec, S. Peng, S. H. Sun, H. Daimon, G. F. Wang, J. Greeley, J. Pearson, A. P. Paulikas, G. Karapetrov, D. Strmcnik, N. M. Markovic, and V. R. Stamenkovic, "Multimetallic Au/FePt3 Nanoparticles as Highly Durable Electrocatalyst," *Nano Letters*, vol. 11, pp. 919-926, Mar 2011.
[114] C. Wang, M. F. Chi, D. G. Li, D. Strmcnik, D. van der Vliett, G. F. Wang, V. Komanicky, K. C. Chang, A. P. Paulikas, D. Tripkovic, J. Pearson, K. L. More, N. M. Markovic, and V. R. Stamenkovic, "Design and Synthesis of Bimetallic Electrocatalyst with Multilayered Pt-Skin Surfaces," *Journal of the American Chemical Society*, vol. 133, pp. 14396-14403, Sep 2011.
[115] J. X. Wang, C. Ma, Y. Choi, D. Su, Y. Zhu, P. Liu, R. Si, M. B. Vukmirovic, Y. Zhang, and R. R. Adzic, "Kirkendall Effect and

Lattice Contraction in Nanocatalysts: A New Strategy to Enhance Sustainable Activity," *Journal of the American Chemical Society*, vol. 133, pp. 13551-13557, Aug 31 2011.
[116] H. I. Karan, K. Sasaki, K. Kuttiyiel, C. A. Farberow, M. Mavrikakis, and R. R. Adzic, "Catalytic Activity of Platinum Mono layer on Iridium and Rhenium Alloy Nanoparticles for the Oxygen Reduction Reaction," *Acs Catalysis*, vol. 2, pp. 817-824, May 2012.
[117] M. Li, P. Liu, and R. R. Adzic, "Platinum Monolayer Electrocatalysts for Anodic Oxidation of Alcohols," *Journal of Physical Chemistry Letters*, vol. 3, pp. 3480-3485, Dec 2012.
[118] H. Q. Liu, C. Koenigsmann, R. R. Adzic, and S. S. Wong, "Probing Ultrathin One-Dimensional Pd-Ni Nanostructures As Oxygen Reduction Reaction Catalysts," *Acs Catalysis*, vol. 4, pp. 2544-2555, Aug 2014.
[119] A. J. Medford, A. Vojvodic, J. S. Hummelshoj, J. Voss, F. Abild-Pedersen, F. Studt, T. Bligaard, A. Nilsson, and J. K. Norskov, "From the Sabatier principle to a predictive theory of transition-metal heterogeneous catalysis," *Journal of Catalysis*, vol. 328, pp. 36-42, Aug 2015.
[120] M. Che, "Nobel Prize in chemistry 1912 to Sabatier: Organic chemistry or catalysis?," *Catalysis Today*, vol. 218, pp. 162-171, Dec 2013.
[121] P. Sabatier, *La catalyse en chimie organique*: Paris et Liége, 1913.
[122] B. Hammer and J. K. Norskov, "Theoretical surface science and catalysis - Calculations and concepts," in *Advances in Catalysis, Vol 45: Impact of Surface Science on Catalysis*. vol. 45, B. C. Gates and H. Knozinger, Eds., ed San Diego: Elsevier Academic Press Inc, 2000, pp. 71-129.
[123] T. Bligaard and J. K. Norskov, "Ligand effects in heterogeneous catalysis and electrochemistry," *Electrochimica Acta*, vol. 52, pp. 5512-5516, May 2007.
[124] A. Vojvodic, J. K. Norskov, and F. Abild-Pedersen, "Electronic Structure Effects in Transition Metal Surface Chemistry," *Topics in Catalysis*, vol. 57, pp. 25-32, Feb 2014.
[125] L. Pettersson and A. Nilsson, "A Molecular Perspective on the d-Band Model: Synergy Between Experiment and Theory," *Topics in Catalysis*, vol. 57, pp. 2-13, Feb 2014.
[126] D. M. Newns, "SELF-CONSISTENT MODEL OF HYDROGEN CHEMISORPTION," *Physical Review*, vol. 178, pp. 1123-&, 1969.

[127] P. W. Anderson, "LOCALIZED MAGNETIC STATES IN METALS," *Physical Review*, vol. 124, pp. 41-&, 1961.
[128] B. Hammer, Y. Morikawa, and J. K. Norskov, "CO chemisorption at metal surfaces and overlayers," *Physical Review Letters*, vol. 76, pp. 2141-2144, Mar 1996.
[129] J. L. Zhang, M. B. Vukmirovic, Y. Xu, M. Mavrikakis, and R. R. Adzic, "Controlling the catalytic activity of platinum-monolayer electrocatalysts for oxygen reduction with different substrates," *Angewandte Chemie-International Edition*, vol. 44, pp. 2132-2135, 2005.
[130] D. Gokcen, Q. Y. Yuan, and S. R. Brankovic, "Nucleation of Pt Monolayers Deposited via Surface Limited Redox Replacement Reaction," *Journal of the Electrochemical Society*, vol. 161, pp. D3051-D3056, 2014.
[131] L. C. Grabow, Q. Y. Yuan, H. A. Doan, and S. R. Brankovic, "Novel 2D RuPt core-edge nanocluster catalyst for CO electro-oxidation," *Surface Science*, vol. 640, pp. 50-58, Oct 2015.
[132] N. M. Markovic, B. N. Grgur, C. A. Lucas, and P. N. Ross, "Electrooxidation of CO and H-2/CO mixtures on Pt(111) in acid solutions," *Journal of Physical Chemistry B*, vol. 103, pp. 487-495, Jan 1999.
[133] T. Toda, H. Igarashi, H. Uchida, and M. Watanabe, "Enhancement of the electroreduction of oxygen on Pt alloys with Fe, Ni, and Co," *Journal of the Electrochemical Society*, vol. 146, pp. 3750-3756, Oct 1999.
[134] Q. Y. Jia, K. Caldwell, K. Strickland, J. M. Ziegelbauer, Z. Y. Liu, Z. Q. Yu, D. E. Ramaker, and S. Mukerjee, "Improved Oxygen Reduction Activity and Durability of Dealloyed PtCox Catalysts for Proton Exchange Membrane Fuel Cells: Strain, Ligand, and Particle Size Effects," *Acs Catalysis*, vol. 5, pp. 176-186, Jan 2015.
[135] Q. Y. Jia, C. U. Segre, D. Ramaker, K. Caldwell, M. Trahan, and S. Mukerjee, "Structure-property-activity correlations of Pt-bimetallic nanoparticles: A theoretical study," *Electrochimica Acta*, vol. 88, pp. 604-613, Jan 2013.
[136] S. Chen, W. C. Sheng, N. Yabuuchi, P. J. Ferreira, L. F. Allard, and Y. Shao-Horn, "Origin of Oxygen Reduction Reaction Activity on "Pt3Co" Nanoparticles: Atomically Resolved Chemical Compositions and Structures," *Journal of Physical Chemistry C*, vol. 113, pp. 1109-1125, Jan 2009.

[137] C. H. Cui, L. Gan, M. Heggen, S. Rudi, and P. Strasser, "Compositional segregation in shaped Pt alloy nanoparticles and their structural behaviour during electrocatalysis," *Nature Materials,* vol. 12, pp. 765-771, Aug 2013.
[138] H. L. Xin, J. A. Mundy, Z. Y. Liu, R. Cabezas, R. Hovden, L. F. Kourkoutis, J. L. Zhang, N. P. Subramanian, R. Makharia, F. T. Wagner, and D. A. Muller, "Atomic-Resolution Spectroscopic Imaging of Ensembles of Nanocatalyst Particles Across the Life of a Fuel Cell," *Nano Letters,* vol. 12, pp. 490-497, Jan 2012.
[139] D. L. Wang, H. L. L. Xin, R. Hovden, H. S. Wang, Y. C. Yu, D. A. Muller, F. J. DiSalvo, and H. D. Abruna, "Structurally ordered intermetallic platinum-cobalt core-shell nanoparticles with enhanced activity and stability as oxygen reduction electrocatalysts," *Nature Materials,* vol. 12, pp. 81-87, Jan 2013.
[140] J. J. Spivey, K. S. Krishna, C. Kumar, K. M. Dooley, J. C. Flake, L. H. Haber, Y. Xu, M. J. Janik, S. B. Sinnott, Y. T. Cheng, T. Liang, D. S. Sholl, T. A. Manz, U. Diebold, G. S. Parkinson, D. A. Bruce, and P. de Jongh, "Synthesis, Characterization, and Computation of Catalysts at the Center for Atomic-Level Catalyst Design," *Journal of Physical Chemistry C,* vol. 118, pp. 20043-20069, Sep 2014.
[141] Q. Y. Jia, W. T. Liang, M. K. Bates, P. Mani, W. Lee, and S. Mukerjee, "Activity Descriptor Identification for Oxygen Reduction on Platinum-Based Bimetallic Nanoparticles: In Situ Observation of the Linear Composition-Strain-Activity Relationship," *Acs Nano,* vol. 9, pp. 387-400, Jan 2015.
[142] E. Antolini, "Carbon supports for low-temperature fuel cell catalysts," *Applied Catalysis B-Environmental,* vol. 88, pp. 1-24, Apr 2009.
[143] P. Trogadas, T. F. Fuller, and P. Strasser, "Carbon as catalyst and support for electrochemical energy conversion," *Carbon,* vol. 75, pp. 5-42, Aug 2014.
[144] Y. J. Wang, D. P. Wilkinson, and J. J. Zhang, "Noncarbon Support Materials for Polymer Electrolyte Membrane Fuel Cell Electrocatalysts," *Chemical Reviews,* vol. 111, pp. 7625-7651, Dec 2011.
[145] R. E. Rettew, N. K. Allam, and F. M. Alamgir, "Interface Architecture Determined Electrocatalytic Activity of Pt on Vertically Oriented TiO2 Nanotubes," *Acs Applied Materials & Interfaces,* vol. 3, pp. 147-151, Feb 2011.
[146] A. L. Dicks, "The role of carbon in fuel cells," *Journal of Power Sources,* vol. 156, pp. 128-141, Jun 2006.

[147] S. Y. Wang, S. P. Jiang, T. J. White, and X. Wang, "Synthesis of Pt and Pd nanosheaths on multi-walled carbon nanotubes as potential electrocatalysts of low temperature fuel cells," *Electrochimica Acta,* vol. 55, pp. 7652-7658, Nov 2010.
[148] H. T. Fang, C. G. Liu, L. Chang, L. Feng, L. Min, and H. M. Cheng, "Purification of single-wall carbon nanotubes by electrochemical oxidation," *Chemistry of Materials,* vol. 16, pp. 5744-5750, Dec 2004.
[149] F. Hasche, M. Oezaslan, and P. Strasser, "Activity, stability and degradation of multi walled carbon nanotube (MWCNT) supported Pt fuel cell electrocatalysts," *Physical Chemistry Chemical Physics,* vol. 12, pp. 15251-15258, Dec 2010.
[150] S. Park, Y. Y. Shao, R. Kou, V. V. Viswanathan, S. A. Towne, P. C. Rieke, J. Liu, Y. H. Lin, and Y. Wang, "Polarization Losses under Accelerated Stress Test Using Multiwalled Carbon Nanotube Supported Pt Catalyst in PEM Fuel Cells," *Journal of the Electrochemical Society,* vol. 158, pp. B297-B302, 2011.
[151] L. Zhao, Z. B. Wang, X. L. Sui, and G. P. Yin, "Effect of multiwalled carbon nanotubes with different specific surface areas on the stability of supported Pt catalysts," *Journal of Power Sources,* vol. 245, pp. 637-643, Jan 2014.
[152] G. Leofanti, M. Padovan, G. Tozzola, and B. Venturelli, "Surface area and pore texture of catalysts," *Catalysis Today,* vol. 41, pp. 207-219, May 1998.
[153] Y. Y. Shao, G. P. Yin, J. Zhang, and Y. Z. Gao, "Comparative investigation of the resistance to electrochemical oxidation of carbon black and carbon nanotubes in aqueous sulfuric acid solution," *Electrochimica Acta,* vol. 51, pp. 5853-5857, Aug 2006.
[154] D. A. Stevens, M. T. Hicks, G. M. Haugen, and J. R. Dahn, "Ex situ and in situ stability studies of PEMFC catalysts," *Journal of the Electrochemical Society,* vol. 152, pp. A2309-A2315, 2005.
[155] F. Coloma, A. Sepulvedaescribano, and F. Rodriguezreinoso, "HEAT-TREATED CARBON-BLACKS AS SUPPORTS FOR PLATINUM CATALYSTS," *Journal of Catalysis,* vol. 154, pp. 299-305, Jul 1995.
[156] F. Coloma, A. Sepulvedaescribano, J. L. G. Fierro, and F. Rodriguezreinoso, "PREPARATION OF PLATINUM SUPPORTED ON PREGRAPHITIZED CARBON-BLACKS," *Langmuir,* vol. 10, pp. 750-755, Mar 1994.
[157] L. Calvillo, V. Celorrio, R. Moliner, and M. J. Lazaro, "Influence of the support on the physicochemical properties of Pt electrocatalysts:

Comparison of catalysts supported on different carbon materials," *Materials Chemistry and Physics*, vol. 127, pp. 335-341, May 2011.
[158] J. Kibsgaard, Z. B. Chen, B. N. Reinecke, and T. F. Jaramillo, "Engineering the surface structure of MoS2 to preferentially expose active edge sites for electrocatalysis," *Nature Materials*, vol. 11, pp. 963-969, Nov 2012.
[159] X. Huang, Z. Y. Yin, S. X. Wu, X. Y. Qi, Q. Y. He, Q. C. Zhang, Q. Y. Yan, F. Boey, and H. Zhang, "Graphene-Based Materials: Synthesis, Characterization, Properties, and Applications," *Small*, vol. 7, pp. 1876-1902, Jul 2011.
[160] A. K. Geim and K. S. Novoselov, "The rise of graphene," *Nature Materials*, vol. 6, pp. 183-191, Mar 2007.
[161] D. Chen, L. H. Tang, and J. H. Li, "Graphene-based materials in electrochemistry," *Chemical Society Reviews*, vol. 39, pp. 3157-3180, 2010.
[162] D. A. C. Brownson, D. K. Kampouris, and C. E. Banks, "An overview of graphene in energy production and storage applications," *Journal of Power Sources*, vol. 196, pp. 4873-4885, Jun 2011.
[163] E. Antolini, "Graphene as a new carbon support for low-temperature fuel cell catalysts," *Applied Catalysis B-Environmental*, vol. 123, pp. 52-68, Jul 2012.
[164] X. Liu, C. Z. Wang, M. Hupalo, W. C. Lu, M. C. Tringides, Y. X. Yao, and K. M. Ho, "Metals on graphene: correlation between adatom adsorption behavior and growth morphology," *Physical Chemistry Chemical Physics*, vol. 14, pp. 9157-9166, 2012 2012.
[165] X. Q. Dai, Y. N. Tang, J. H. Zhao, and Y. W. Dai, "Absorption of Pt clusters and the induced magnetic properties of graphene," *Journal of Physics-Condensed Matter*, vol. 22, Aug 2010.
[166] K. T. Chan, J. B. Neaton, and M. L. Cohen, "First-principles study of metal adatom adsorption on graphene," *Physical Review B*, vol. 77, Jun 2008.
[167] H. K. He and C. Gao, "Graphene nanosheets decorated with Pd, Pt, Au, and Ag nanoparticles: Synthesis, characterization, and catalysis applications," *Science China-Chemistry*, vol. 54, pp. 397-404, Feb 2011.
[168] S. H. Sun, G. X. Zhang, N. Gauquelin, N. Chen, J. G. Zhou, S. L. Yang, W. F. Chen, X. B. Meng, D. S. Geng, M. N. Banis, R. Y. Li, S. Y. Ye, S. Knights, G. A. Botton, T. K. Sham, and X. L. Sun, "Single-atom Catalysis Using Pt/Graphene Achieved through Atomic Layer Deposition," *Scientific Reports*, vol. 3, May 2013.

[169] J. A. Von Fraunhofer and C. Banks, *Potentiostat and its applications*. Hartford, Conn.: Daniel Davey, 1972.
[170] W. M. Haynes, D. R. Lide, and T. J. Bruno, *CRC handbook of chemistry and physics : a ready-reference book of chemical and physical data*. Boca Raton, Fla: CRC Press, 2014.
[171] R. E. Rettew, "NEAR-SURFACE STUDY OF STRUCTURE-PROPERTY RELATIONSHIPS IN ELECTROCHEMICALLY FABRICATED MULTI-COMPONENT CATALYSTS," Doctor of Philosophy, Materials Science and Engineering, Georgia Institute of Technology, 2011.
[172] E. Leiva, "Recent developments in the theory of metal upd," *Electrochimica Acta,* vol. 41, pp. 2185-2206, 1996.
[173] O. A. Oviedo, P. Velez, V. A. Macagno, and E. P. M. Leiva, "Underpotential deposition: From planar surfaces to nanoparticles," *Surface Science,* vol. 631, pp. 23-34, Jan 2015.
[174] O. A. Oviedo, C. F. A. Negre, M. M. Mariscal, C. G. Sanchez, and E. P. M. Leiva, "Underpotential deposition on free nanoparticles: Its meaning and measurement," *Electrochemistry Communications,* vol. 16, pp. 1-5, Mar 2012.
[175] O. A. Oviedo, L. Reinaudi, and E. P. M. Leiva, "The limits of underpotential deposition in the nanoscale," *Electrochemistry Communications,* vol. 21, pp. 14-17, Jul 2012.
[176] Nicholso.Rs, "THEORY AND APPLICATION OF CYCLIC VOLTAMMETRY FOR MEASUREMENT OF ELECTRODE REACTION KINETICS," *Analytical Chemistry,* vol. 37, pp. 1351-&, 1965.
[177] A. J. Bard and L. R. Faulkner, *Electrochemical methods : fundamentals and applications*. Hoboken: John Wiley & Sons, 2007.
[178] U. A. Paulus, T. J. Schmidt, H. A. Gasteiger, and R. J. Behm, "Oxygen reduction on a high-surface area Pt/Vulcan carbon catalyst: a thin-film rotating ring-disk electrode study," *Journal of Electroanalytical Chemistry,* vol. 495, pp. 134-145, Jan 2001.
[179] J. Zhai, M. Huang, and S. Dong, "Electrochemical designing of Au/Pt core shell nanoparticles as nanostructured catalyst with tunable activity for oxygen reduction," *Electroanalysis,* vol. 19, pp. 506-509, Feb 2007.
[180] S. C. Zignani, E. Antolini, and E. R. Gonzalez, "Evaluation of the stability and durability of Pt and Pt-Co/C catalysts for polymer electrolyte membrane fuel cells," *Journal of Power Sources,* vol. 182, pp. 83-90, Jul 2008.

[181] S. D. Kelly, D. Hesterberg, and B. Ravel, "Analysis of Soils and Minerals Using X-ray Absorption Spectroscopy," in *Methods of Soil Analysis. Part 5. Mineralogical Methods*, ed 677 S. Segoe Road, Madison: Soil Science Society of America, 2008, pp. 387-584.
[182] J. F. Watts and J. Wolstenholme. (2003). *An introduction to surface analysis by XPS and AES*. Available: http://search.ebscohost.com/login.aspx?direct=true&scope=site&db=nlebk&db=nlabk&AN=90295
[183] National Institute of Standards and Technology. (2012). *NIST X-ray Photoelectron Spectroscopy Database, Version 4.1*. Available: http://srdata.nist.gov/xps/
[184] A. Rosengren and B. Johansson, "CALCULATED TRANSITION-METAL SURFACE CORE-LEVEL BINDING-ENERGY SHIFTS," *Physical Review B,* vol. 22, pp. 3706-3709, 1980.
[185] L. Ley, S. P. Kowalczyk, F. R. McFeely, and D. A. Shirley, "CRYSTAL-FIELD EFFECTS ON APPARENT SPIN-ORBIT-SPLITTING OF CORE AND VALENCE LEVELS OBSERVED BY X-RAY PHOTOEMISSION," *Physical Review B,* vol. 10, pp. 4881-4888, 1974.
[186] C. E. Bryson, "SURFACE-POTENTIAL CONTROL IN XPS," *Surface Science,* vol. 189, pp. 50-58, Oct 1987.
[187] D. C. Koningsberger and R. Prins, *X-ray absorption : principles, applications, techniques of EXAFS, SEXAFS, and XANES*. New York: Wiley, 1988.
[188] T. Tanaka, K. K. Bando, N. Matsubayashi, M. Imamura, and H. Shimada, "Measurement of X-ray absorption spectra (XAS) of insulators by the partial electron yield method using an electron flood gun," *Journal of Electron Spectroscopy and Related Phenomena,* vol. 114, pp. 1077-1081, Mar 2001.
[189] D. E. Sayers, E. A. Stern, and F. W. Lytle, "NEW TECHNIQUE FOR INVESTIGATING NONCRYSTALLINE STRUCTURES - FOURIER ANALYSIS OF EXTENDED X-RAY - ABSORPTION FINE STRUCTURE," *Physical Review Letters,* vol. 27, pp. 1204-&, 1971.
[190] B. Ravel and M. Newville, "ATHENA, ARTEMIS, HEPHAESTUS: data analysis for X-ray absorption spectroscopy using IFEFFIT," *Journal of Synchrotron Radiation,* vol. 12, pp. 537-541, Jul 2005.
[191] E. Herrero, L. J. Buller, and H. D. Abruna, "Underpotential deposition at single crystal surfaces of Au, Pt, Ag and other materials," *Chemical Reviews,* vol. 101, pp. 1897-1930, Jul 2001.

[192] A. A. Gewirth and B. K. Niece, "Electrochemical applications of in situ scanning probe microscopy," *Chemical Reviews,* vol. 97, pp. 1129-1162, Jun 1997.
[193] Y.-G. Kim, J. Y. Kim, D. Vairavapandian, and J. L. Stickney, "Platinum nanofilm formation by EC-ALE via redox replacement of UPD copper: Studies using in-situ scanning tunneling microscopy," *Journal of Physical Chemistry B,* vol. 110, pp. 17998-18006, Sep 14 2006.
[194] S. R. Brankovic, J. X. Wang, and R. R. Adzic, "Metal monolayer deposition by replacement of metal adlayers on electrode surfaces," *Surface Science,* vol. 474, pp. L173-L179, Mar 1 2001.
[195] N. Jayaraju, D. Vairavapandian, Y. G. Kim, D. Banga, and J. L. Stickney, "Electrochemical Atomic Layer Deposition (E-ALD) of Pt Nanofilms Using SLRR Cycles," *Journal of the Electrochemical Society,* vol. 159, pp. D616-D622, 2012.
[196] M. F. Mrozek, Y. Xie, and M. J. Weaver, "Surface-enhanced Raman scattering on uniform platinum-group overlayers: Preparation by redox replacement of underpotential-deposited metals on gold," *Analytical Chemistry,* vol. 73, pp. 5953-5960, Dec 2001.
[197] D. Gokcen, S. E. Bae, and S. R. Brankovic, "Stoichiometry of Pt Submonolayer Deposition via Surface-Limited Redox Replacement Reaction," *Journal of the Electrochemical Society,* vol. 157, pp. D582-D587, 2010.
[198] X. S. Li, W. W. Cai, J. H. An, S. Kim, J. Nah, D. X. Yang, R. Piner, A. Velamakanni, I. Jung, E. Tutuc, S. K. Banerjee, L. Colombo, and R. S. Ruoff, "Large-Area Synthesis of High-Quality and Uniform Graphene Films on Copper Foils," *Science,* vol. 324, pp. 1312-1314, Jun 2009.
[199] G. Eda, G. Fanchini, and M. Chhowalla, "Large-area ultrathin films of reduced graphene oxide as a transparent and flexible electronic material," *Nature Nanotechnology,* vol. 3, pp. 270-274, May 2008.
[200] Q. K. Yu, J. Lian, S. Siriponglert, H. Li, Y. P. Chen, and S. S. Pei, "Graphene segregated on Ni surfaces and transferred to insulators," *Applied Physics Letters,* vol. 93, Sep 2008.
[201] P. W. Sutter, J. I. Flege, and E. A. Sutter, "Epitaxial graphene on ruthenium," *Nature Materials,* vol. 7, pp. 406-411, May 2008.
[202] J. W. Suk, A. Kitt, C. W. Magnuson, Y. F. Hao, S. Ahmed, J. H. An, A. K. Swan, B. B. Goldberg, and R. S. Ruoff, "Transfer of CVD-Grown Monolayer Graphene onto Arbitrary Substrates," *Acs Nano,* vol. 5, pp. 6916-6924, Sep 2011.

[203] J. Chan, A. Venugopal, A. Pirkle, S. McDonnell, D. Hinojos, C. W. Magnuson, R. S. Ruoff, L. Colombo, R. M. Wallace, and E. M. Vogel, "Reducing Extrinsic Performance-Limiting Factors in Graphene Grown by Chemical Vapor Deposition," *Acs Nano,* vol. 6, pp. 3224-3229, Apr 2012.
[204] A. Reina, X. T. Jia, J. Ho, D. Nezich, H. B. Son, V. Bulovic, M. S. Dresselhaus, and J. Kong, "Large Area, Few-Layer Graphene Films on Arbitrary Substrates by Chemical Vapor Deposition," *Nano Letters,* vol. 9, pp. 30-35, Jan 2009.
[205] D. Zhao and B.-Q. Xu, "Enhancement of Pt utilization in electrocatalysts by using gold nanoparticles," *Angewandte Chemie-International Edition,* vol. 45, pp. 4955-4959, 2006 2006.
[206] H. Tang, J. H. Chen, M. Y. Wang, L. H. Nie, Y. F. Kuang, and S. Z. Yao, "Controlled synthesis of platinum catalysts on Au nanoparticles and their electrocatalytic property for methanol oxidation," *Applied Catalysis a-General,* vol. 275, pp. 43-48, Nov 8 2004.
[207] R. E. Rettew, J. W. Guthrie, C. Jayeb, D. Fischer, and F. M. Alamgir, "Synthesis and Characterization of Monolayer Bimetallic Surfaces: A Synchrotron NEXAFS and XPS Study," *ECS Transactions,* vol. 19, pp. 97-106, 2009.
[208] H. Yang, N. Alonso-Vante, J. M. Leger, and C. Lamy, "Tailoring, structure, and activity of carbon-supported nanosized Pt-Cr alloy electrocatalysts for oxygen reduction in pure and methanol-containing electrolytes," *Journal of Physical Chemistry B,* vol. 108, pp. 1938-1947, Feb 2004.
[209] M. Wakisaka, S. Asizawa, H. Uchida, and M. Watanabe, "In situ STM observation of morphological changes of the Pt(111) electrode surface during potential cycling in 10 mM HF solution," *Physical Chemistry Chemical Physics,* vol. 12, pp. 4184-4190, 2010.
[210] M. Matsumoto, T. Miyazaki, and H. Imai, "Oxygen-Enhanced Dissolution of Platinum in Acidic Electrochemical Environments," *Journal of Physical Chemistry C,* vol. 115, pp. 11163-11169, Jun 2011.
[211] P. J. Cumpson and M. P. Seah, "Elastic scattering corrections in AES and XPS .2. Estimating attenuation lengths and conditions required for their valid use in overlayer/substrate experiments," *Surface and Interface Analysis,* vol. 25, pp. 430-446, Jun 1997.
[212] S. Sen, F. Sen, and G. Gokagac, "Preparation and characterization of nano-sized Pt-Ru/C catalysts and their superior catalytic activities for

methanol and ethanol oxidation," *Physical Chemistry Chemical Physics,* vol. 13, pp. 6784-6792, 2011 2011.
[213] J. Greeley, J. K. Norskov, and M. Mavrikakis, "Electronic structure and catalysis on metal surfaces," *Annual Review of Physical Chemistry,* vol. 53, pp. 319-348, 2002.
[214] V. Stamenkovic, B. S. Mun, K. J. J. Mayrhofer, P. N. Ross, N. M. Markovic, J. Rossmeisl, J. Greeley, and J. K. Norskov, "Changing the activity of electrocatalysts for oxygen reduction by tuning the surface electronic structure," *Angewandte Chemie-International Edition,* vol. 45, pp. 2897-2901, 2006.
[215] J. Luo, L. Wang, D. Mott, P. N. Njoki, Y. Lin, T. He, Z. Xu, B. N. Wanjana, I. I. S. Lim, and C. J. Zhong, "Core/Shell Nanoparticles as Electrocatalysts for Fuel Cell Reactions," *Advanced Materials,* vol. 20, pp. 4342-4347, Nov 2008.
[216] Y. Zhu, W. H. H. Zhu, and B. J. Tatarchuk, "Performance comparison between high temperature and traditional proton exchange membrane fuel cell stacks using electrochemical impedance spectroscopy," *Journal of Power Sources,* vol. 256, pp. 250-257, Jun 2014.
[217] Q. F. Li, R. H. He, J. A. Gao, J. O. Jensen, and N. J. Bjerrum, "The CO poisoning effect in PEMFCs operational at temperatures up to 200 degrees C," *Journal of the Electrochemical Society,* vol. 150, pp. A1599-A1605, Dec 2003.
[218] H. Xu, Y. Song, H. R. Kunz, and J. M. Fenton, "Operation of PEM fuel cells at 120-150 degrees C to improve CO tolerance," *Journal of Power Sources,* vol. 159, pp. 979-986, Sep 2006.
[219] O. V. Yazyev and S. G. Louie, "Electronic transport in polycrystalline graphene," *Nature Materials,* vol. 9, pp. 806-809, Oct 2010.
[220] H. Y. Nan, Z. H. Ni, J. Wang, Z. Zafar, Z. X. Shi, and Y. Y. Wang, "The thermal stability of graphene in air investigated by Raman spectroscopy," *Journal of Raman Spectroscopy,* vol. 44, pp. 1018-1021, Jul 2013.
[221] Y. L. Liu and X. Chen, "Mechanical properties of nanoporous graphene membrane," *Journal of Applied Physics,* vol. 115, Jan 2014.
[222] J. S. Bunch, S. S. Verbridge, J. S. Alden, A. M. van der Zande, J. M. Parpia, H. G. Craighead, and P. L. McEuen, "Impermeable atomic membranes from graphene sheets," *Nano Letters,* vol. 8, pp. 2458-2462, Aug 2008.
[223] M. E. Suk and N. R. Aluru, "Water Transport through Ultrathin Graphene," *Journal of Physical Chemistry Letters,* vol. 1, pp. 1590-1594, May 2010.

[224] J. Hong, S. Lee, H. Han, C. Mahata, H. W. Yeon, B. Koo, S. I. Kim, T. Nam, K. Byun, B. W. Min, Y. W. Kim, H. Kim, Y. C. Joo, and T. Lee, "Graphene as an atomically thin barrier to Cu diffusion into Si," *Nanoscale*, vol. 6, pp. 7503-7511, 2014.
[225] C. P. Y. Wong, T. J. H. Koek, Y. P. Liu, K. P. Loh, K. E. J. Goh, C. Troadec, and C. A. Nijhuis, "Electronically Transparent Graphene Barriers against Unwanted Doping of Silicon," *Acs Applied Materials & Interfaces*, vol. 6, pp. 20464-20472, Nov 2014.
[226] Y. D. Zhao, Y. Z. Xie, Z. K. Liu, X. S. Wang, Y. Chai, and F. Yan, "Two-Dimensional Material Membranes: An Emerging Platform for Controllable Mass Transport Applications," *Small*, vol. 10, pp. 4521-4542, Nov 2014.
[227] W. K. Morrow, S. J. Pearton, and F. Ren, "Review of Graphene as a Solid State Diffusion Barrier," *Small*, vol. 12, pp. 120-134, Jan 2016.
[228] J. A. Herron and M. Mavrikakis, "On the composition of bimetallic near-surface alloys in the presence of oxygen and carbon monoxide," *Catalysis Communications*, vol. 52, pp. 65-71, Jul 2014.
[229] P. W. Allen and L. E. Sutton, "TABLES OF INTERATOMIC DISTANCES AND MOLECULAR CONFIGURATIONS OBTAINED BY ELECTRON DIFFRACTION IN THE GAS PHASE," *Acta Crystallographica*, vol. 3, pp. 46-72, 1950.
[230] J.-D. Qiu, G.-C. Wang, R.-P. Liang, X.-H. Xia, and H.-W. Yu, "Controllable Deposition of Platinum Nanoparticles on Graphene As an Electrocatalyst for Direct Methanol Fuel Cells," *Journal of Physical Chemistry C*, vol. 115, pp. 15639-15645, Aug 11 2011.
[231] Y. A. Tang, Z. X. Yang, and X. Q. Dai, "Noble metals induced magnetic properties of graphene," *Journal of Magnetism and Magnetic Materials*, vol. 323, pp. 2441-2447, Oct 2011.
[232] C. C. Huang, C. Li, and G. Q. Shi, "Graphene based catalysts," *Energy & Environmental Science*, vol. 5, pp. 8848-8868, Oct 2012.
[233] S. H. Hur and J. N. Park, "Graphene and its application in fuel cell catalysis: a review," *Asia-Pacific Journal of Chemical Engineering*, vol. 8, pp. 218-233, Mar-Apr 2013.
[234] B. F. Machado and P. Serp, "Graphene-based materials for catalysis," *Catalysis Science & Technology*, vol. 2, pp. 54-75, 2012.
[235] X. Wang, W. Z. Li, Z. W. Chen, M. Waje, and Y. S. Yan, "Durability investigation of carbon nanotube as catalyst support for proton exchange membrane fuel cell," *Journal of Power Sources*, vol. 158, pp. 154-159, Jul 2006.

[236] P. Wynblatt and N. A. Gjostein, "Supported metal crystallites," *Progress in Solid State Chemistry Progress in Solid State Chemistry,* vol. 9, pp. 21-58, 1975.
[237] A. Cao and G. Veser, "Exceptional high-temperature stability through distillation-like self-stabilization in bimetallic nanoparticles," *Nature Materials,* vol. 9, pp. 75-81, Jan 2010.
[238] J. A. Farmer and C. T. Campbell, "Ceria Maintains Smaller Metal Catalyst Particles by Strong Metal-Support Bonding," *Science,* vol. 329, pp. 933-936, Aug 2010.
[239] W. Y. Song, Z. X. Chen, C. Yang, Z. P. Yang, J. P. Tai, Y. L. Nan, and H. B. Lu, "Carbon-coated, methanol-tolerant platinum/graphene catalysts for oxygen reduction reaction with excellent long-term performance," *Journal of Materials Chemistry A,* vol. 3, pp. 1049-1057, 2015.
[240] N. C. Cheng, M. N. Banis, J. Liu, A. Riese, X. Li, R. Y. Li, S. Y. Ye, S. Knights, and X. L. Sun, "Extremely Stable Platinum Nanoparticles Encapsulated in a Zirconia Nanocage by Area-Selective Atomic Layer Deposition for the Oxygen Reduction Reaction," *Advanced Materials,* vol. 27, pp. 277-281, Jan 2015.
[241] J. K. Norskov, J. Rossmeisl, A. Logadottir, L. Lindqvist, J. R. Kitchin, T. Bligaard, and H. Jonsson, "Origin of the overpotential for oxygen reduction at a fuel-cell cathode," *Journal of Physical Chemistry B,* vol. 108, pp. 17886-17892, Nov 2004.
[242] O. Antoine, Y. Bultel, and R. Durand, "Oxygen reduction reaction kinetics and mechanism on platinum nanoparticles inside Nafion (R)," *Journal of Electroanalytical Chemistry,* vol. 499, pp. 85-94, Feb 2001.
[243] D. B. Sepa, M. V. Vojnovic, and A. Damjanovic, "REACTION INTERMEDIATES AS A CONTROLLING FACTOR IN THE KINETICS AND MECHANISM OF OXYGEN REDUCTION AT PLATINUM-ELECTRODES," *Electrochimica Acta,* vol. 26, pp. 781-793, 1981.
[244] A. M. Gomez-Marin and J. M. Feliu, "New Insights into the Oxygen Reduction Reaction Mechanism on Pt(111): A Detailed Electrochemical Study," *Chemsuschem,* vol. 6, pp. 1091-1100, Jun 2013.
[245] Z. H. Ni, Y. Y. Wang, T. Yu, and Z. X. Shen, "Raman Spectroscopy and Imaging of Graphene," *Nano Research,* vol. 1, pp. 273-291, Oct 2008.

[246] P. Venezuela, M. Lazzeri, and F. Mauri, "Theory of double-resonant Raman spectra in graphene: Intensity and line shape of defect-induced and two-phonon bands," *Physical Review B*, vol. 84, Jul 2011.